

DISSERTATION

EMERGENT TOPOLOGICAL PHENOMENA IN LOW-D SYSTEMS INDUCED BY GAUGE
POTENTIALS

Submitted by

Aidan Winblad

Department of Physics

In partial fulfillment of the requirements

For the Degree of Doctor of Philosophy

Colorado State University

Fort Collins, Colorado

Fall 2024

Doctoral Committee:

Advisor: Hua Chen

Richard Eykholt

Martin Gelfand

Olivier Pinaud

Copyright by Aidan Winblad 2024

All Rights Reserved

ABSTRACT

EMERGENT TOPOLOGICAL PHENOMENA IN LOW-D SYSTEMS INDUCED BY GAUGE POTENTIALS

Abstract goes here

ACKNOWLEDGEMENTS

I would like to thank the CSU Graduate Student Council and the CSU Graduate School for initiating, commissioning and supporting this project. I would also like to thank Nicole Ramo for her support and ensuring that we followed through with this project to completion. I would like to thank Leif Anderson, who created and supported the previous LaTeX template for a number of years. Although I have never met Leif, his work was invaluable in the creation of this package and has helped many students get their thesis approved by the CSU graduate school. Finally, I would like to thank everyone who helps to contribute to this package. Your work will help many CSU graduate students to create professional, beautiful and compelling theses and dissertations using LaTeX. Last but not least, thank you to the creators and maintainers of \LaTeX for creating a fantastic typesetting tool.

DEDICATION

I would like to dedicate this dissertation to my dog Zeta.

TABLE OF CONTENTS

ABSTRACT	ii
ACKNOWLEDGEMENTS	iii
DEDICATION	iv
LIST OF TABLES	vii
LIST OF FIGURES	viii
Chapter 1 Introduction	1
1.1 Introduction	1
1.2 Maxwell's equations	2
1.3 Gauge transformations	2
1.4 Minimal coupling and Canonical momentum	4
1.5 Peierls phase in tight-binding models	7
1.6 Majorana fermions and topological superconductors	9
1.6.1 Kitaev chain	11
1.6.2 Half-quantum vortices in p -wave superconductors	13
1.6.3 Braiding	16
1.6.4 T-junction qubit	17
1.6.5 Effective p -wave superconductors	19
1.7 Landau levels in condensed matter	24
Chapter 2 Superconducting Triangular Islands as a Platform for Manipulating Majorana Zero Modes	28
2.1 Introduction	28
2.2 Kitaev Triangle	30
2.3 Hollow Triangles	33
2.4 Braiding MZM in a small network of triangles	40
2.5 Additional results using inhomogeneous vector fields	41
2.6 Discussion	44
Chapter 3 Floquet Landau Levels	48
3.1 Introduction	48
3.2 Toy model	49
3.3 Floquet LLs in 2DEG	51
3.3.1 2DEG Numerical Approach	52
3.4 Floquet LLs in Dirac systems	55
3.4.1 Dirac Numerical Approach	57
3.5 Discussion and conclusion	59
Chapter 4 Conclusion and Discussion	62
Appendices	63

Appendix Chapter A	Superconducting Triangular Islands	63
A.1	Kitaev chain	63
A.2	Vector potential and gauge invariance	79
A.3	Analytic solution of the Kitaev triangle	81
A.4	Kitaev Triangle and Peierls substitution	87
Appendix Chapter B	Floquet Landau levels	89
B.1	Quantum harmonic oscillator	89
B.2	Dirac equation in the presence of a magnetic field	92
B.3	Van-Vleck expansion of modulated circularly polarized light on a 2DEG	94
B.4	Tight-binding model 2DEG	100
B.5	Tight-binding model Dirac	104
Bibliography		117

LIST OF TABLES

LIST OF FIGURES

1.1	The top chain represents the system in a trivial topology where each complex fermion $c_j = \frac{1}{2}(a_j + ib_j)$ is a linear combination of intraconnected MFs. The bottom chain represents the system in a non-trivial topology where each complex fermion $\tilde{c}_j = \frac{1}{2}(a_j + ib_{j+1})$ is a linear combination of interconnected MFs, leaving the non-localized complex fermion $f = \frac{1}{2}(a_0 + ib_N)$, and thus leaving one MF located at each end of the chain.	12
1.2	The order phase φ and angle α of \mathbf{d} rotate by π : $(\varphi, \mathbf{d}) \rightarrow (\varphi + \pi, -\mathbf{d})$. The order parameter θ maps to itself, $(0, 2\pi)$, under simultaneous change of both \mathbf{d} and φ : $\theta = \varphi + \alpha$	14
1.3	Two vortices in an elementary braid exchange.	16
1.4	Braid group relation for $T_i T_{i+1} T_i = T_{i+1} T_i T_{i+1}$	17
1.5	Braiding two Majorana fermions on a T-junction.	18
1.6	Ladder junction schematic for hosting and braiding multiple Majorana fermions.	18
2.1	Schematics of two triangle structures proposed in this work. (a) Three-site Kitaev triangle with bond-dependent Peierls phases. (b) Hollow triangular island with a uniform vector potential.	30
2.2	(a) Evolution of the eigenvalues of the 3-site Kitaev triangle along the closed parameter path for ϕ on the three edges. (b) MZM wavefunctions at different points of the parameter path. Clockwise from the upper left panel: $\phi_1 \rightarrow \frac{1}{2}(\phi_1 + \phi_2) \rightarrow \phi_2 \rightarrow \phi_3$	33
2.3	(a) Topological phase diagram for a $W = 1$ triangular chain with the Hamiltonian Eq. (2.7) obtained by superimposing the $\mathcal{M}(A, \mu)$ plots of 1D chains with $\mathbf{A} = A\mathbf{y}$ and $\mathbf{A} = A(\frac{\sqrt{3}}{2}\mathbf{x} + \frac{1}{2}\mathbf{y})$. Color scheme: white— $\mathcal{M} = 1$, dark blue— $\mathcal{M} = -1$, light blue— $\mathcal{M} = 0$ (b) Near-gap BdG eigen-energies vs A for a finite triangle with edge length $L = 50$, $W = 1$, and $\mu = 1.6$	35
2.4	(a) Spectral flow of a hollow triangle with $W = 1$, $L = 50$, $\mu = 1.6$, and $A = 2.75$ with increasing rotation angle φ , defined through $\mathbf{A} = A(-\sin \varphi \mathbf{x} + \cos \varphi \mathbf{y})$. (b-d) BdG eigenfunction $ \Psi ^2$ summed over the two zero modes at $\varphi = 0, \frac{\pi}{6}$, and $\frac{\pi}{3}$, respectively.	37
2.5	(a) Topological phase diagram for a $W = 3$ hollow triangle obtained by overlapping the $\mathcal{M}(A, \mu)$ plots of 1D chains with $\mathbf{A} = A\mathbf{y}$ and $\mathbf{A} = A(\frac{\sqrt{3}}{2}\mathbf{x} + \frac{1}{2}\mathbf{y})$. Color scheme: white— $\mathcal{M} = 1$, dark blue— $\mathcal{M} = -1$, light blue— $\mathcal{M} = 0$ (b) Near-gap BdG eigen-energies vs A for a finite triangle with edge length $L = 50$, $W = 3$, and $\mu = 1.6$. (c) BdG eigenfunction $ \Psi ^2$ summed over the two zero modes at $A = 2.4709$	38
2.6	(a) Spectral flow of a hollow triangle with $W = 3$, $L = 50$, $\mu = 1.6$, and $A = 2.75$ with increasing rotation angle φ , defined through $\mathbf{A} = A(-\sin \varphi \mathbf{x} + \cos \varphi \mathbf{y})$. (b-c) BdG eigenfunction $ \Psi ^2$ summed over the two zero modes at $\varphi = 0$ and $\frac{\pi}{3}$, respectively.	39

2.7	(a) Spectral flow for the critical step of swapping γ_2 and γ_3 in the example of Fig. 5 in the main text, calculated using four corner-sharing triangles of $W = 1$ and $L = 50$, with $\mu = 1.6$ and $A = 2.6$. Vector potential for the middle triangle in the bottom row can rotate according to $\mathbf{A} = A(-\sin\varphi\mathbf{x} + \cos\varphi\mathbf{y})$ from $\varphi = \frac{\pi}{6}$ to $\frac{\pi}{3}$, while the other three have fixed $\varphi = 0$. (b)-(g) BdG eigenfunction $ \Psi ^2$ summed over the four zero modes at equally-spaced points along the rotation path. The black arrow indicates the direction of the vector potential for the bottom middle triangle.	40
2.8	(a) Spectral flow of a hollow triangle with $W = 1$, $L = 50$, and $\mu = 1.6$ for increasing heaviside vector potential strength defined by $\mathbf{A} = A[1 - 2\Theta(x)]\mathbf{y}$ (b) BdG eigenfunction $ \Psi ^2$ summed over the two zero modes at $A = 2.7409$	41
2.9	(a) Spectral flow of a hollow triangle with $W = 1$, $L = 50$, and $\mu = 1.6$ for increasing tanh vector potential strength defined by $\mathbf{A} = -A \tanh(x/2w)\mathbf{y}$, $w = a/2$ (b) BdG eigenfunction $ \Psi ^2$ summed over the two zero modes at $A = 2.7409$	42
2.10	(a) Spectral flow of a hollow triangle with $W = 3$, $L = 50$, and $\mu = 1.6$ for increasing heaviside vector potential strength defined by $\mathbf{A} = A[1 - 2\Theta(x)]\mathbf{y}$ (b) BdG eigenfunction $ \Psi ^2$ summed over the two zero modes at $A = 2.7409$	43
2.11	(a) Spectral flow of a hollow triangle with $W = 3$, $L = 50$, and $\mu = 1.6$ for increasing tanh vector potential strength defined by $\mathbf{A} = -A \tanh(x/2w)\mathbf{y}$, $w = a/2$ (b) BdG eigenfunction $ \Psi ^2$ summed over the two zero modes at $A = 2.7409$	43
2.12	Spectral flow of a hollow triangle with $L = 50$, and $\mu = 0$ for increasing linear vector potential strength defined by $\mathbf{A} = -Axy$ (a) $W = 1$ and (b) $W = 3$ (c-d) Wavefunctions of the MZM at $A = 0.0499$ for both widths, respectively.	44
2.13	Spectral flow of a hollow triangle with $L = 50$, and $\mu = 1.6$ for increasing linear vector potential strength defined by $\mathbf{A} = -Axy$ (a) $W = 1$ and (b) $W = 3$. (c-d) Wavefunctions of the MZM at $A = 0.0598$ for both widths, respectively.	45
2.14	Representative steps for braiding four MZM in four triangles sharing corners. (a) Initialization of four MZM $\gamma_1, \gamma_2, \gamma_3, \gamma_4$. All three edges of the bottom-middle and the top triangles are in the trivial phase by e.g. controlling the chemical potential. The bottom-left and bottom-right triangles have $\varphi = 0$ so that their bottom edges are nontrivial. (b) Moving γ_3 by “switching on” the middle triangle by changing the chemical potential under a fixed vector potential at $\varphi = \frac{\pi}{6}$, and then turning on the top triangle with similar means except $\varphi = 0$. (c) Transporting γ_2 to the right triangle through rotating the vector potential in the middle triangle counterclockwise by $\pi/6$. (d) Moving γ_3 to the left triangle by “switching off” the top triangle followed by the middle triangle.	46

Chapter 1

Introduction

EM gauge potential appears in electronic Hamiltonian in CM

1. Review Maxwell theory -> gauge potential
2. Minimal coupling $-i\hbar\nabla \rightarrow -i\hbar\nabla + q\mathbf{A}$ or $-i\partial_\mu \rightarrow -i\partial_\mu + qA_\mu$
3. TB Hamiltonian and Peierls phase

Topological phenomena in CM considered in thesis

1.1 Introduction

In this dissertation we discuss how gauge potentials can be used as a key ingredient for inducing topological phase transitions in condensed matter systems, such as conductors, insulators, and superconductors. We will cover some important background physics: Maxwell's equation, gauge invariance, minimal coupling, and Peierls phase. A review of how one can achieve Majorana fermions in superconductors is shown and their importance to topological quantum computing. Followed by some basics of Landau level in relation to the Chern number, a parameter that indicates if a system is in a non-trivial topological phase. Then, applying these concepts to superconductors and conductors, for 2D electron gases (2DEG) and Dirac systems, we see topological phenomena occur.

In the case of a superconductor we can induce topological phase transitions that allow for Majorana Fermions to be hosted and rotated along the corners of a hollow equilateral triangle, a basic building block for a topological quantum logic gate. This provides a potential new avenue for achieving a topological quantum computation where a network of interconnected triangular islands allows for braiding of Majorana fermions.

For 2DEG and Dirac systems we show oblique incident circularly polarized light can using Floquet theory can achieve Landau Levels, or quantum Hall effect, where the effective magnetic

field is related to the electric field of the laser light. Outside of having the electric field as a useful parameter for achieving a QHE device this lets us explore non-equilibrium systems which is a burgeoning field of interest in condensed matter physics.

1.2 Maxwell's equations

Let us start with Maxwell's equations, given as

$$\nabla \cdot \mathbf{E} = \frac{1}{\epsilon_0} \rho, \quad (1.1)$$

$$\nabla \cdot \mathbf{B} = 0, \quad (1.2)$$

$$\nabla \times \mathbf{E} = -\partial_t \mathbf{B}, \quad (1.3)$$

$$\nabla \times \mathbf{B} = \mu_0 \mathbf{J} + \mu_0 \epsilon_0 \partial_t \mathbf{E}, . \quad (1.4)$$

We want to write Maxwell's equations as a function of potentials, V and \mathbf{A} . One recalls the magnetic field, $\mathbf{B} = \nabla \times \mathbf{A}$, and electric field, $\mathbf{E} = -\nabla V - \partial_t \mathbf{A}$. We notice Eq. (1.2) and (1.3) provide nothing new. The remaining Maxwell's equation then become

$$\frac{1}{\epsilon_0} \rho = -\nabla^2 V - \partial_t \nabla \cdot \mathbf{A}, \quad (1.5)$$

$$-\mu_0 \mathbf{J} = \nabla^2 \mathbf{A} - \mu_0 \epsilon_0 \partial_t^2 \mathbf{A} - \nabla (\nabla \cdot \mathbf{A} + \mu_0 \epsilon_0 \partial_t V). \quad (1.6)$$

1.3 Gauge transformations

We now move on to gauge transformations. Suppose $\mathbf{A}' = \mathbf{A} + \boldsymbol{\alpha}$ and $V' = V + \beta$. Both vector potentials give the same magnetic field,

$$\mathbf{B} = \nabla \times \mathbf{A} = \nabla \times \mathbf{A}' = \nabla \times (\mathbf{A} + \boldsymbol{\alpha}),$$

$$\boldsymbol{\alpha} = \nabla \lambda. \quad (1.7)$$

The two potentials should also give the same electric field,

$$\mathbf{E} = -\nabla V - \partial_t \mathbf{A} = -\nabla V' - \partial_t \mathbf{A}'$$

$$\mathbf{E} = -\nabla V - \nabla \beta - \partial_t \mathbf{A} - \partial_t \nabla \lambda$$

$$\text{then } \beta = -\partial_t \tilde{\lambda} = -\partial_t \lambda + k(t)$$

$$\mathbf{A}' = \mathbf{A} + \nabla \lambda \quad (1.8)$$

$$V' = V - \partial_t \tilde{\lambda} \quad (1.9)$$

From the above set of expressions we arrive at the general gauge transformations of potentials. We make note that a change in V and \mathbf{A} does not change the electric and magnetic fields, i.e. gauge invariant, and are tuned to adjust the divergence of \mathbf{A} . This allows one to solve the scalar and vector potentials readily depending on the gauge.

One common example of gauge is the Coulomb gauge, which is used in magnetostatics. We assert the following for a Coulomb gauge, $\nabla \cdot \mathbf{A} = 0$, which makes $\nabla^2 V = -\frac{1}{\epsilon_0} \rho$. Recall Eq. (1.6), it simplifies to

$$(\nabla^2 - \mu_0 \epsilon_0 \partial_t^2) \mathbf{A} = -\mu_0 \mathbf{J} + \mu_0 \epsilon_0 \nabla \partial_t V$$

$$\square^2 \mathbf{A} = -\mu_0 \mathbf{J} + \mu_0 \epsilon_0 \nabla \partial_t V \quad (1.10)$$

where we have used \square as the d'Alembertian [1].

1.4 Minimal coupling and Canonical momentum

Minimal coupling comes from the following substitution

$$-i\hbar\nabla \rightarrow -i\hbar\nabla - q\mathbf{A}, \quad (1.11)$$

which can be derived from the canonical momentum operator when a charged particle is present in a vector potential field. In this case minimal coupling means the field is coupling the orbital and potential only, ignoring higher order multipole moments. This also allows the system to have a local gauge invariance under U(1) transformations, i.e. $\mathbf{A} \rightarrow \mathbf{A} + \nabla\lambda$ [2].

Next, we derive the canonical momentum operator and demonstrate its gauge invariance. Start with the Lagrangian for charged particle in a scalar and vector potential field,

$$\begin{aligned} \mathcal{L} &= T - U \\ &= \frac{1}{2}m\dot{\mathbf{r}}^2 - qV + q\dot{\mathbf{r}} \cdot \mathbf{A}(\mathbf{r}, t), \end{aligned} \quad (1.12)$$

where $T = \frac{1}{2}m\dot{\mathbf{r}}^2$ and $U = qV - q\dot{\mathbf{r}} \cdot \mathbf{A}(\mathbf{r}, t)$. One recalls from classical mechanics that

$$\begin{aligned} \mathbf{p}_{\text{can}} &= \frac{\partial \mathcal{L}}{\partial \dot{\mathbf{r}}} \\ \mathbf{p}_{\text{can}} &= \mathbf{p}_{\text{kin}} + q\mathbf{A}. \end{aligned} \quad (1.13)$$

With the canonical momentum defined the Hamiltonian is

$$\begin{aligned}
\mathcal{H} &= \mathbf{p}_{\text{can}} \cdot \dot{\mathbf{r}} - \mathcal{L} \\
&= \frac{1}{2m} \mathbf{p}_{\text{kin}}^2 + qV \\
&= \frac{1}{2m} (\mathbf{p}_{\text{can}} - q\mathbf{A})^2 + qV.
\end{aligned} \tag{1.14}$$

Thus, we have shown that in the presence of a vector potential field we have the minimal coupling expression $i\hbar\nabla - q\mathbf{A}$.

For simplicity, we show the previous Hamiltonian without a scalar potential is gauge invariant (it can be shown with the scalar potential but it is irrelevant for our purposes). Suppose $\mathcal{H}|\psi\rangle = \epsilon|\psi\rangle$ and that

$$\mathcal{H} = \frac{1}{2m} (\mathbf{p} - q\mathbf{A})^2. \tag{1.15}$$

Let $\mathbf{A}' = \mathbf{A} + \nabla\lambda$, where λ is a scalar. Then,

$$\mathcal{H}|\psi\rangle = \frac{1}{2m} (\mathbf{p} - q\mathbf{A}' + q\nabla\lambda)^2 |\psi\rangle = \epsilon|\psi\rangle, \tag{1.16}$$

and also allow

$$\begin{aligned}
\mathcal{H}'|\psi'\rangle &= \frac{1}{2m} (\mathbf{p} - q\mathbf{A}')^2 |\psi'\rangle, \\
\mathcal{H}'|\psi'\rangle &= \frac{1}{2m} (\mathbf{p} - q\mathbf{A} - q\nabla\lambda)^2 |\psi'\rangle = \epsilon|\psi'\rangle.
\end{aligned} \tag{1.17}$$

Let $|\psi'\rangle = U|\psi\rangle$, where U is a unitary operator such that $U^\dagger U = \mathbf{1}$. Position and momentum expectation values should be the same under both gauge choices. Starting with position operator we derive one useful commutation relation

$$\langle \psi' | \mathbf{r} | \psi' \rangle = \langle \psi | U^\dagger \mathbf{r} U | \psi \rangle = \langle \psi | \mathbf{r} | \psi \rangle$$

$$U^\dagger \mathbf{r} U = \mathbf{r}$$

$$\mathbf{r} U = U \mathbf{r}$$

$$[\mathbf{r}, U] = 0. \quad (1.18)$$

We can then extrapolate to $[\mathbf{A}(\mathbf{r}), U] = 0$. With the momentum operator we can derive another useful commutation relation

$$\langle \psi' | \mathbf{p} - q\mathbf{A}' | \psi' \rangle = \langle \psi | U^\dagger (\mathbf{p} - q\mathbf{A}') U | \psi \rangle = \langle \psi | \mathbf{p} - q\mathbf{A} | \psi \rangle$$

$$U^\dagger \mathbf{p} U - U^\dagger q\mathbf{A}' U = \mathbf{p} - q\mathbf{A}$$

$$\mathbf{p} U - q\mathbf{A} U - q\nabla\lambda U = U\mathbf{p} - Uq\mathbf{A}$$

$$[\mathbf{p}, U] = -i\hbar\partial_{\mathbf{r}}U = q\nabla\lambda U. \quad (1.19)$$

This leads us to find $U = \exp[iq\lambda/\hbar]$. The gauged Hamiltonian is related to the original basis by

$$\begin{aligned}
\mathcal{H}'|\psi'\rangle &= (\mathbf{p} - q\mathbf{A} - q\nabla\lambda)^2|\psi'\rangle \\
&= (\mathbf{p} - q\mathbf{A} - q\nabla\lambda) \cdot (\mathbf{p}U - q\mathbf{A}U - q\nabla\lambda U)|\psi\rangle \\
&= (\mathbf{p} - q\mathbf{A} - q\nabla\lambda) \cdot U(\mathbf{p} - q\mathbf{A})|\psi\rangle \\
&= U(\mathbf{p} - q\mathbf{A})^2|\psi\rangle \\
&= U\epsilon|\psi\rangle.
\end{aligned} \tag{1.20}$$

We see the local phase of the wavefunction is changed but it still represents the same energy shown by

$$\begin{aligned}
\langle\psi'|\mathcal{H}'|\psi'\rangle &= \langle\psi|U^\dagger\mathcal{H}'U|\psi\rangle = \langle\psi|U^\dagger U\epsilon|\psi\rangle = \epsilon, \\
\langle\psi|\mathcal{H}|\psi\rangle &= \langle\psi|\epsilon|\psi\rangle = \epsilon,
\end{aligned} \tag{1.21}$$

and in other words $U^\dagger\mathcal{H}'U = \mathcal{H}$ [3].

1.5 Peierls phase in tight-binding models

We next show how to incorporate a vector potential field into a tight-binding Hamiltonian. There are a few ways to derive a Peierls phase and we will use the differential geometry approach. Before we showed minimal coupling and now we would like to express it in terms of a covariant derivative

$$D_\mu = \partial_\mu - iA_\mu. \tag{1.22}$$

Let us now envision how a wavefunction will evolve in the presence of a vector potential field. Using the covariant derivative with the parallel transport along curves we can obtain an expression for the phase accumulation on the wave function. The covariant derivative should vanish if it is parallel transported along the curve \mathcal{C} defined by points x and $x' = x + v t$. The expression is as follows

$$\nabla_\nu s = 0 \rightarrow t v^\mu D_\mu s_{x(t)} = 0 \quad (1.23)$$

$$\begin{aligned} &= t \dot{x}^\mu(t) (\partial_\mu - i A_\mu) s_{x(t)} \\ &= t \frac{\partial x^\mu}{\partial t} \frac{\partial}{\partial x_\mu} s_{x(t)} - i t \dot{x}^\mu(t) A_{x(t),\mu} s_{x(t)} \\ &\rightarrow \dot{s}_{x(t)} - i \dot{x}^\mu(t) A_{x(t),\mu} s_{x(t)} = 0 \\ &\rightarrow s_{x(t)} = s_{x(0)} \exp \left[i \int_0^t \dot{x}^\mu A_{x(t'),\mu} dt' \right] \\ &s_{x(t)} = s_{x(0)} \exp \left[i \int_{\mathcal{C}} dx^\mu A_{x(t'),\mu} \right] \end{aligned}$$

and in general we can rewrite to the following expression $\psi(t) = \psi(0) \exp \left[\frac{iq}{\hbar} \int_{\mathcal{C}} \mathbf{A}(\mathbf{r}) \cdot d\mathbf{l} \right]$ [2].

Given the following tight-binding Hamiltonian

$$\mathcal{H}_t = -t \sum_{\langle j,l \rangle} c_j^\dagger c_l + h.c., \quad (1.24)$$

we can apply a vector potential to a system making the following Peierls phase transform, a unitary transform, to its creation/annihilation operators

$$\begin{aligned}
c_j &\rightarrow c_j \exp \left[\frac{iq}{\hbar} \int^{\mathbf{r}_j} \mathbf{A} \cdot d\mathbf{l} \right] \\
c_j^\dagger c_l &\rightarrow c_j^\dagger c_l \exp \left[\frac{iq}{\hbar} \int_{\mathbf{r}_j}^{\mathbf{r}_l} \mathbf{A} \cdot d\mathbf{l} \right].
\end{aligned} \tag{1.25}$$

The Hamiltonian in the new basis takes the following form

$$\mathcal{H}_t = \sum_{\langle j,l \rangle} -t_{j,l} c_j^\dagger c_l + h.c., \tag{1.26}$$

where $t_{j,l} = t \exp \left[\frac{iq}{\hbar} \int_{\mathbf{r}_j}^{\mathbf{r}_l} \mathbf{A} \cdot d\mathbf{l} \right]$.

1.6 Majorana fermions and topological superconductors

Before we define Majorana fermions we will discuss characteristics of fermions. Fermions are particles that follow Fermi-Dirac statistics and the Pauli exclusion principle and have half-integer spin (spin 1/2, 3/2, etc.). Both Enrico Fermi and Paul Dirac derived the Fermi-Dirac distribution at roughly the same time in 1926 and independently of one another. There are three types of fermions: Dirac, Weyl, Majorana. Dirac's equation led to the derivation of a (complex) wavefunction solution for spin-half fermions that have mass and charge, and an antiparticle, coined as the positron. A few years later, Hermann Weyl derived from Dirac's equation a simplified solution for describing massless fermions. Then, in 1937 Ettore Majorana hypothesized from Dirac's equation a (real) wavefunction solution that showed that these fermions were both particle and antiparticle and neutrally charged.

Examples of observed fermions include electrons, neutrinos, neutron, and protons. Weyl and Majorana fermions have yet to be observed. The Standard Model does allow for neutrinos to potentially be Majorana fermions. The MAJORANA project: neutrinoless double beta decay, is one experiment for detecting neutrino Majorana fermions and has yielded negative results thus far. The particle physics community has not found either Weyl and Majorana fermions in

any experiment yet. There are, however, avenues for pursuing them as quasiparticles in condensed matter systems. For example, in 2011 Weyl fermions were theorized to be in topological semimetals then quickly observed by 2015 in TaAs semimetals using angle-resolved photoemission spectroscopy (ARPES) [4–6].

To understand where Majorana fermions come from let's look at what quasiparticles exist in superconductors. Since 2001 it has been hypothesized that Majorana fermions can be found on p -wave superconductors in pairs of 2 and non-localized in half-quantum vortices and at the ends of wires [7, 8]. In conventional superconductors there are Cooper pairs that make up the supercurrent. These Cooper pairs are made up of two electrons (or holes) with opposite spin and momenta caused by the electron-phonon interaction, are bosonic and condensate, and are in a ground state with allowed excited states. A Bogoliubov quasiparticle is the first excited state of a Cooper pair condensate, this is when an electron and hole with opposite momenta become paired. This usually happens when the system's chemical potential allows the electron and hole bands to cross one another in the Brillouin space and the superconducting order parameter, Δ , dictates the type of spin coupling. For example, superconductors that are s -wave pair electrons and holes with opposite spin, while p -wave pairs electrons and holes that are spin-polarized or spinless. In a p -wave superconductor if the Bogoliubov quasiparticle is a zero-energy excitation it can be written as a Majorana fermion and because of the particle-hole symmetry in the system they come in pairs. Should I mention anything about singlets and triplets and mention a generalized 2×2 d vector notation for order parameter?

We have yet to physically realize a p -wave superconductor experimentally, however, we can use heterostructures in proximity to an s -wave superconductor to achieve an effective p -wave superconducting interface, which is explained and referenced in later chapters. Majorana fermions are dictated by non-Abelian exchange statistics, which allows for building a universal quantum computer, hence why they are highly sought after. Another boon of using a non-trivial topological superconductor is the ability to protect Majorana fermions from local perturbations.

1.6.1 Kitaev chain

Ivanov first showed how to derive Majorana fermions in a 2D p -wave superconductor. However, we find it easier to understand Kitaev's approach first. Let us go ahead and show how Kitaev derived Majorana zero modes (MZMs), Majorana(MFs), on a 1D spinless p -wave superconductor. Start with a 1D spinless p -wave superconductor tight-binding Hamiltonian

$$\mathcal{H} = \sum_j^{N-1} (-tc_j^\dagger c_{j+1} + \Delta c_j c_{j+1} + h.c.) - \sum_j^N \mu c_j^\dagger c_j, \quad (1.27)$$

where t is hopping amplitude, superconducting order parameter $\Delta = |\Delta|$ for simplicity, μ is chemical potential, and $c^\dagger(c)$ is the creation (annihilation) operator for a complex fermion. We use a basis tranformation to convert to the Majorana fermion basis, where $c_j^\dagger = \frac{1}{2}(a_j - ib_j)$, $\{a_j^\dagger, a_{j'}\} = \{a_j, a_{j'}\} = 2\delta_{j,j'}$ since they are Majorana fermions, and $\{a_j, b_j'\} = 0$. After some algebra we arrive at

$$\mathcal{H} = \frac{i}{2} \sum_j (-\mu a_j b_j + (t + \Delta) b_j a_{j+1} + (-t + \Delta) a_j b_{j+1}). \quad (1.28)$$

In the trivial topology phase, there are no Majorana fermions, $\mu \neq 0$ and $t = \Delta = 0$,

$$\mathcal{H} = -\mu \frac{1}{2} \sum_j a_j b_j. \quad (1.29)$$

For non-trivial topology phase, there are Majorana fermions present, $\mu = 0$, and $t = \Delta > 0$,

$$\mathcal{H} = it \sum_j b_j a_{j+1}. \quad (1.30)$$

Notice the terms a_0 and b_N are missing in the non-trivial topology Hamiltonian, we can say there is a non-localized zero energy mode present in the system defined by $f = \frac{1}{2}(a_0 + ib_N)$, hence the name Majorana zero modes. Figure 1.1 shows the wire in both topological phases. One quick note on terminology, sometimes non-trivial topology is referred to as the topological phase, for the purposes of this dissertation we will use the former option. Now, slightly outside

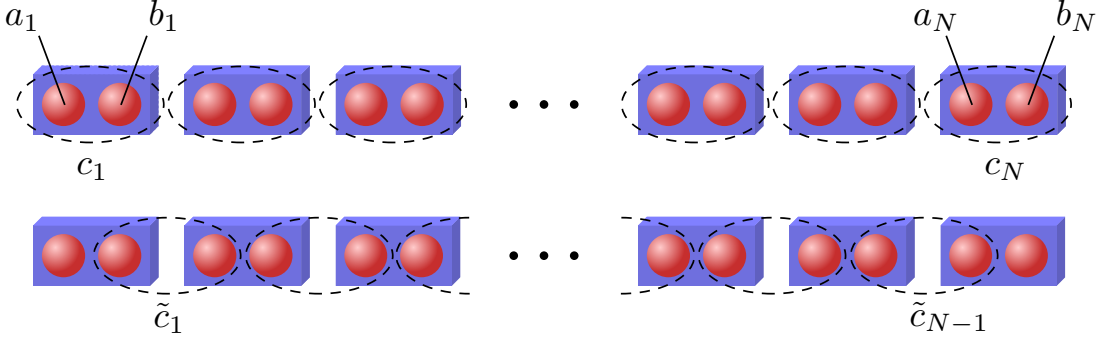


Figure 1.1: The top chain represents the system in a trivial topology where each complex fermion $c_j = \frac{1}{2}(a_j + ib_j)$ is a linear combination of intraconnected MFs. The bottom chain represents the system in a non-trivial topology where each complex fermion $\tilde{c}_j = \frac{1}{2}(a_j + ib_{j+1})$ is a linear combination of interconnected MFs, leaving the non-localized complex fermion $f = \frac{1}{2}(a_0 + ib_N)$, and thus leaving one MF located at each end of the chain.

the Kitaev limit for non-trivial topology, we can limit $|\mu| < 2t$ and $t = |\Delta| > 0$ and still achieve non-trivial topology with Majorana zero modes at the interface of trivial and non-trivial topology.

To understand why this is still true we can determine the topological invariant for the system, also known as the Majorana number, a type of Winding number for 1D superconducting systems. While calculating the Majorana number is straight forward enough, its proof on the other hand is not, this can be found in the appendix REFERENCE appendix here. We write the Hamiltonian in the Majorana basis, $A = -iU\mathcal{H}U^\dagger$, then take the sign of the Pfaffian,

$$\mathcal{M} = \text{sgn}[\text{Pf}(A)]. \quad (1.31)$$

This calculation can be reduced down if we can write the Hamiltonian in momentum space. Employing the following symmetry $\epsilon(-k) = -\epsilon(k)$ we find there are n positive and n negative eigenvalues in the system for any given k value.

$$\mathcal{M} = \begin{cases} \text{sgn}[\text{Pf}(A_{k=0})\text{Pf}(A_{k=\pi})], & \text{if } L \text{ is even,} \\ \text{sgn}[\text{Pf}(A_{k=0})], & \text{if } L \text{ is odd,} \end{cases} \quad (1.32)$$

where L is the number of lattice sites from our lattice Hamiltonian. We find that under the Kitaev limit, if $|\mu| < 2t$, then $\mathcal{M} = -1$, and if $|\mu| > 2t$, then $\mathcal{M} = 1$. When a section of the material is in a non-trivial topology and either the other material is trivial or vacuum, which is also trivial, Majorana zero modes will be localized at interfaces of differing topological number, this is also known as bulk-edge correspondence and will be used later in our topological quantum logic gate. As a last note, when $|\mu| = 2t$ this is a critical point and where the gap opens and closes, it is not an ideal region of parameter space for the band gap is too small [8]. *Originally, Kitaev's proposal was to design topological quantum storage.

1.6.2 Half-quantum vortices in p -wave superconductors

We now transition back to Ivanov's derivation of MFs and begin to introduce *braiding* for topological quantum computing as a key reason for hosting and manipulating MFs. It was proposed by Read and Green that the Pfaffian quantum Hall state derived by Moore and Read belongs to the same topological class as the BCS pairing state. Ivanov then verified this was the case for a BCS pairing state. Since the Pfaffian state was shown to exhibit non-Abelian statistics for half-quantum vortices the same is true for p -wave superconductors. To answer why this is the case we need to understand how the superconducting order parameter acts for different pairing potentials composing of singlet or triplet states.

The superconducting order parameter, called order parameter or pairing potential for short, tells us the correlation between two fermionic operators in a superconductor and thus requires the state to be antisymmetric. These states are made up of a spatial and spin component. When the two electrons in a cooper pair are a spin-singlet the spin component is antisymmetric and requires the spatial component be symmetric; this occurs in s - and d -wave superconductors. If instead the electrons in a cooper pair are a spin-triplet the spin component is symmetric and requires the spatial component be antisymmetric; this occurs in p - and f -wave superconductors. In terms of Pauli matrices we can in general encode the order parameter with

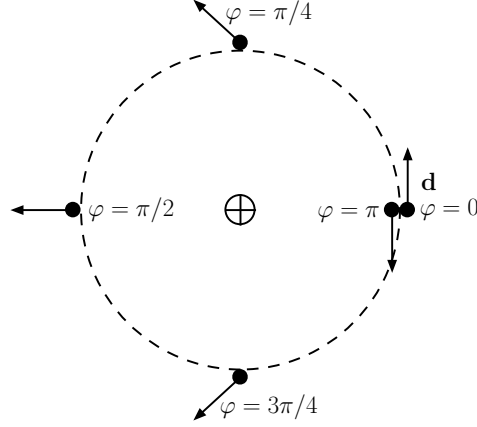


Figure 1.2: The order phase φ and angle α of \mathbf{d} rotate by π : $(\varphi, \mathbf{d}) \rightarrow (\varphi + \pi, -\mathbf{d})$. The order parameter θ maps to itself, $(0, 2\pi)$, under simultaneous change of both \mathbf{d} and φ : $\theta = \varphi + \alpha$.

$$\Delta(\mathbf{k}) = (\Delta_0(\mathbf{k}) + \mathbf{d}(\mathbf{k}) \cdot \boldsymbol{\sigma}) i\sigma_y, \quad (1.33)$$

with the following antisymmetric definition $\Delta(\mathbf{k}) = \Delta^T(-\mathbf{k})$, we see $\Delta_0(\mathbf{k})$ encodes spin-singlet components and $\mathbf{d}(\mathbf{k})$ encodes spin-triplet components, and at the end σ_y is there to keep the matrix antisymmetric. The direction vector \mathbf{d} needs to be a three dimensional vector to ensure we account for the three spin configurations $|\uparrow\uparrow\rangle$, $|\uparrow\downarrow\rangle + |\downarrow\uparrow\rangle$, and $|\downarrow\downarrow\rangle$. To account for even-parity in the symmetric spatial component the momentum is of even powers proportional with the even spherical harmonics, while odd-parity in the antisymmetric component the momentum is of odd powers proportional to the odd spherical harmonics. For example, in s -wave superconductors, $l = 0$ and $Y_{0,0} = \text{const.}$ and has no momentum dependence and $\Delta_s(\mathbf{k}) = i\Delta_0\sigma_y$. In the case of p -wave superconductors, $l = 1$ and $Y_{1,\pm 1} \propto k_x \pm ik_y$ leading to linear dependence in momentum such that the order parameter becomes $\Delta_p(\mathbf{k}) = i\Delta(\mathbf{d} \cdot \boldsymbol{\sigma})(k_x + ik_y)\sigma_y$.

In Ivanov's case he picked a slightly different basis for the triplet-pairing order parameter,

$$\Delta(\mathbf{k}) = \Delta e^{i\varphi} [d_x\sigma_0 + id_y\sigma_z + d_z\sigma_x] (k_x + ik_y) \quad (1.34)$$

it still follows the antisymmetric definition $\Delta(\mathbf{k}) = -\Delta^T(-\mathbf{k})$. For a half-quantum vortex to exist, we must allow \mathbf{d} to rotate in 3D or on a plane. Additionally, the order parameter maps to itself, which requires the change of sign of \mathbf{d} and shift in the phase φ by π simultaneously. This mapping is $(\varphi, \mathbf{d}) \mapsto (\varphi + \pi, -\mathbf{d})$ and can be seen in Figure 1.2.

We now reduce to a 2D superconductor, this forces \mathbf{d} to point and rotate in the x-y plane and removes the coupling of spin-up and -down fermions from the order parameter. The order parameter can then be written in polar coordinates

$$\begin{aligned}\Delta(\mathbf{k}, r, \theta) &= \Delta(r) e^{i\varphi} \begin{bmatrix} e^{i\alpha} & 0 \\ 0 & e^{-i\alpha} \end{bmatrix} (k_x + i k_y) \\ &= \Delta(r) \begin{bmatrix} e^{i\theta} & 0 \\ 0 & 1 \end{bmatrix} (k_x + i k_y),\end{aligned}\tag{1.35}$$

where α is the angle of \mathbf{d} , remembering its simultaneous change w.r.t. φ . We see that the spin-up fermions have a vortex while the spin-down do not have a vortex (and thus no low energy states). The Hamiltonian for spin-up or spinful fermions can now be described by

$$\mathcal{H} = \int d^2\mathbf{r} \left[-\Psi^\dagger \left(\frac{\nabla^2}{2m} + \epsilon_F \right) \Psi + \Psi^\dagger \left[e^{i\theta} \Delta(r) * (\partial_x + i\partial_y) \right] \Psi^\dagger + h.c. \right],\tag{1.36}$$

where $*$ is the symmetrized product $[A * B = (AB + BA)/2]$. One can diagonalize the Hamiltonian using the quasiparticle operator $\gamma^\dagger = u\Psi^\dagger + v\Psi$. The creation annihilation of the same fermion is related by the parameters u and v , causing the energy eigenstates to be symmetric about zero-energy forcing $\gamma^\dagger(E) = \gamma(E)$. It then leads to the zero-energy eigenstate being self-conjugate, a Majorana fermion, $\gamma^\dagger(E=0) = \gamma(E=0)$. The spinful nature eliminates the spin degree of freedom and shows the creation and annihilation operators are coupled due to superconductivity, making the Majorana fermion possible through self-conjugacy.

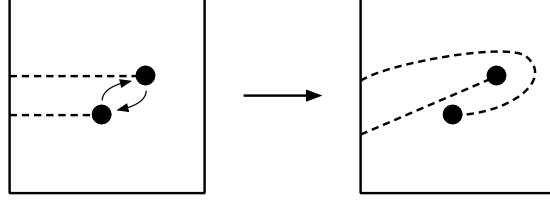


Figure 1.3: Two vortices in an elementary braid exchange.

1.6.3 Braiding

Let us now talk about gauge symmetry. Under $U(1)$ gauge transformation, if the superconducting gap is shifted by ϕ , it is the same as rotating the creation annihilation operator by half the shift. Thus, $\Psi_\alpha \mapsto e^{i\phi/2}\Psi_\alpha$, which leads to the Majorana fermion operator weights transforming as $(u, v) \mapsto (ue^{i\phi/2}, v^{-i\phi/2})$. We can see with a change of superconducting order parameter by 2π the Majorana fermion changes sign, $\gamma \mapsto -\gamma$.

This change of sign is important in braiding transformations since it allows for non-Abelian statistics. We can circumvent a global phase by introducing branch cuts for the vortices to cross, causing a 2π phase change in the Majorana fermion. Vortices can be exchanged as described in Figure 1.3, with a "bird's eye" view. We can define the braiding operators as the following

$$T_i : \begin{cases} \gamma_i \mapsto \gamma_{i+1} \\ \gamma_{i+1} \mapsto -\gamma_i \\ \gamma_j \mapsto \gamma_j \quad \text{for } j \neq i \text{ and } j \neq i+1. \end{cases} \quad (1.37)$$

This leads us to the following braiding relations

$$\begin{aligned} T_i T_j &= T_j T_i, \quad |i - j| > 1, \\ T_i T_j T_i &= T_j T_i T_j, \quad |i - j| = 1. \end{aligned} \quad (1.38)$$

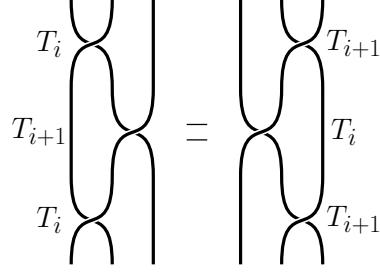


Figure 1.4: Braid group relation for $T_i T_{i+1} T_i = T_{i+1} T_i T_{i+1}$.

Figure 1.4 demonstrates three neighboring vortices and their braiding statistics having two means of achieving the same braiding exchange. One can write the braiding operators in terms of fermionic operators with the following

$$\tau(T_i) = \exp\left(\frac{\pi}{4}\gamma_{i+1}\gamma_i\right) = \frac{1}{\sqrt{2}}(1 + \gamma_{i+1}\gamma_i). \quad (1.39)$$

This can be further carried out for a number of Majorana fermions and builds a set of braiding operators for that system [7].

1.6.4 T-junction qubit

The simplest qubit theorized for braiding Majorana fermions is on 1D wires connected in a T-junction, which can be extrapolated to a ladder junction for $2n$ Majorana fermions. In the T-junction we define the quasi-1D Hamiltonian

$$\mathcal{H} = -\mu \sum_j c_j^\dagger c_j - \sum_j \left(t c_j^\dagger c_{j+1} + |\Delta| e^{i\phi} c_j c_{j+1} + h.c. \right), \quad (1.40)$$

where $c_j = e^{-i\phi/2}(\gamma_{j+1,1} + i\gamma_{j,2})/2$. We additionally have to define the pairing as $|\Delta|e^{i\phi}c_j c_{j+1}$ such that the site indices have the following definitions

- Increase moving \rightarrow / \uparrow in the horizontal/vertical wires: $\phi = 0$,
- Decrease moving \leftarrow / \downarrow in the horizontal/vertical wires: $\phi = \pi$.

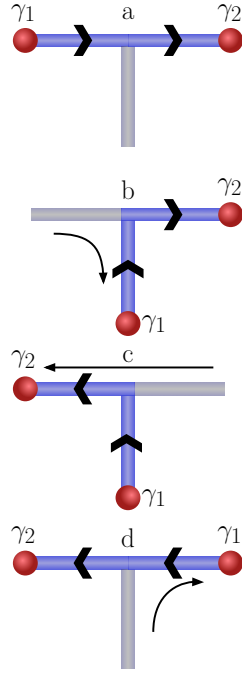


Figure 1.5: Braiding two Majorana fermions on a T-junction.

The braiding of two Majorana fermions in a T-junction is achieved by adiabatically tuning the voltage gate, or chemical potential, of the wires which can be seen in Figure 1.5. Then we can extrapolate to a ladder junction as shown in Figure 1.6 [9]. While this approach is simple in theory and being seriously pursued, it is difficult to build, manipulate, and read experimentally. Another difficulty for these wires is due to not having any truly p -wave superconductors, currently they need to be built from heterostructures to make an effective p -wave superconductor.

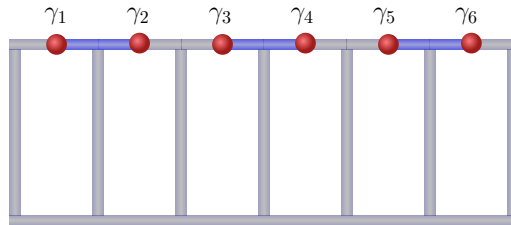


Figure 1.6: Ladder junction schematic for hosting and braiding multiple Majorana fermions.

1.6.5 Effective p -wave superconductors

There are several ways to build an effective p -wave superconductor. We go over one example given by Sau et. al. [10]. A zinc-blende semiconductor quantum well grown along the (100) direction is considered. We start with the relevant noninteracting Hamiltonian

$$\mathcal{H}_0 = \sum_{\mathbf{k}} c_{\mathbf{k}}^\dagger \left[\frac{k^2}{2m} - \mu + \alpha(\sigma^x k_y - \sigma^y k_x) \right] c_{\mathbf{k}} \quad (1.41)$$

where m is the effective mass, μ is the chemical potential, α is the Rashba spin-orbit (referenced in Alicea's paper as ref 23) coupling strength, and σ^i are the Pauli matrices that act on the spin degrees of freedom in $c_{\mathbf{k}}$. We have set $\hbar = 1$ throughout.

We next introduce a ferromagnetic insulator and a magnetic field. The ferromagnetic insulator has magnetization pointing perpendicular to the 2D semiconductor.

$$\mathcal{H}_Z = V_z \sum_{\mathbf{k}} c_{\mathbf{k}}^\dagger \sigma^z c_{\mathbf{k}} \quad (1.42)$$

but negligible orbital coupling. If we look at the combined Hamiltonian it becomes obvious there is a constant energy plus the energy eigenvalues of the Pauli matrices terms. We can easily solve the eigenvalue problem of

$$\begin{bmatrix} V_z & \alpha(k_y + i k_x) \\ \alpha(k_y - i k_x) & -V_z \end{bmatrix} \quad (1.43)$$

giving $\epsilon'_\pm(\mathbf{k}) = \pm \sqrt{V_z^2 + \alpha^2 k^2}$ with eigenvectors

$$u_+(\mathbf{k}) = \begin{pmatrix} A_\uparrow(\mathbf{k}) \\ -A_\downarrow(\mathbf{k}) \frac{k_y - ik_x}{k} \end{pmatrix} \quad (1.44)$$

$$(1.45)$$

$$u_-(\mathbf{k}) = \begin{pmatrix} B_\uparrow(\mathbf{k}) \frac{k_y + ik_x}{k} \\ B_\downarrow(\mathbf{k}) \end{pmatrix} \quad (1.46)$$

One can find $A_\sigma = A_\sigma^*$ and $B_\sigma = B_\sigma^*$ and the coefficients are

$$A_\uparrow(\mathbf{k}) = \frac{-\alpha k}{\sqrt{2\epsilon'_+(\mathbf{k})}} \sqrt{\frac{1}{\epsilon'_+(\mathbf{k}) - V_z}} \quad (1.47)$$

$$A_\downarrow(\mathbf{k}) = \sqrt{\frac{\epsilon'_+(\mathbf{k}) - V_z}{2\epsilon'_+(\mathbf{k})}} \quad (1.48)$$

$$B_\uparrow(\mathbf{k}) = \sqrt{\frac{\epsilon'_-(\mathbf{k}) + V_z}{2\epsilon'_-(\mathbf{k})}} \quad (1.49)$$

$$B_\downarrow(\mathbf{k}) = \frac{\alpha k}{\sqrt{2\epsilon'_-(\mathbf{k})}} \sqrt{\frac{1}{\epsilon'_-(\mathbf{k}) + V_z}} \quad (1.50)$$

The expressions for $A_{\uparrow,\downarrow}$ and $B_{\uparrow,\downarrow}$ can be written in convenient terms as

$$f_p(\mathbf{k}) = A_\uparrow(\mathbf{k}) A_\downarrow(-\mathbf{k}) = B_\uparrow(-\mathbf{k}) B_\downarrow(\mathbf{k}) \quad (1.51)$$

$$= \frac{-\alpha k}{2\epsilon'_+(\mathbf{k})} \quad (1.52)$$

When putting the semiconductor in contact with an s -wave superconductor a pairing term is generated by the proximity effect. The full Hamiltonian becomes $\mathcal{H} = \mathcal{H}_0 + \mathcal{H}_Z + \mathcal{H}_{SC}$ with

$$\mathcal{H}_{SC} = \sum_{\mathbf{k}} \Delta c_{\uparrow, \mathbf{k}}^{\dagger} c_{\downarrow, -\mathbf{k}}^{\dagger} + H.c. \quad (1.53)$$

We now want to write the pairing potential in terms of c_{\pm} using a basis transformation.

$$c_{\uparrow, \mathbf{k}} = \langle \uparrow | u_+(\mathbf{k}) \rangle c_{\mathbf{k}, +} + \langle \uparrow | u_-(\mathbf{k}) \rangle c_{\mathbf{k}, -} \quad (1.54)$$

$$= A_{\uparrow}(\mathbf{k}) c_{\mathbf{k}, +} + B_{\uparrow}(\mathbf{k}) \frac{k_y + i k_x}{k} c_{\mathbf{k}, -} \quad (1.55)$$

$$c_{\downarrow, -\mathbf{k}} = \langle \downarrow | u_+(-\mathbf{k}) \rangle c_{-\mathbf{k}, +} + \langle \downarrow | u_-(-\mathbf{k}) \rangle c_{-\mathbf{k}, -} \quad (1.56)$$

$$= A_{\downarrow}(-\mathbf{k}) \frac{k_y - i k_x}{k} c_{-\mathbf{k}, +} + B_{\downarrow}(-\mathbf{k}) c_{-\mathbf{k}, -} \quad (1.57)$$

with the adjoints being

$$c_{\uparrow, \mathbf{k}}^{\dagger} = A_{\uparrow}(\mathbf{k}) c_{\mathbf{k}, +}^{\dagger} + B_{\uparrow}(\mathbf{k}) \frac{k_y - i k_x}{k} c_{\mathbf{k}, -}^{\dagger} \quad (1.58)$$

$$c_{\downarrow, -\mathbf{k}}^{\dagger} = A_{\downarrow}(-\mathbf{k}) \frac{k_y + i k_x}{k} c_{-\mathbf{k}, +}^{\dagger} + B_{\downarrow}(-\mathbf{k}) c_{-\mathbf{k}, -}^{\dagger} \quad (1.59)$$

Continue reducing the pairing potential which becomes

$$\begin{aligned} \Delta c_{\uparrow, \mathbf{k}}^{\dagger} c_{\downarrow, -\mathbf{k}}^{\dagger} &= \Delta [A_{\uparrow}(\mathbf{k}) A_{\downarrow}(-\mathbf{k}) \frac{k_y + i k_y}{k} c_{\mathbf{k}, +}^{\dagger} c_{-\mathbf{k}, +}^{\dagger} + B_{\uparrow}(\mathbf{k}) B_{\downarrow}(-\mathbf{k}) \frac{k_y - i k_y}{k} c_{\mathbf{k}, -}^{\dagger} c_{-\mathbf{k}, -}^{\dagger} \\ &\quad + (A_{\uparrow}(\mathbf{k}) B_{\downarrow}(-\mathbf{k}) + B_{\uparrow}(\mathbf{k}) A_{\downarrow}(-\mathbf{k})) c_{\mathbf{k}, +}^{\dagger} c_{-\mathbf{k}, -}^{\dagger}] \end{aligned} \quad (1.60)$$

We will use a more convenient notation by making the following substitutions

$$\Delta_{++}(\mathbf{k}) = \Delta f_p(\mathbf{k}) \frac{k_y + i k_x}{k} \quad (1.61)$$

$$\Delta_{--}(\mathbf{k}) = \Delta f_p(-\mathbf{k}) \frac{k_y - i k_x}{k} \quad (1.62)$$

$$\Delta_{+-}(\mathbf{k}) = \Delta f_s(\mathbf{k}) \quad (1.63)$$

Where

$$f_s(\mathbf{k}) = (A_\uparrow(\mathbf{k})B_\downarrow(-\mathbf{k}) + B_\uparrow(\mathbf{k})A_\downarrow(-\mathbf{k})) \quad (1.64)$$

The pairing potential Hamiltonian then becomes

$$\mathcal{H}_{SC} = \sum_{\mathbf{k}} \Delta_{++} c_{\mathbf{k},+}^\dagger c_{-\mathbf{k},+}^\dagger + \Delta_{--} c_{\mathbf{k},-}^\dagger c_{-\mathbf{k},-}^\dagger + \Delta_{+-} c_{\mathbf{k},+}^\dagger c_{-\mathbf{k},-}^\dagger + h.c. \quad (1.65)$$

Writing the full Hamiltonian in matrix form we will use the following Nambu spinor

$$\Psi = (c_{\mathbf{k},+}, c_{\mathbf{k},-}, c_{-\mathbf{k},+}^\dagger, c_{-\mathbf{k},-}^\dagger)^T \quad (1.66)$$

Then we write the Hamiltonian as, where we have used the conventional BdG approach of applying the anticommutation relation and reindexing the momentum vector of the second term to give

$$\mathcal{H} = \frac{1}{2} \sum_{\mathbf{k}} \Psi^\dagger H_{BdG} \Psi \quad (1.67)$$

with

$$H_{BdG} = \begin{bmatrix} \epsilon_+(\mathbf{k}) & 0 & 2\Delta_{++}(\mathbf{k}) & \Delta_{+-}(\mathbf{k}) \\ 0 & \epsilon_-(\mathbf{k}) & -\Delta_{+-}(-\mathbf{k}) & 2\Delta_{--}(\mathbf{k}) \\ 2\Delta_{++}^*(\mathbf{k}) & -\Delta_{+-}^*(-\mathbf{k}) & -\epsilon_+(-\mathbf{k}) & 0 \\ \Delta_{+-}^*(\mathbf{k}) & 2\Delta_{--}^*(\mathbf{k}) & 0 & -\epsilon_-(-\mathbf{k}) \end{bmatrix} \quad (1.68)$$

where

$$\epsilon_{\pm}(\mathbf{k}) = \frac{k^2}{2m} - \mu + \epsilon'_{\pm}(\mathbf{k}) \quad (1.69)$$

We can rearrange our matrix into a more block diagonal form with off terms to give

$$H_{BdG} = \begin{bmatrix} \epsilon_+(\mathbf{k}) & 2\Delta_{++} & 0 & \Delta_{+-}(\mathbf{k}) \\ 2\Delta_{++}^* & -\epsilon_+(-\mathbf{k}) & -\Delta_{+-}^*(-\mathbf{k}) & 0 \\ 0 & -\Delta_{+-}(-\mathbf{k}) & \epsilon_-(\mathbf{k}) & 2\Delta_{--} \\ \Delta_{+-}^*(\mathbf{k}) & 0 & 2\Delta_{--}^* & -\epsilon_-(-\mathbf{k}) \end{bmatrix} \quad (1.70)$$

Upon studying $V_z \gg \alpha$ we see that near the fermi surface the interband pairing has little affect on the band gap. Scaling it's effect from $0 \rightarrow 1$ we see the intraband gap appears at a slightly smaller momentum as the interband pairing is turned off. We thus use the approximation $\Delta_{+-}(k_f) \approx 0$. We also set μ such that it only crosses the lower bands, thus allowing $c_+^{\dagger} \rightarrow 0$.

$$H_{BdG} = \begin{bmatrix} \epsilon_-(\mathbf{k}) & 2\Delta_{--}(\mathbf{k}) \\ 2\Delta_{--}^*(\mathbf{k}) & -\epsilon_-(-\mathbf{k}) \end{bmatrix} \quad (1.71)$$

Solving for the dispersion relation of the system we arrive at

$$E_{\pm}(\mathbf{k}) = \pm \sqrt{(\epsilon_-(\mathbf{k}))^2 + 4|\Delta_{--}(\mathbf{k})|^2}, \quad (1.72)$$

an effective p -wave superconductor with opening and closing band gaps.

1.7 Landau levels in condensed matter

We are also interested in producing Landau levels in 2DEG and Dirac models using non-uniform circularly polarized laser light. To understand how Landau levels appear we need to solve the Hamiltonian associated with a 2DEG in the presence of a Magnetic field. We can start with the square lattice tight-binding Hamiltonian for a 2DEG

$$\mathcal{H} = - \sum_{\langle j,l \rangle} t c_j^\dagger c_l + h.c., \quad (1.73)$$

and in momentum space

$$\mathcal{H} = - \sum_{\mathbf{p}} 2t \left(\cos(p_x a) + \cos(p_y a) \right) c_{\mathbf{p}}^\dagger c_{\mathbf{p}}. \quad (1.74)$$

Then in the limit of small momenta k we arrive at

$$\begin{aligned} \mathcal{H} &= - \sum_{\mathbf{p}} 2t \left(2 - \frac{p_x^2 a^2}{2} - \frac{p_y^2 a^2}{2} \right) c_{\mathbf{p}}^\dagger c_{\mathbf{p}}, \\ \mathcal{H}(\mathbf{p}) &= \left(\frac{p_x^2 + p_y^2}{2m} \right), \end{aligned} \quad (1.75)$$

we have thus arrived at Schrodingers equation for a 2DEG in the limit of small momenta. Let us assume a 2DEG in the x - y plane and has a magnetic field that points in the positive \mathbf{z} direction, $\mathbf{B} = B\mathbf{z}$ or $\mathbf{A} = Bxy$. The Hamiltonian in momentum space then becomes

$$\mathcal{H} = \frac{1}{2m} (\hat{p}_x^2 + (\hat{p}_y - qB\hat{x})^2) \quad (1.76)$$

Recall $[\hat{r}_\alpha, \hat{p}_\beta] = i\hbar\delta_{\alpha,\beta}$, that means our magnetic term commutes with \hat{p}_y , so let us assume that $\Psi(x, y) = e^{ik_y y} \psi(x)$. Acting the Hamiltonian on the ansatz wavefunction yields

$$\begin{aligned}
\mathcal{H}\Psi &= \frac{1}{2m} (\hat{p}_x^2 + (qB\hat{x} - \hbar k_y)^2) e^{ik_y y} \psi(x) \\
\mathcal{H} &= \frac{1}{2m} (\hat{p}_x^2 + q^2 B^2 \hat{x}^2) \\
&= \frac{\hat{p}_x^2}{2m} + \frac{1}{2} m \omega^2 \hat{x}^2,
\end{aligned} \tag{1.77}$$

where we let $x - \frac{\hbar k_y}{mqB} \rightarrow x$, since it is just a shift in x coordinates. Notice that we arrive at the expression for a quantum harmonic oscillator. A derivation for the energy solutions can be found in [B.1](#). With the energy solutions

$$E_n = \hbar \omega \left(n + \frac{1}{2} \right) = \frac{\hbar q B}{m} \left(n + \frac{1}{2} \right). \tag{1.78}$$

An alteration to the lattice model can have slightly different results. Using a honeycomb lattice, provided by graphene, gives the following Hamiltonian

$$\mathcal{H} = -t \sum_{\substack{j,l \\ \alpha\beta}} c_{j\alpha}^\dagger c_{l\beta} + h.c., \tag{1.79}$$

with lattice vectors $\mathbf{a}_1 = \sqrt{3}a\mathbf{x}$ and $\mathbf{a}_2 = \frac{\sqrt{3}}{2}a\mathbf{x} + \frac{3}{2}a\mathbf{y}$. In momentum space

$$\begin{aligned}
\mathcal{H} &= -t \sum_{\mathbf{p}} \begin{bmatrix} 0 & 1 + e^{i\mathbf{p} \cdot \mathbf{a}_1} + e^{i\mathbf{p} \cdot \mathbf{a}_2} \\ 1 + e^{-i\mathbf{p} \cdot \mathbf{a}_1} + e^{-i\mathbf{p} \cdot \mathbf{a}_2} & 0 \end{bmatrix}, \\
\mathcal{H}(\mathbf{p}) &= \begin{bmatrix} 0 & t(\mathbf{p}) \\ t^*(\mathbf{p}) & 0 \end{bmatrix},
\end{aligned}$$

where the hopping can be rewritten as

$$t(\mathbf{p}) = -te^{i\sqrt{3}p_x a/2} \left(2 \cos \left(\frac{\sqrt{3}p_x a}{2} \right) + e^{i3p_y a/2} \right) \tag{1.80}$$

which gives the following energy spectrum

$$E(\mathbf{p}) = \pm t \sqrt{3 + 2 \cos(\sqrt{3} p_x a) + 4 \cos\left(\frac{\sqrt{3} p_x a}{2}\right) \cos\left(\frac{3 p_y a}{2}\right)}. \quad (1.81)$$

There are several high symmetry points on the corners of the Brillouin zone, one such point is $\mathbf{K} = \frac{4\pi}{3\sqrt{3}a} \mathbf{x}$. Going back to the Hamiltonian and expanding about \mathbf{K} with small \mathbf{q} , $\mathbf{q} = \mathbf{p} + \mathbf{K}$, gives the following hopping amplitude

$$\begin{aligned} t(\mathbf{q}) &= -t e^{i\sqrt{3}q_x a/2} e^{i\sqrt{3}K a/2} \left(2 \cos\left(\frac{\sqrt{3}q_x a}{2} + \frac{\sqrt{3}K a}{2}\right) + e^{i3p_y a/2} \right) \\ t(\mathbf{q}) &= -t e^{i\sqrt{3}q_x a/2} e^{i2\pi/3} \left(2 \cos\left(\frac{\sqrt{3}q_x a}{2} + \frac{2\pi}{3}\right) + e^{i3p_y a/2} \right) \\ t(\mathbf{q}) &= -t e^{i\sqrt{3}q_x a/2} e^{i2\pi/3} \left(-\cos\left(\frac{\sqrt{3}q_x a}{2}\right) - \sqrt{3} \sin\left(\frac{\sqrt{3}q_x a}{3}\right) + e^{i3p_y a/2} \right) \\ t(\mathbf{q}) &\approx t e^{i2\pi/3} \left(\frac{3q_x a}{2} - \frac{i3q_y a}{2} \right) \\ t(\mathbf{q}) &= v_f e^{i2\pi/3} (q_x - i q_y), \\ t^*(\mathbf{q}) &= v_f e^{-i2\pi/3} (q_x + i q_y), \end{aligned}$$

where we keep the leading order in \mathbf{q} and $v_f = \frac{3ta}{2}$. Using a gauge transformation and redefining $\mathbf{q} \rightarrow \mathbf{p}$ we arrive at the Dirac equation

$$\mathcal{H}(\mathbf{p}) = v_f \boldsymbol{\sigma} \cdot \mathbf{p}. \quad (1.82)$$

With graphene spanning the x - y plane in the presence of a magnetic field $\mathbf{B} = B\mathbf{z}$, $\mathbf{A} = Bx\mathbf{y}$, the Dirac equation becomes

$$\mathcal{H}(\mathbf{p}) = v_f \boldsymbol{\sigma} \cdot (\mathbf{p} - \mathbf{q}\mathbf{A}). \quad (1.83)$$

A derivation for the energy solution can be found in [B.2](#). The quantized energy solutions for a 2D Dirac equation in the presence of perpendicular magnetic field is

$$E_n = v_f \sqrt{2\hbar q B n} \quad (1.84)$$

Landau Level and Hofstadter butterfly

- i solve for LL in 2DEG — why it's topological, chern number, TKNN quantum Hall
- ii square lattice — hofstadter butterfly (on other lattices, honeycomb)

Chapter 2

Superconducting Triangular Islands as a Platform for Manipulating Majorana Zero Modes

2.1 Introduction

For more than twenty years, Majorana zero modes (MZM) in condensed matter systems have been highly sought after due to their potential for serving as building blocks of topological quantum computation, thanks to their inherent robustness against decoherence and non-Abelian exchange statistics [7, 9, 11–13]. MZM were originally proposed to be found in half-quantum vortices of two-dimensional (2D) topological p -wave superconductors and at the ends of 1D spinless p -wave superconductors [8, 14]. Whether a pristine p -wave superconductor [15] has been found is still under debate. However, innovative heterostructures proximate to ordinary s -wave superconductors have been proposed to behave as effective topological superconductors in both 1D and 2D. These include, for example, semiconductor nanowires subject to magnetic fields [16–18], ferromagnetic atomic spin chains [19–24], 3D topological insulators [25–28], quantum anomalous Hall insulators [29–31], quasi-2D spin-orbit-coupled superconductors with a perpendicular Zeeman field [10, 32–36], and planar Josephson junctions [37–43], etc. It has been a challenging task to decisively confirm the existence of MZM in the various experimental systems due to other competing mechanisms that can potentially result in similar features as MZM do in different probes [40, 41, 44–49]. Other proposals for constructing Kitaev chains through a bottom-up approach, based on, e.g. magnetic tunnel junctions proximate to spin-orbit-coupled superconductors [50], and quantum dots coupled through superconducting links [51–53] are therefore promising. In particular, the recent experiment [53] of a designer minimal Kitaev chain based on two quantum dots coupled through

tunable crossed Andreev reflections (CAR) offers a compelling route towards MZM platforms based on exactly solvable building blocks.

In parallel with the above efforts of realizing MZM in different materials systems, scalable architectures for quantum logic circuits based on MZM have also been intensely studied over the past decades. A major proposal among these studies is to build networks of T-junctions, which are minimal units for swapping a pair of MZM hosted at different ends of a junction, that allow braiding-based TQC [13]. Alternatively, networks based on coupled wires forming the so-called tetrons and hexons, aiming at measurement-based logic gate operations [54], have also been extensively investigated. To counter the technical challenges of engineering networks with physical wires or atomic chains, various ideas based on effective Kitaev chains, such as quasi-1D systems in thin films [55], cross Josephson junctions [43], scissor cuts on a quantum anomalous Hall insulator [31], and rings of magnetic atoms [56], etc. have been proposed. However, due to the same difficulty of obtaining or identifying genuine MZM in quasi-1D systems mentioned above, it remains unclear how practical these strategies are in the near future.

In this Letter, we propose an alternative structural unit for manipulating MZM, triangular superconducting islands, motivated by the above challenges associated with wire geometries and by the fact that triangular islands routinely appear spontaneously in epitaxial growth [57] on close-packed atomic surfaces. We first show that a minimal “Kitaev triangle” consisting of three sites hosts MZM at different pairs of vertices controlled by Peierls phases on the three edges [Fig. 2.1 (a)], which can be readily realized using quantum dots. To generalize the minimal model to triangular structures involving more degrees of freedom, we study the topological phase transitions of quasi-1D ribbons driven by Peierls phases, which can be created by magnetic fields or supercurrents [58, 59], and use the resulting phase diagram as a guide to construct finite-size triangles with a hollow interior that host MZM [Fig. 2.1 (b)]. In the end we discuss possible experimental systems that can realize our proposals and scaled-up networks of triangles for implementing braiding operations of MZM.

2.2 Kitaev Triangle

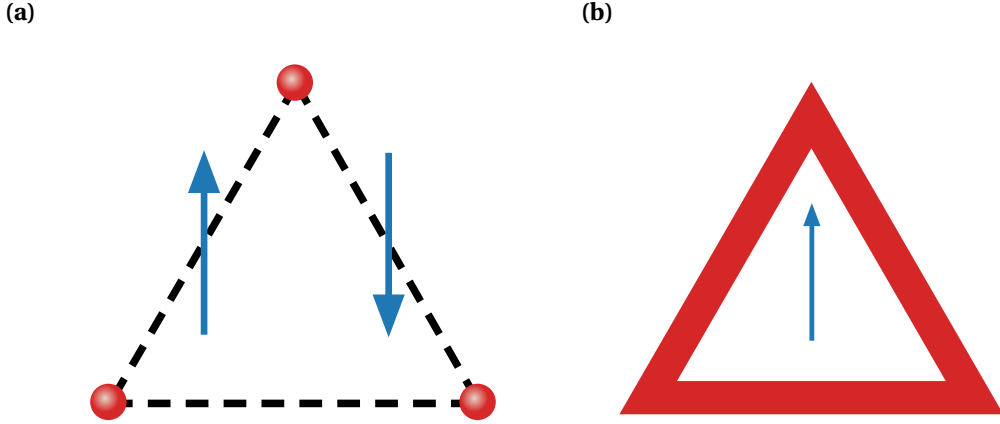


Figure 2.1: Schematics of two triangle structures proposed in this work. (a) Three-site Kitaev triangle with bond-dependent Peierls phases. (b) Hollow triangular island with a uniform vector potential.

In this section we present an exactly solvable minimal model with three sites forming a “Kitaev triangle” that can host MZM at different pairs of vertices controlled by Peierls phases on the edges. The Bogoliubov-de Gennes (BdG) Hamiltonian includes complex hopping and p -wave pairing between three spinless fermions forming an equilateral triangle [Fig. 2.1 (a)]:

$$\mathcal{H} = \sum_{\langle jl \rangle} (-te^{i\phi_{jl}} c_j^\dagger c_l + \Delta e^{i\theta_{jl}} c_j c_l + \text{h.c.}) - \sum_j \mu c_j^\dagger c_j, \quad (2.1)$$

where t is the hopping amplitude, Δ is the amplitude of the (2D) p -wave pairing, μ is the chemical potential, θ_{jl} is the polar angle of $\mathbf{r}_{jl} = \mathbf{r}_l - \mathbf{r}_j$ (the x axis is chosen to be along \mathbf{r}_{12}), consistent with $\{c_l^\dagger, c_j^\dagger\} = 0$. ϕ_{jl} is the Peierls phase due to a bond-dependent vector potential \mathbf{A} to be specified below (the nearest neighbor distance a is chosen to be the length unit hereinbelow):

$$\phi_{jl} = \frac{e}{\hbar} \int_{\mathbf{r}_j}^{\mathbf{r}_l} \mathbf{A} \cdot d\mathbf{l} = -\phi_{lj} \quad (2.2)$$

where $e > 0$ is the absolute value of the electron charge. Below we use the natural units $e = \hbar = 1$. To get the conditions for having MZM in this model we rewrite \mathcal{H} in the Majorana fermion basis $a_j = c_j + c_j^\dagger$, $b_j = \frac{1}{i}(c_j - c_j^\dagger)$:

$$\begin{aligned} \mathcal{H} = & -\frac{i}{2} \sum_{\langle jl \rangle} \left[(t \sin \phi_{jl} - \Delta \sin \theta_{jl}) a_j a_l \right. \\ & + (t \sin \phi_{jl} + \Delta \sin \theta_{jl}) b_j b_l \\ & + (t \cos \phi_{jl} - \Delta \cos \theta_{jl}) a_j b_l \\ & \left. - (t \cos \phi_{jl} + \Delta \cos \theta_{jl}) b_j a_l \right] - \frac{i\mu}{2} \sum_j a_j b_j \end{aligned} \quad (2.3)$$

For concreteness we consider the Kitaev limit $t = \Delta$, $\mu = 0$, and choose $\phi_{12} = 0$ so that sites 1 and 2 alone form a minimal Kitaev chain with $\mathcal{H}_{12} = i t b_1 a_2$ and hosting MZM a_1 and b_2 . In order for the MZM to persist in the presence of site 3, one can choose ϕ_{23} and ϕ_{31} so that all terms involving these Majorana operators cancel out. For example, consider the 2–3 bond, for which $\theta_{23} = 2\pi/3$, we require

$$\sin \phi_{23} + \sin \frac{2\pi}{3} = \cos \phi_{23} + \cos \frac{2\pi}{3} = 0 \quad (2.4)$$

which means $\phi_{23} = -\pi/3$. Similarly one can find $\phi_{31} = -\phi_{13} = -\pi/3$. The three Peierls phases can be realized by the following staggered vector potential

$$\mathbf{A} = [1 - 2\Theta(x)] \frac{2\pi}{3\sqrt{3}} \mathbf{y} \quad (2.5)$$

where $\Theta(x)$ is the Heaviside step function. In fact, using a uniform $\mathbf{A} = \frac{2\pi}{3\sqrt{3}} \mathbf{y}$, which corresponds to $\phi_{23} = -\pi/3 = -\phi_{31}$ also works, since the existence of a_1 is unaffected by ϕ_{23} . However, in this case the counterpart of b_2 is not localized on a single site. For the same reason, the above condition for MZM localized at triangle corners can be generalized to Kitaev chains forming a triangular loop, as well as to finite-size triangles of 2D spinless p -wave superconductors in

the Kitaev limit, as the existence of a_1 and b_2 are only dictated by the vector potential near the corresponding corners. It should be noted that in the latter case, 1D Majorana edge states will arise when the triangle becomes larger, and effectively diminish the gap that protects the corner MZM. On the other hand, for the longer Kitaev chain, due to the potential practical difficulty of controlling further-neighbor hopping and pairing amplitudes, it is better to resort to the approach of controlling the individual topological phases of the three edges which will be detailed in the next section.

We next show that the minimal Kitaev triangle suffices to demonstrate braiding of MZM. To this end we consider a closed parameter path linearly interpolating between the following sets of values of ϕ_{jl} :

$$\begin{aligned}
(\phi_{12}, \phi_{23}, \phi_{31}) &= \left(0, -\frac{\pi}{3}, -\frac{\pi}{3}\right) \equiv \boldsymbol{\phi}_1 \\
&\rightarrow \left(-\frac{\pi}{3}, -\frac{\pi}{3}, 0\right) \equiv \boldsymbol{\phi}_2 \\
&\rightarrow \left(-\frac{\pi}{3}, 0, -\frac{\pi}{3}\right) \equiv \boldsymbol{\phi}_3 \\
&\rightarrow \boldsymbol{\phi}_1
\end{aligned} \tag{2.6}$$

It is straightforward to show that at $\boldsymbol{\phi}_2$ and $\boldsymbol{\phi}_3$ there are MZM located at sites 3, 1 and 2, 3, respectively. Therefore the two original MZM at sites 1, 2 should switch their positions at the end of the adiabatic evolution.

Indeed, Fig. 2.2 shows that the MZM stays at zero energy throughout the parameter path that interchanges their positions. To show that such an operation indeed realizes braiding, we explicitly calculated the many-body Berry phase of the evolution [9, 56, 60] and found the two degenerate many-body ground states acquire a $\frac{\pi}{2}$ difference in their Berry phases as expected [9]. Compared to the minimum T-junction model with four sites [9], our Kitaev triangle model only requires three sites to achieve braiding between two MZM, and is potentially also easier

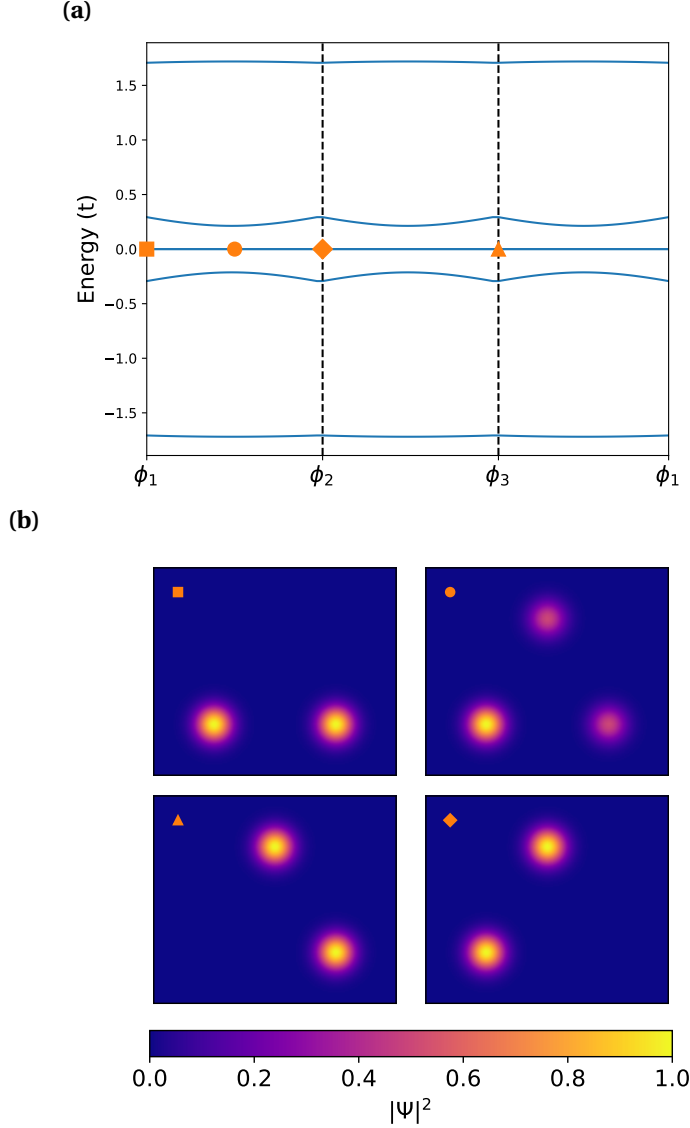


Figure 2.2: (a) Evolution of the eigenvalues of the 3-site Kitaev triangle along the closed parameter path for ϕ on the three edges. (b) MZM wavefunctions at different points of the parameter path. Clockwise from the upper left panel: $\phi_1 \rightarrow \frac{1}{2}(\phi_1 + \phi_2) \rightarrow \phi_2 \rightarrow \phi_3$.

to engineer experimentally. In the next section we will show that a more mesoscopic hollow-triangle structure can achieve similar results and may be preferred in other materials platforms.

2.3 Hollow Triangles

For systems with less fine-tuned Hamiltonians than the minimal model in the previous section, it is more instructive to search for MZM based on topological arguments. In this section

we show that MZM generally appear at the corners of a hollow triangle, which can be approximated by joining three finite-width chains or ribbons whose bulk topology is individually tuned by the same uniform vector potential.

To this end, we first show that topological phase transitions can be induced by a vector potential in a spinless p -wave superconductor ribbon. In comparison with similar previous proposals that mostly focused on vector potentials or supercurrents flowing along the chain [58,59], we consider in particular the tunability by varying the direction of the vector potential relative to the length direction of the ribbon, which will become instrumental in a triangular structure.

Consider Eq. (A.98) on a triangular lattice defined by unit-length lattice vectors $(\mathbf{a}_1, \mathbf{a}_2) = (\mathbf{x}, \frac{1}{2}\mathbf{x} + \frac{\sqrt{3}}{2}\mathbf{y})$ with W unit cells along \mathbf{a}_2 but infinite unit cells along \mathbf{a}_1 , and assume the Peierls phases are due to a uniform vector potential \mathbf{A} so that $\phi_{jl} = \mathbf{A} \cdot \mathbf{r}_{jl}$. We also introduce $\mathbf{a}_3 \equiv -\mathbf{a}_1 + \mathbf{a}_2$ for later convenience. The Hamiltonian is periodic along x and can be Fourier transformed through $c_{m,n}^\dagger = \frac{1}{\sqrt{N}} \sum_k c_{k,n}^\dagger e^{-ikm}$, where m, n label the lattice sites as $\mathbf{r}_{m,n} = m\mathbf{a}_1 + n\mathbf{a}_2$. The resulting momentum space Hamiltonian can be written as the following block form up to a constant

$$\begin{aligned} \mathcal{H} &= \frac{1}{2} \sum_k \Psi_k^\dagger \begin{pmatrix} h_t(k) & h_\Delta(k) \\ h_\Delta^\dagger(k) & -h_t^*(-k) \end{pmatrix} \Psi_k \\ &\equiv \frac{1}{2} \sum_k \Psi_k^\dagger H(k) \Psi_k \end{aligned} \quad (2.7)$$

where $\Psi_k \equiv (c_{k,1}, \dots, c_{k,W}, c_{-k,1}^\dagger, \dots, c_{-k,W}^\dagger)^T$. $h_t(k)$ is a $W \times W$ Hermitian tridiagonal matrix with $(h_t)_{n,n} = -2t \cos(k + \mathbf{A} \cdot \mathbf{a}_1) - \mu$ and $(h_t)_{n,n+1} = -t(e^{i(-k+\mathbf{A} \cdot \mathbf{a}_3)} + e^{i\mathbf{A} \cdot \mathbf{a}_2})$. $h_\Delta(k)$ is a $W \times W$ tridiagonal matrix with $(h_\Delta)_{n,n} = -2i\Delta \sin k$ and $(h_\Delta)_{n,n\pm 1} = \mp \Delta \left[e^{-i(\pm k + \frac{2\pi}{3})} + e^{-i\frac{\pi}{3}} \right]$.

By transforming Eq. (2.7) to the Majorana basis using the unitary transformation:

$$U \equiv \frac{1}{\sqrt{2}} \begin{pmatrix} 1 & 1 \\ -i & i \end{pmatrix} \otimes \mathbb{I} \quad (2.8)$$

where \mathbb{I} is a $W \times W$ identity matrix, and defining $A_k \equiv -iUH(k)U^\dagger$, not to be confused with the vector potential, one can calculate the Majorana number [8] \mathcal{M} of the 1D ribbon as [61]

$$\mathcal{M} = \text{sgn} [\text{Pf}(A_{k=0})\text{Pf}(A_{k=\pi})] \quad (2.9)$$

where Pf stands for the Pfaffian of a skew-symmetric matrix [8]. When $\mathcal{M} = -1$, the 1D system is in a nontrivial topological phase with MZM appearing at open ends of semi-infinite ribbons, and otherwise for $\mathcal{M} = 1$.

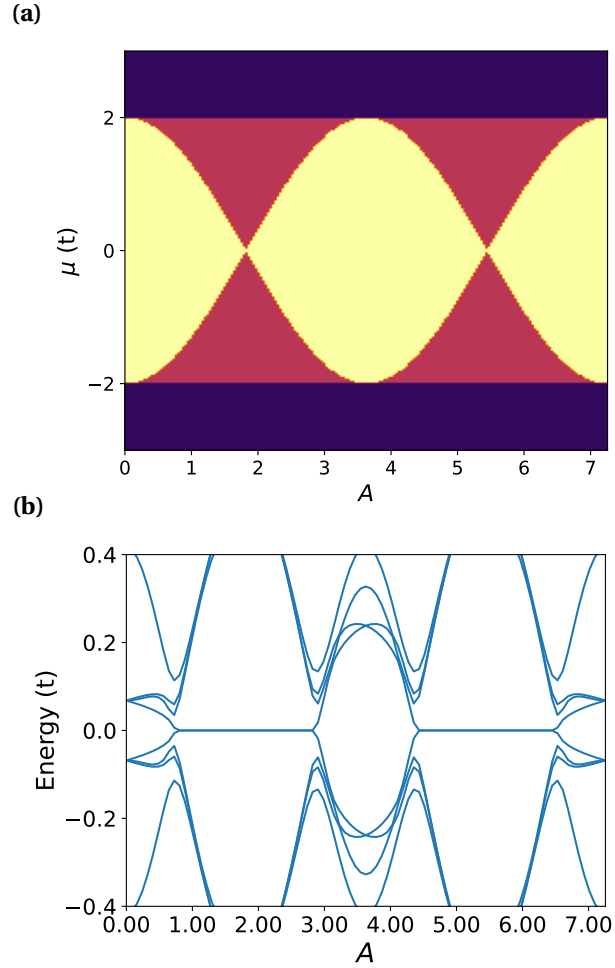


Figure 2.3: (a) Topological phase diagram for a $W = 1$ triangular chain with the Hamiltonian Eq. (2.7) obtained by superimposing the $\mathcal{M}(A, \mu)$ plots of 1D chains with $\mathbf{A} = A\mathbf{y}$ and $\mathbf{A} = A(\frac{\sqrt{3}}{2}\mathbf{x} + \frac{1}{2}\mathbf{y})$. Color scheme: white— $\mathcal{M} = 1$, dark blue— $\mathcal{M} = -1$, light blue— $\mathcal{M} = 0$ (b) Near-gap BdG eigen-energies vs A for a finite triangle with edge length $L = 50$, $W = 1$, and $\mu = 1.6$.

In Fig. 2.3 (a) we show the topological phase diagrams for a 1D ribbon with width $W = 1$, $\mathbf{A} = A\mathbf{y}$ and $\mathbf{A} = A(\frac{\sqrt{3}}{2}\mathbf{x} + \frac{1}{2}\mathbf{y})$ superimposed (see below). We found that the vector potential component normal to the ribbon length direction has no effect on the Majorana number, nor does the sign of its component along the ribbon length direction. However, topological phase transitions can be induced by varying the size of the vector potential component along the ribbon, consistent with previous results [58, 59]. These properties motivate us to consider the structure of a hollow triangle formed by three finite-width ribbons subject to a uniform vector potential $\mathbf{A} = A\mathbf{y}$ as illustrated in Fig. 2.1 (b). The light blue color on the phase diagram Fig. 2.3 (a) therefore means that the bottom edge and the two upper edges of the hollow triangle have different \mathcal{M} , which should give rise to MZM localized at the two bottom corners if the triangle is large enough so that bulk-edge correspondence holds, and gap closing does not occur at other places along its edges.

To show that corner MZM indeed appear when the conditions given by the phase diagram Fig. 2.3 (a) are met, we directly diagonalize the BdG Hamiltonian of a finite hollow triangle with edge length $L = 50$ and width $W = 1$. Fig. 2.3 (b) shows the spectral flow (BdG eigen-energies evolving with increasing vector potential A) close to zero energy at chemical potential $\mu = 1.6$. Indeed, zero-energy modes appear in the regions of μ and A consistent with the phase diagram (except when the bulk band gap is too small; see [60] for some examples.). Hollow triangles with larger W also have qualitatively similar behavior, although the phase diagrams are more complex [60]. The eigenfunctions for the zero-energy modes at $A = 2.75$ and $\mu = 1.6$ in Fig. 2.4 (b) also confirm their spatial localization at the bottom corners of the triangle.

We finally show that rotating the uniform vector potential in-plane can manipulate the positions of the MZM without hybridizing them with bulk states for certain ranges of μ and A . Fig. 2.4 (a) plots the spectral flow versus the in-plane azimuthal angle of \mathbf{A} , which clearly shows that the zero-energy modes persist throughout the rotation and the bulk gap never closes. Figs. 2.4 (b-d) plot the BdG wavefunctions of the MZM at special values of φ . One can see that the two MZM appear to cycle through the three vertices by following the rotation of \mathbf{A} . The robustness

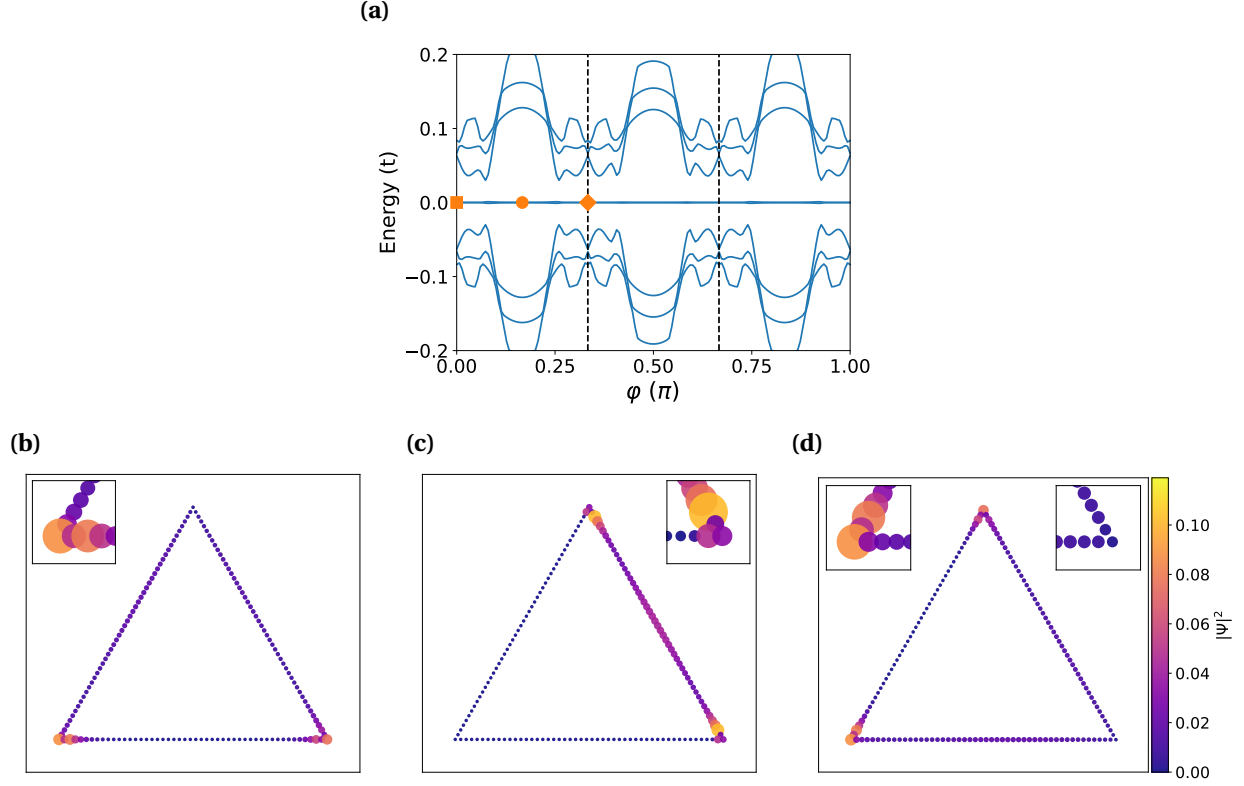


Figure 2.4: (a) Spectral flow of a hollow triangle with $W = 1$, $L = 50$, $\mu = 1.6$, and $A = 2.75$ with increasing rotation angle φ , defined through $\mathbf{A} = A(-\sin \varphi \mathbf{x} + \cos \varphi \mathbf{y})$. (b-d) BdG eigenfunction $|\Psi|^2$ summed over the two zero modes at $\varphi = 0, \frac{\pi}{6}$, and $\frac{\pi}{3}$, respectively.

of the MZM therefore requires the condition of two edges being in a different topological phase from the third one to be satisfied throughout the rotation. Such a criterion combined with the individual phase diagrams of the edges can help isolate the desired parameter regions of μ and A . We also note that the positions of the MZM do not interchange after φ increases from 0 to π , different from the situation of the minimal Kitaev triangle in Fig. 2.2. The reason is that the MZM in the latter case are not due to bulk-boundary correspondence [the values of $A = \frac{2\pi}{3\sqrt{3}}$ and $\mu = 0$ are a critical point in the phase diagram Fig. 2.3 (a)]. While the positions of the MZM at special points along the parameter path in the hollow triangle case have to be additionally constrained by the bulk topological phases of the three edges, that for the Kitaev triangle have more flexibility and are also protected by the finite size of the system.

A model that is closer to a realistic hollow triangular island is the finite-width triangular chain or ribbon. An example, illustrated in Figure 2.5 (c), has its edge length $L = 50$ and width

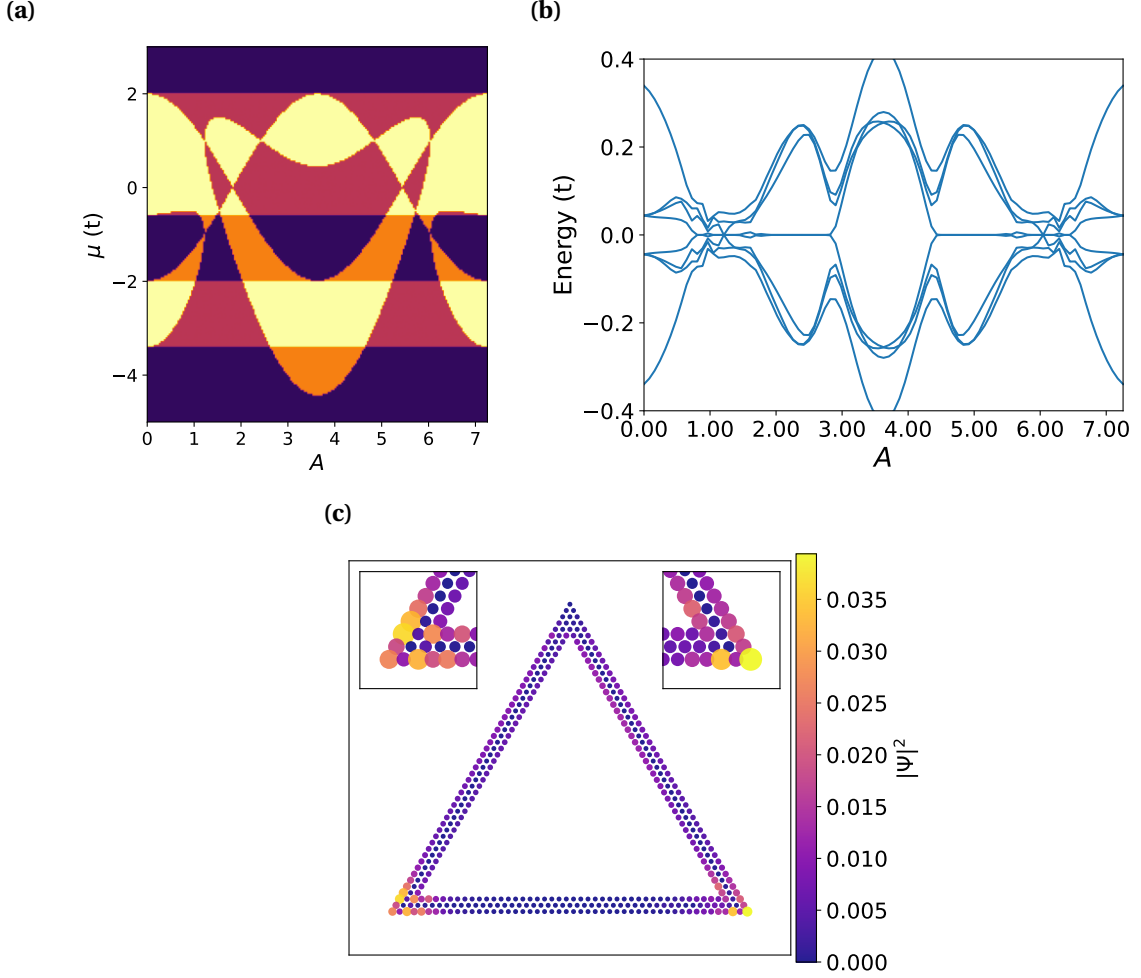


Figure 2.5: (a) Topological phase diagram for a $W = 3$ hollow triangle obtained by overlapping the $\mathcal{M}(A, \mu)$ plots of 1D chains with $\mathbf{A} = A\mathbf{y}$ and $\mathbf{A} = A(\frac{\sqrt{3}}{2}\mathbf{x} + \frac{1}{2}\mathbf{y})$. Color scheme: white— $\mathcal{M} = 1$, dark blue— $\mathcal{M} = -1$, light blue— $\mathcal{M} = 0$ (b) Near-gap BdG eigen-energies vs A for a finite triangle with edge length $L = 50$, $W = 3$, and $\mu = 1.6$. (c) BdG eigenfunction $|\Psi|^2$ summed over the two zero modes at $A = 2.4709$.

$W = 3$. The phase diagram Fig. 2.5 (a) is created in a similar way as that in Fig. 2.3 (a), assuming a constant vector potential and infinitely long $W = 3$ ribbons. The spectral flow for the actual triangle with $\mu = 1.6$ in Fig. 2.5 (b) shows MZM in the parameter regions in agreement with the phase diagram. Fig. 2.5 (c) plots the MZM wavefunction for $A = 2.7409$ and $\mu = 1.6$ that are indeed well localized at the bottom corners.

We next rotate the uniform vector potential to examine how the MZM move on a hollow triangle. Figure 2.6 shows the spectral flow and eigenfunctions as we rotate $\varphi = 0$ to $\varphi = \pi$ counterclockwisely. The two MZM cycle through the three vertices in a similar manner as that

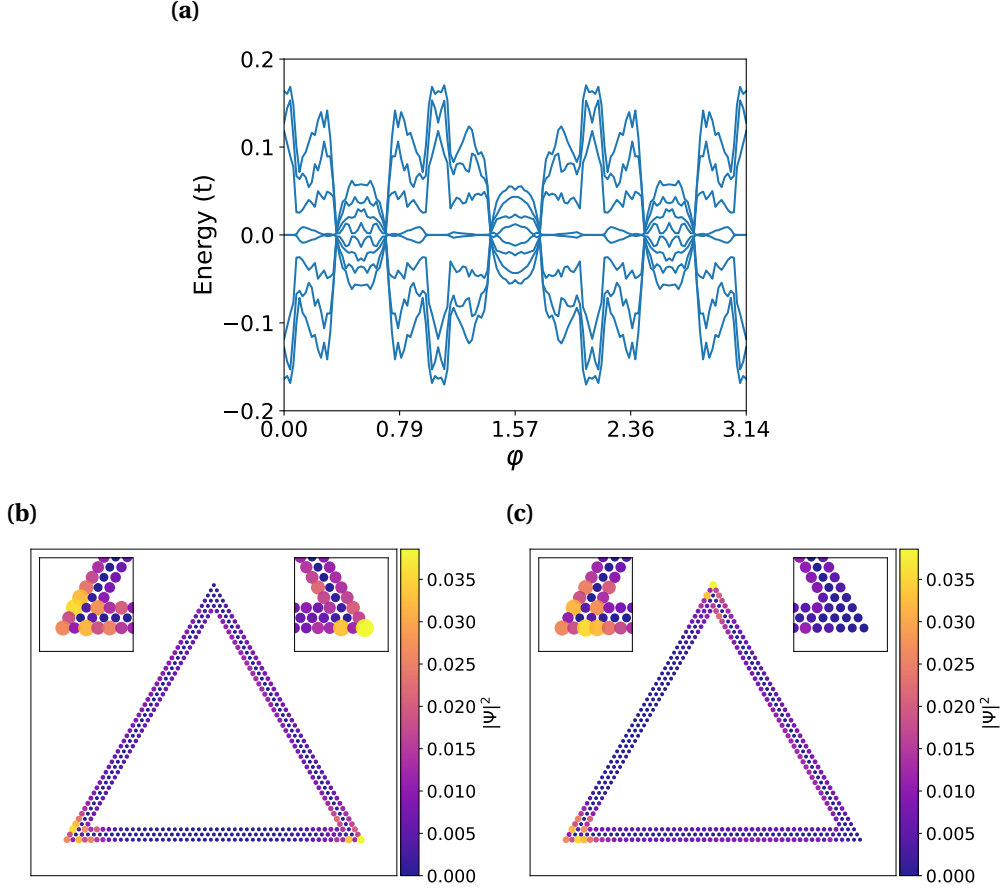


Figure 2.6: (a) Spectral flow of a hollow triangle with $W = 3$, $L = 50$, $\mu = 1.6$, and $A = 2.75$ with increasing rotation angle φ , defined through $\mathbf{A} = A(-\sin \varphi \mathbf{x} + \cos \varphi \mathbf{y})$. (b-c) BdG eigenfunction $|\Psi|^2$ summed over the two zero modes at $\varphi = 0$ and $\frac{\pi}{3}$, respectively.

in Fig. 4 of the main text (only the MZM wavefunctions at $\varphi = 0$ and $\frac{\pi}{3}$ are plotted as representatives of the $\varphi = n\pi/3$ cases). Note that the spectral flow has 3-fold rotation symmetry but not 6-fold, since increasing φ by $\frac{2\pi}{3}$ is equivalent to rotating the coordinate system clockwise by $\frac{2\pi}{3}$. In contrast, rotating the vector potential by $\frac{\pi}{3}$, if without an additional sign change of the p -wave pairing potential, is not an exact symmetry of the finite triangle. Also we did not try to scrutinize the phase diagram to find a parameter path in which the bulk gap does not close, as in the $W = 1$ case in the main text. Here we just point out that identifying a system-specific parameter path for adiabatic manipulation of MZM is in principle always possible, especially if one is allowed to have more knobs other than φ in real structures, such as tuning the chemical potential of individual edges or the size of the vector potential, etc.

2.4 Braiding MZM in a small network of triangles

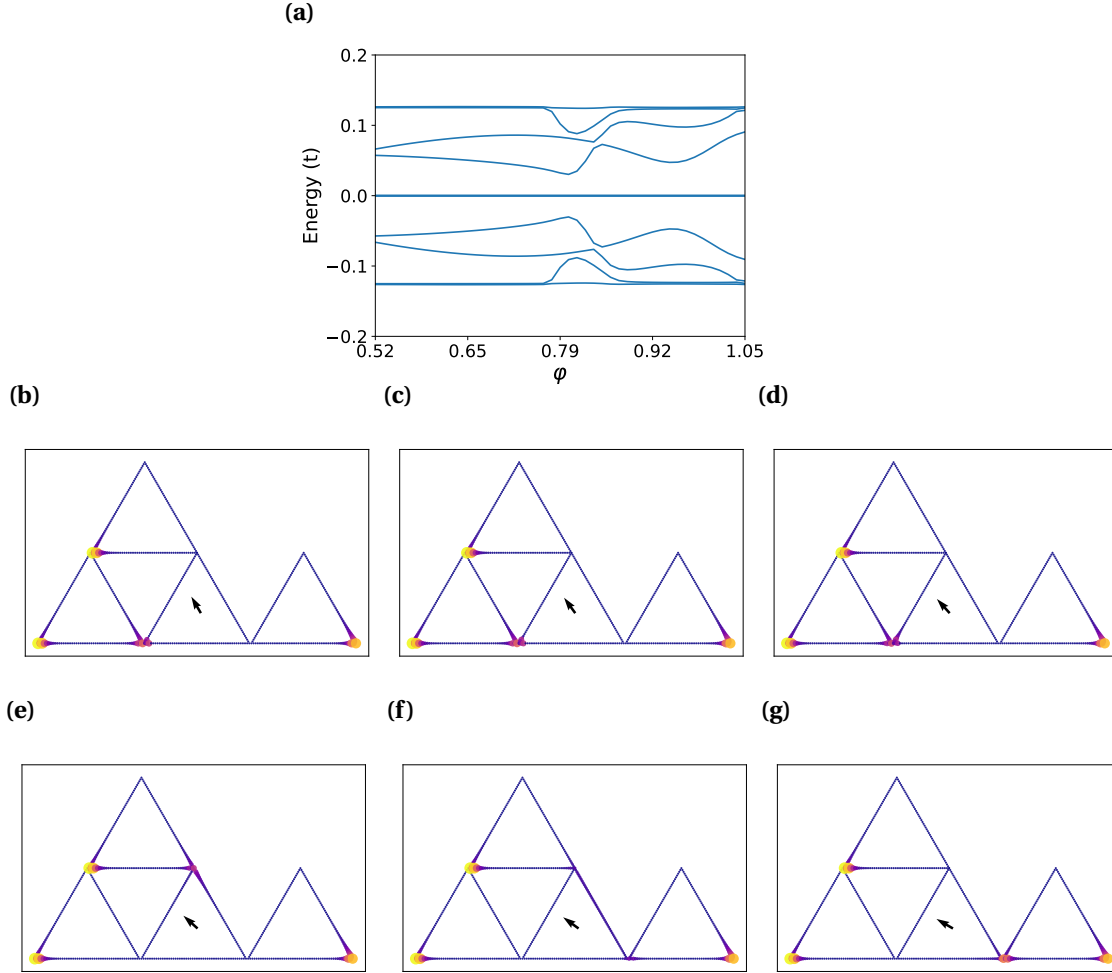


Figure 2.7: (a) Spectral flow for the critical step of swapping γ_2 and γ_3 in the example of Fig. 5 in the main text, calculated using four corner-sharing triangles of $W = 1$ and $L = 50$, with $\mu = 1.6$ and $A = 2.6$. Vector potential for the middle triangle in the bottom row can rotate according to $\mathbf{A} = A(-\sin \phi \mathbf{x} + \cos \phi \mathbf{y})$ from $\phi = \frac{\pi}{6}$ to $\frac{\pi}{3}$, while the other three have fixed $\phi = 0$. (b)-(g) BdG eigenfunction $|\Psi|^2$ summed over the four zero modes at equally-spaced points along the rotation path. The black arrow indicates the direction of the vector potential for the bottom middle triangle.

In this section we show that one can braid two out of four MZM, a minimal setting for non-trivial manipulation of the degenerate many-body ground states, by using a small network of corner-sharing triangles. We focus on the critical step of swapping γ_2 and γ_3 as labeled in Fig. 5 of the main text. This can be done by rotating the vector potential of the triangle in the middle of the bottom row from $\phi = \frac{\pi}{6}$ to $\frac{\pi}{3}$. More specifically, when $\phi = \frac{\pi}{6}$, with the chosen values of μ

and A , only the right edge of the said triangle is topologically nontrivial. The chain that hosts $\gamma_{3,4}$ thus extends through this nontrivial edge to the top triangle as in Fig. 2.7 (b). On the other hand, when φ increases to $\frac{\pi}{3}$, the nontrivial edge of the middle triangle changes from right to left, which leads to γ_2 hopping from its left corner to the right through the top corner, while γ_3 is unaffected [Figs. 2.7 (c-g)]. As a result the γ_2, γ_3 swapping is done without closing the bulk gap, as can be seen from the spectral flow in Fig. 2.7 (a).

2.5 Additional results using inhomogeneous vector fields

While we have showed a constant vector field works to induce and manipulate MZM for a triangular chain and hollow triangle it remains to be seen if inhomogeneous vector potential fields can reproduce the same results. We expect this to be the case due to the topological phase diagram seen in 2.3 (a) and 2.5 (a) and the results that followed for a constant vector potential.

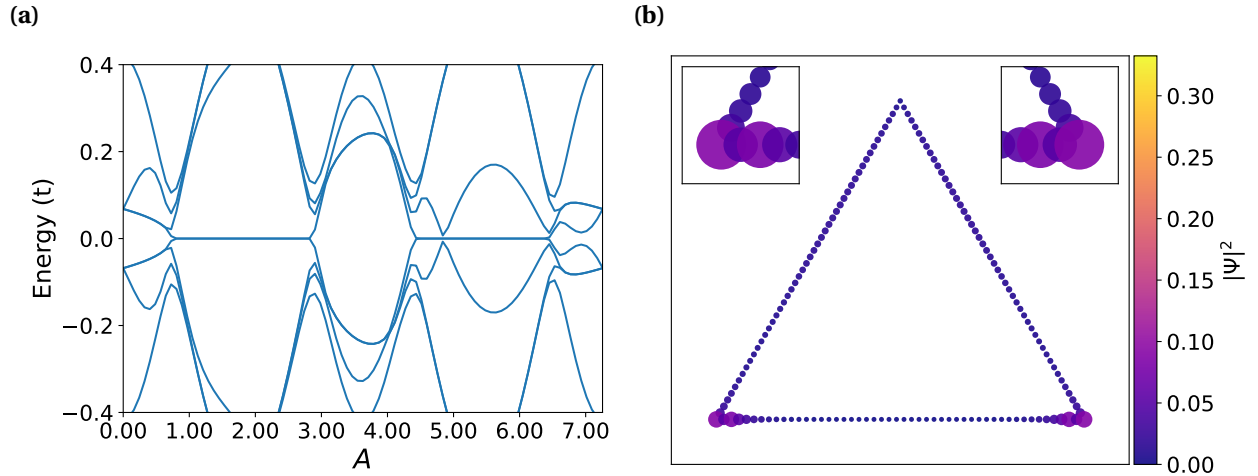


Figure 2.8: (a) Spectral flow of a hollow triangle with $W = 1$, $L = 50$, and $\mu = 1.6$ for increasing heaviside vector potential strength defined by $\mathbf{A} = A[1 - 2\Theta(x)]\mathbf{y}$ (b) BdG eigenfunction $|\Psi|^2$ summed over the two zero modes at $A = 2.7409$.

For hollow triangle of width, $W = 1$ subject to a heaviside vector potential we see a similar spectral flow and MZM in Fig. 2.8 to match 2.3. If the heaviside vector potential is not so easily made in lab it may be easier to model a tanh function instead. Also, in the limit that the tanh's

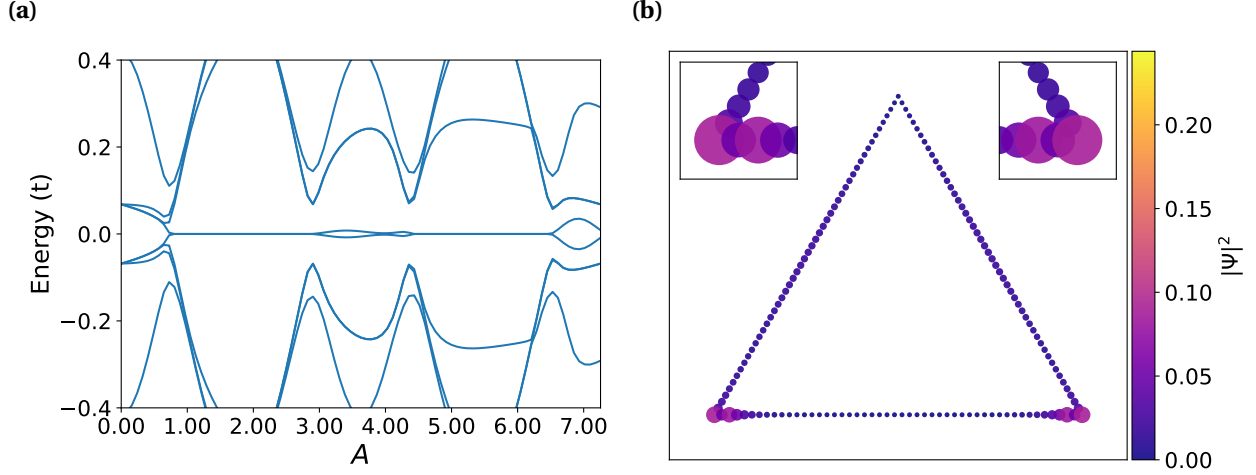


Figure 2.9: (a) Spectral flow of a hollow triangle with $W = 1$, $L = 50$, and $\mu = 1.6$ for increasing tanh vector potential strength defined by $\mathbf{A} = -A \tanh(x/2w)\mathbf{y}$, $w = a/2$ (b) BdG eigenfunction $|\Psi|^2$ summed over the two zero modes at $A = 2.7409$.

function width, w , goes to zero it is equivalent to the heaviside function. A tanh vector potential can match the same results as seen in Fig. 2.9. It should be mentioned that the width of the tanh function should be on the order or smaller than the distance between neighboring lattice points, if two neighboring sites overall phase accumulation is not large enough to match the topological phase diagram then the bulk edge correspondence at the tanh's inflection point would cause additional MZM to appear. In other words, the top edges of the triangle should be one long bent trivial edge but if the tanh's width is too large the two edges become separated by a small non-trivial topological corner-edge because the Peierls phase is too small. Increasing the width of the hollow triangle to $W = 3$, we see similar results for heaviside, Fig. 2.10, and tanh, Fig. 2.11, compared to a constant vector potential, Fig. 2.5.

We look at a linear vector potential next. A topological phase diagram for a linear vector potential is possible to compute, however, it requires a lattice space matrix instead of momentum space matrix due to having no periodic boundary conditions. It also requires separate calculations for longer triangular lattice ribbons. Computation times can become unruly when modeling large triangles for a high density phase diagram of A and μ values. We could, however, use the topological phase diagram in Fig. 2.3 to guess the topology for the varying Peierls phases

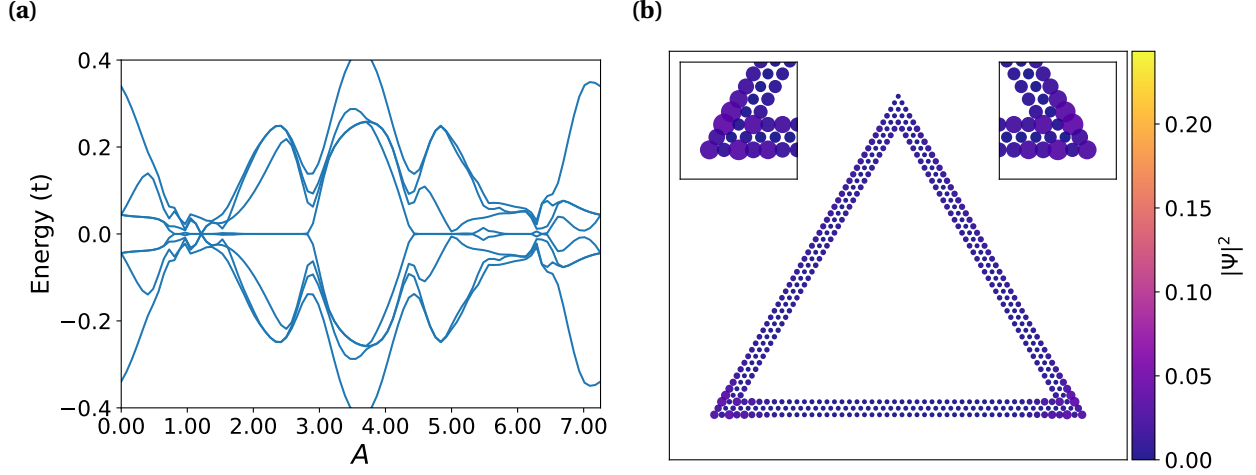


Figure 2.10: (a) Spectral flow of a hollow triangle with $W = 3$, $L = 50$, and $\mu = 1.6$ for increasing heaviside vector potential strength defined by $\mathbf{A} = A[1 - 2\Theta(x)]\mathbf{y}$ (b) BdG eigenfunction $|\Psi|^2$ summed over the two zero modes at $A = 2.7409$.

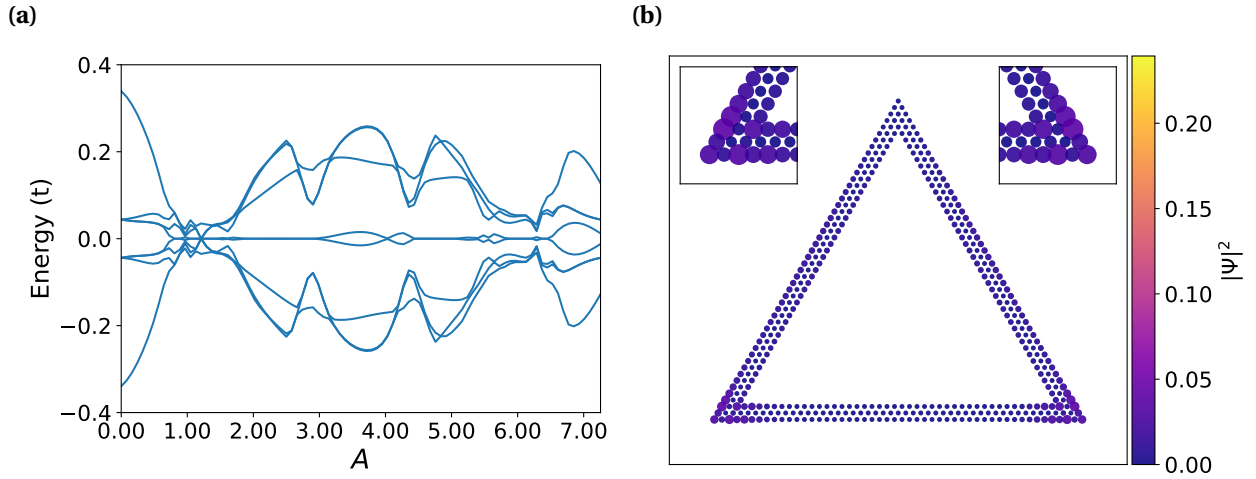


Figure 2.11: (a) Spectral flow of a hollow triangle with $W = 3$, $L = 50$, and $\mu = 1.6$ for increasing tanh vector potential strength defined by $\mathbf{A} = -A \tanh(x/2w)\mathbf{y}$, $w = a/2$ (b) BdG eigenfunction $|\Psi|^2$ summed over the two zero modes at $A = 2.7409$.

along an edge. Fig. 2.12 shows some critical points for MZMs to appear with $\mu = 0$ for a hollow triangle of $W = 1$ and $W = 3$, respectively. Fig. 2.13 shows apparent zero modes for a range of A values for a hollow triangle of $W = 1$ and $W = 3$, respectively. For similar reasons why the tanh function width needs to be small, it may be difficult to have the upper parts of the triangles top edges be all trivial topology, a small section may centered on the top corner may be non-trivial, thus hosting additional MZMs, as seen in Fig. 2.13 (c-d) half way up the triangles.

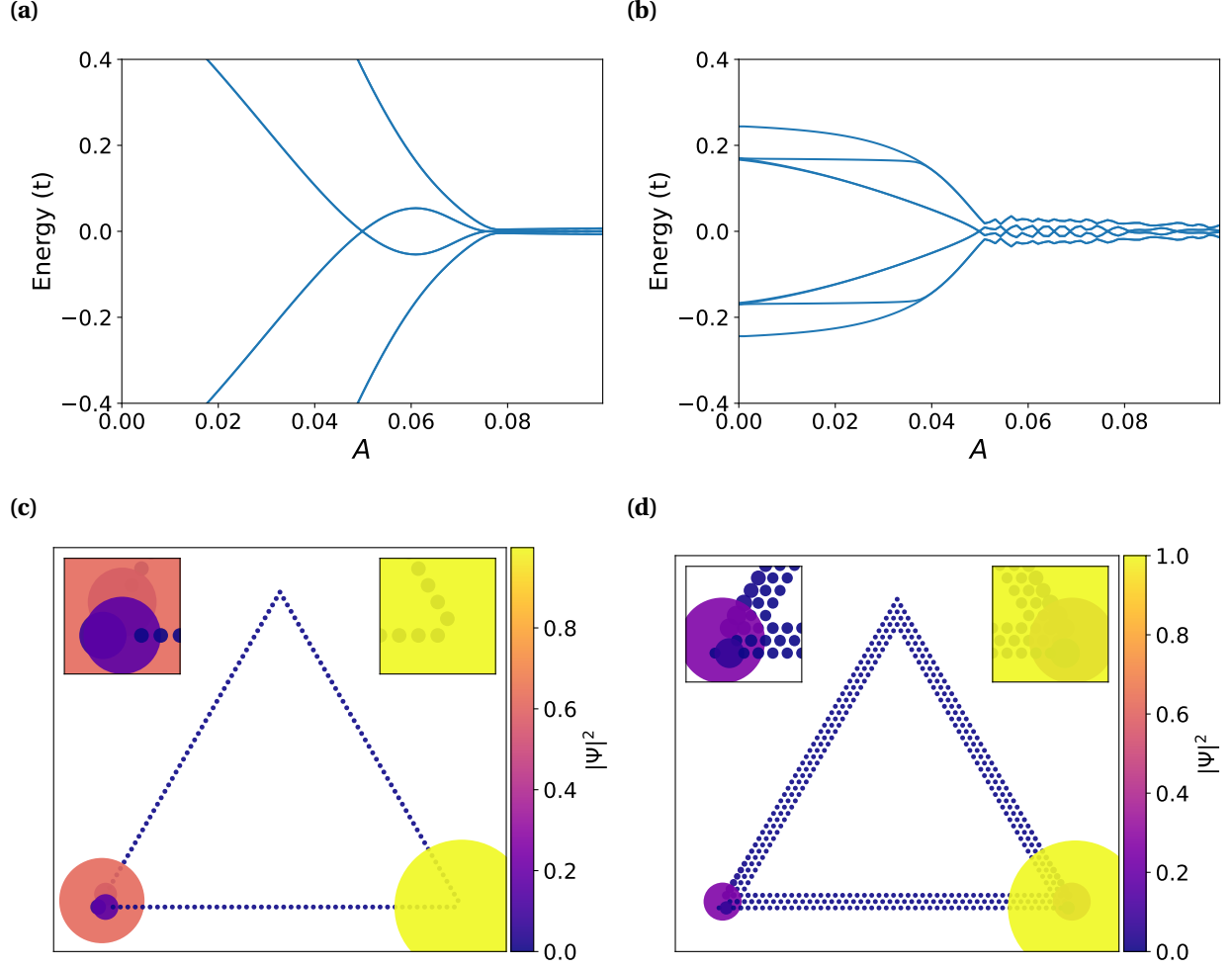


Figure 2.12: Spectral flow of a hollow triangle with $L = 50$, and $\mu = 0$ for increasing linear vector potential strength defined by $\mathbf{A} = -A\mathbf{x}\mathbf{y}$ (a) $W = 1$ and (b) $W = 3$ (c-d) Wavefunctions of the MZM at $A = 0.0499$ for both widths, respectively.

2.6 Discussion

The hollow interior of the triangles considered in this work is needed for two reasons: (1) $W \ll L$ is required for bulk-edge correspondence based on 1D topology to hold; (2) A finite W is needed to gap out the chiral edge states of a 2D spinless p -wave superconductor based on which Eq. (2.7) is written. The latter is not essential if one does not start with a spinless p -wave superconductor but a more realistic model such as the Rashba+Zeeman+s-wave pairing model. On the other hand, the former constraint may also be removed if one uses the Kitaev triangle. Nonetheless, an effective 3-site Kitaev triangle may emerge as the effective theory of triangular

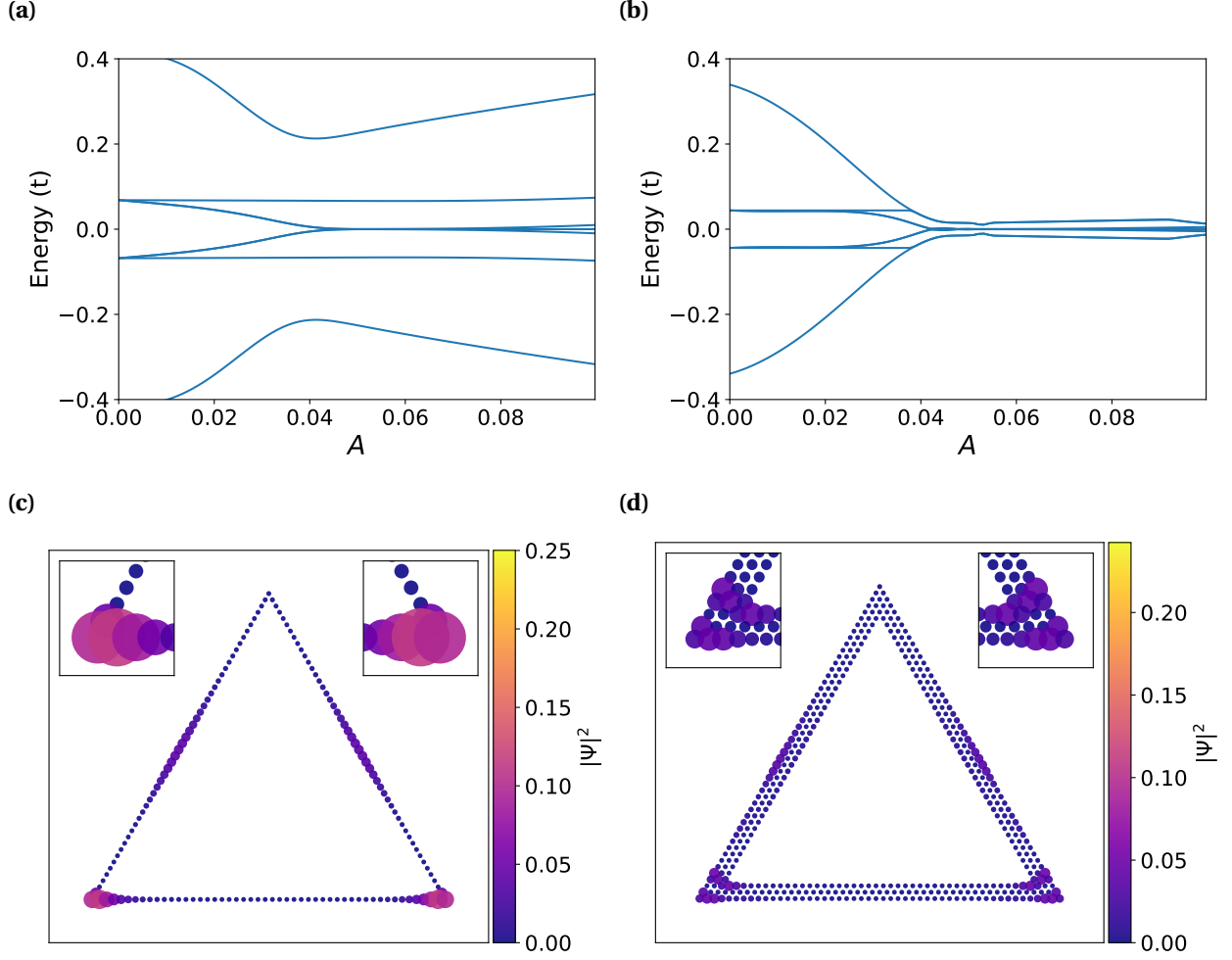


Figure 2.13: Spectral flow of a hollow triangle with $L = 50$, and $\mu = 1.6$ for increasing linear vector potential strength defined by $\mathbf{A} = -A\mathbf{xy}$ (a) $W = 1$ and (b) $W = 3$. (c-d) Wavefunctions of the MZM at $A = 0.0598$ for both widths, respectively.

structures if a three-orbital low-energy Wannier basis can be isolated, similar to the continuum theory of moiré structures. We also note in passing that the corner MZM in our triangles appear due to different reasons from that in higher-order topological superconductors [47, 62].

For possible physical realizations of our triangles, immediate choices are quantum dots forming a Kitaev triangle [53], planar Josephson junctions or cuts on quantum anomalous Hall insulator/superconductor heterostructures [31] that form a hollow triangle, and triangular atomic chains assembled by an STM tip [24] on a close-packed surface. The quantum-dot platform may be advantageous in the convenience of implementing parity readout by turning the third

vertex temporarily into a normal quantum dot [63–65]. Looking into the future, it is more intriguing to utilize the spontaneously formed triangular islands in epitaxial growth [57] with the center region removed either physically by lithography/ablation, or electrically by gating. To create a staggered vector potential or supercurrent profile for the Kitaev triangle, one can use a uniform magnetic field, corresponding to a constant vector potential gradient, plus a uniform supercurrent that controls the position of the zero. It is also possible to use two parallel superconducting wires with counter-propagating supercurrents proximate to the triangle.

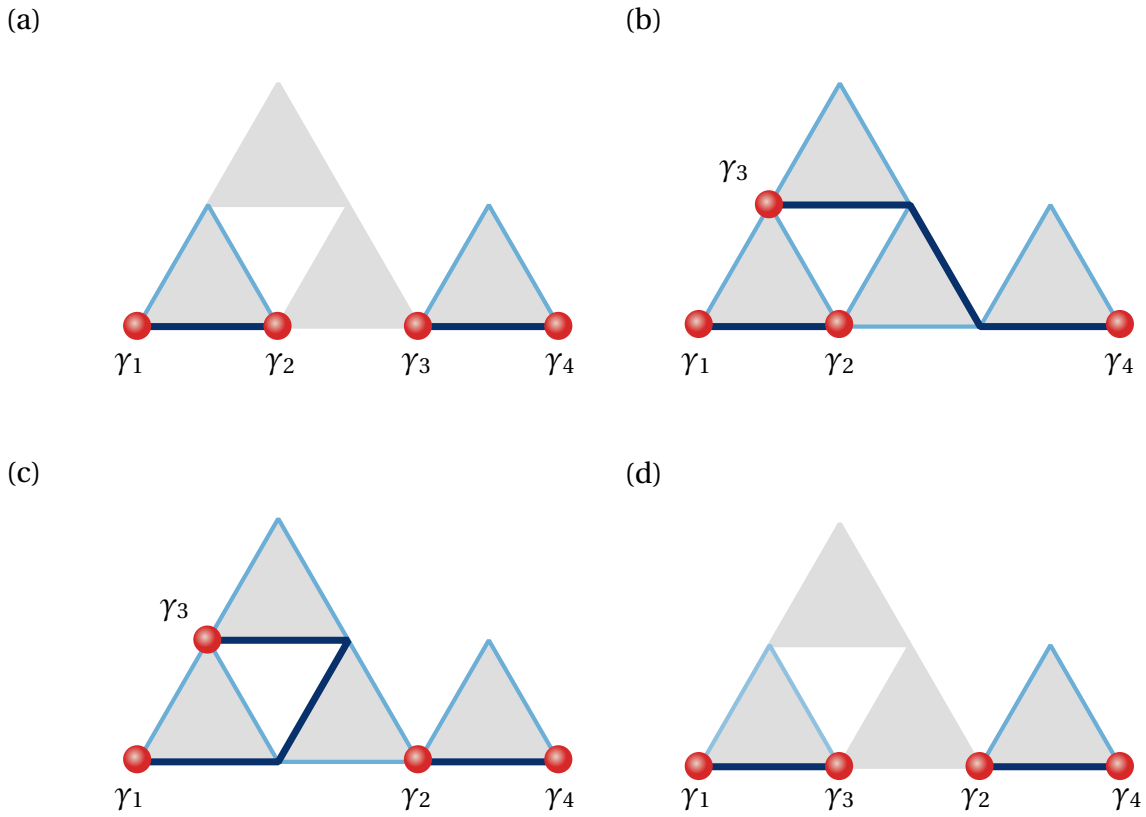


Figure 2.14: Representative steps for braiding four MZM in four triangles sharing corners. (a) Initialization of four MZM $\gamma_1, \gamma_2, \gamma_3, \gamma_4$. All three edges of the bottom-middle and the top triangles are in the trivial phase by e.g. controlling the chemical potential. The bottom-left and bottom-right triangles have $\varphi = 0$ so that their bottom edges are nontrivial. (b) Moving γ_3 by “switching on” the middle triangle by changing the chemical potential under a fixed vector potential at $\varphi = \frac{\pi}{6}$, and then turning on the top triangle with similar means except $\varphi = 0$. (c) Transporting γ_2 to the right triangle through rotating the vector potential in the middle triangle counterclockwise by $\pi/6$. (d) Moving γ_3 to the left triangle by “switching off” the top triangle followed by the middle triangle.

A tentative design for braiding more than two MZM, illustrated in Fig. 2.14, consists of four triangles sharing corners with their neighbors. The critical step of transporting γ_2 to the left vertex of the rightmost triangle, corresponding to Figs. 2.14 (b,c), can be achieved by rotating the vector potential of the bottom-middle triangle counterclockwise from $\varphi = \frac{\pi}{6}$ to $\frac{\pi}{3}$, which swaps the topological phases of the two side edges as shown in Fig. 2.4. In [60] we show this operation does not involve gap closing at least for certain parameter regions. Our work provides a versatile platform for manipulating MZM based on currently available candidate MZM systems and for potentially demonstrating the non-Abelian nature of MZM in near-term devices.

Chapter 3

Floquet Landau Levels

3.1 Introduction

The quantum Hall effect (QHE) in conventional two-dimensional electron gas (2DEG) is one of the most remarkable phenomena in condensed matter physics [66]. This effect is indeed associated with a uniform external perpendicular magnetic field, which splits the electron energy spectrum into discrete Landau levels (LLs). Subject to a strong magnetic field, the diagonal (longitudinal) electric conductivity is vanishingly small, while the nondiagonal (Hall) conductivity is quantized. This happens due to the fact that, when the Fermi energy lies in the gap between two LLs, it is referred to as integer QHE as the Hall conductivity takes values of $2(n+1)e^2/h$ with an integer n . Recent experimental realization of graphene has stimulated additional interest to explore QHE in two dimensional systems [67–69]. Graphene exhibits unusual quantized Hall conductivity values of $2(2n+1)e^2/h$ due to application of the magnetic field [69], which are different from conventional 2DEG.

This significant effect is important to explore in Floquet systems [70, 71] because one may want to observe new phases in an alternative venue that can be experimentally realized [72–75]. Time periodically modulated Floquet theory has been extensively studied and well established for a large class of systems [71, 76–80]. Therefore, one may employ the high frequency expansions [71, 79–86] such as the well known Floquet-Magnus expansion [84–87] and Van Vleck expansion [71, 79]. The significant difference is that latter provides an explicit formulas for the time evolution operator starting at initial time $t_0 = 0$ rather than former starting with finite time t_0 [60]. In such nonequilibrium systems, a circularly polarized laser light made topology nontrivial in spite of triviality in equilibrium [88]. This nontrivial topology is similar to the quantum Anomalous Hall effect proposed by Haldane [89]. Further, optical manipulation of matter is emerging as a promising way of exploring novel phases [90, 91]. This leads to Floquet-

Bloch states exhibiting emerging physical properties that are otherwise inaccessible in equilibrium [92], i.e., the Floquet Chern insulator [93], Floquet notion of magnetic and other strongly-correlated phases [94], topological classifications, symmetry-breaking concept, and symmetry-protected topological phases in nonequilibrium quantum many-body systems [94, 95]. Furthermore, it is important to note that these studies have been demonstrated in the presence of time-periodic homogeneous laser lights. However, the application of spatially inhomogeneous [96–100] laser lights have not been considered so far to best of our knowledge.

In this Letter, it is stirring to unveil that QHE can be observed in Floquet systems without need of uniform magnetic field. We show that two linearly polarized lights are an effective and versatile way of realizing QHE either in graphene-like 2D systems or in conventional 2DEG. Additionally, any one or both lights need to be spatially inhomogeneous. Employing the Floquet theory, we rely on the standard degenerate perturbation formalism and use the Van Vleck expansion [60, 71, 79]. Finally, to obtain the effective Hamiltonian and corresponding band-structure, we employ the long wavelength limit for spatially inhomogeneous modulation. We believe that our work provides a new platforms for realizing QHE and related novel phases in nonequilibrium systems.

3.2 Toy model

A quick derivation of how the center of mass changes when we add a parabolic term to the 2DEG Landau Level system. Start with the Landau level Hamiltonian with a perpendicular magnetic field and additional parabolic term

$$\mathcal{H} = \frac{p_x^2}{2m} + \frac{1}{2m}(p_y - qBx)^2 + d^2 x^2 \quad (3.1)$$

We want to utilize the Laughlin pump argument. we imagine the y-axis is wrapped around to make a cylinder with circumference L which makes $k = \frac{2\pi m}{L}$. Then add in a flux term $\Phi(t)$ along the x-axis, the Hamiltonian becomes

$$\mathcal{H} = \frac{p_x^2}{2m} + \frac{1}{2m} (qBx + q\Phi - \hbar k)^2 + d^2 x^2 \quad (3.2)$$

Performing a shift in coordinates of $x' = x + \frac{\Phi}{BL} - \frac{\hbar k}{qB}$

$$\begin{aligned} \mathcal{H} &= \frac{p_x^2}{2m} + \frac{q^2 B^2 x'^2}{2m} + d^2 \left(x' - \frac{\Phi}{BL} + \frac{\hbar k}{qB} \right)^2 \\ &= \frac{p_x^2}{2m} + \frac{q^2 B^2 x'^2}{2m} + d^2 x'^2 - 2d^2 \Phi'(k) x' + d^2 \Phi'^2(k) \\ &= \frac{p_x^2}{2m} + \frac{q^2 B'^2}{2m} \left(x'^2 - \frac{4md^2 \Phi'(k) x'}{q^2 B'^2} + \frac{4m^2 d^4 \Phi'^2(k)}{q^4 B'^4} \right) - \frac{2md^4 \Phi'^2(k)}{q^2 B'^2} + d^2 \Phi'^2 \\ &= \frac{p_x^2}{2m} + \frac{q^2 B'^2}{2m} \left(x' - \frac{2md^2 \Phi'(k) x'}{q^2 B'^2} \right)^2 - \frac{d^2 \Phi'^2(k)}{q^2 B'^2} (2md^2 - q^2 B'^2) \\ &= \frac{p_x^2}{2m} + \frac{q^2 B'^2 x'^2}{2m} - \frac{d^2 \Phi'^2(k) B^2}{B'^2} \end{aligned} \quad (3.3)$$

where

$$\begin{aligned} x'' &= x' - \frac{2md^2 \Phi'(k)}{q^2 B'^2} \\ &= x + \Phi'(k) \frac{B^2}{B'^2} \\ &= x + \left(\frac{\Phi}{BL} - \frac{\hbar k}{qB} \right) \frac{B^2}{B'^2} \\ &= x + \left(\frac{2\pi\Phi}{\Phi_0} - kL \right) \frac{\hbar B}{qLB'^2} \\ &= x - \left(m - \frac{\Phi}{\Phi_0} \right) \frac{\hbar B}{qLB'^2} \end{aligned} \quad (3.4)$$

3.3 Floquet LLs in 2DEG

We consider the case of Schrödinger electrons under the application of two linearly polarized laser lights. The unperturbed Hamiltonian for 2DEG is

$$H = \frac{\pi_x^2}{2m^*} + \frac{\pi_y^2}{2m^*}, \quad (3.5)$$

where m^* is the effective mass of electron. By changing the Hamiltonian into a time-dependent form by applying two linearly polarized lights such that $\boldsymbol{\pi} \rightarrow \mathbf{p} - q\mathbf{A}(t)$. Therefore, Eq. (3.5) is written as

$$H(t) = \frac{1}{2m^*} [p_x - qA_x(t)]^2 + \frac{1}{2m^*} [p_y - qA_y(t)]^2, \quad (3.6)$$

where the electric field components for two spatially inhomogeneous linearly polarized laser lights are

$$\begin{aligned} \mathbf{E}_1 &= E \sin(Kx) \cos(\omega t) \mathbf{x}, \\ \mathbf{E}_2 &= -E \sin(Kx) \sin(\omega t) \mathbf{y}. \end{aligned} \quad (3.7)$$

The field given in Eq. (3.7) lead to the following vector potential $\mathbf{A}(t)$

$$\mathbf{A}(t) = -\frac{E}{\omega} \sin(Kx) \langle \sin(\omega t), \cos(\omega t), 0 \rangle. \quad (3.8)$$

Substituting into the Schrodinger Hamiltonian we arrive at

$$\mathcal{H}(t) = \frac{1}{2m} [p_x^2 + p_y^2 + V^2 \sin^2(Kx) + V^2 \sin(\omega t) (p_x \sin(Kx) + \sin(Kx) p_x) + 2V p_y \sin(Kx) \cos(\omega t)] \quad (3.9)$$

where $V = qE/\omega$. Because of the time-translation symmetry through $A(t+T) = A(t)$ with $T = 2\pi/\omega$, one can apply the Floquet theory [60, 71, 79] and obtain an effective Hamiltonian from

Eq. (3.9). After performing the Fourier transform of the time-periodicity, first order expansion in $\hbar\omega$ terms and in the long wavelength limit leads to the final effective Hamiltonian as

$$\begin{aligned}\mathcal{H}_{\text{eff}} &= \frac{1}{2m} \left[p_x^2 + p_y^2 + V^2 K^2 x^2 + \frac{\hbar V^2}{4m\omega} (K^2 - 2K^4 x^2) - \frac{2V^2 K^2}{m\omega} p_y x \right] \\ \mathcal{H} &= \frac{1}{2m} \left[p_x^2 + p_y^2 - \frac{2V^2 K^2}{m\omega} p_y x + \left(1 - \frac{\hbar K^2}{2m\omega} \right) V^2 K^2 x^2 + \frac{\hbar V^2 K^2}{4m\omega} \right]\end{aligned}\quad (3.10)$$

Notice here we have quantum harmonic oscillator (QHO) in x-axis and also coupling between p_y and x . The coupling can allow for flux pumping. While we may have Landau levels, from the QHO, it still needs to be shown if our system has topological edge states.

3.3.1 2DEG Numerical Approach

We now consider a 2D square lattice tight-binding model. The incident laser light doesn't allow for translation symmetry along the x-axis in which we will only consider a finite radius along the x-axis and treat the y-axis as infinite. Our unit cell will still only contain one atom per cell, this will not be the case for Dirac. Lattice vectors are described as follows $\mathbf{a}_1 = a\mathbf{x}$, and $\mathbf{a}_2 = a\mathbf{y}$. We will use a Peierls phase to introduce the vector potential field to the tight-binding Hamiltonian. In general, the Hamiltonian has the following form:

$$\mathcal{H}(t) = - \sum_{jl} h_{j,j+1}(t) c_{j,l}^\dagger c_{j+1,l} + h_{l,l+1} c_{j,l}^\dagger c_{j,l+1} + h.c. \quad (3.11)$$

where h , hopping amplitude, takes the following phase contributions

$$h_{j,j+1}(t) = \exp \left[i \frac{qE}{\hbar\omega} (x_{j+1} - x_j) \sin(K\bar{x}_{j,j+1}) \sin\omega t \right]$$

$$h_{j,j+1}(t) = \exp [iZ_1 \sin\omega t] \quad (3.12)$$

$$h_{j+1,j}(t) = \exp [-iZ_1 \sin\omega t] \quad (3.13)$$

$$h_{l,l+1}(t) = \exp \left[i \frac{qE}{\hbar\omega} (y_{l+1} - y_l) \sin(Kx_j) \cos\omega t \right]$$

$$h_{l,l+1}(t) = \exp [iZ_2 \cos\omega t] \quad (3.14)$$

$$h_{l+1,l}(t) = \exp [-iZ_2 \cos\omega t] \quad (3.15)$$

where $Z = qEa/\hbar\omega$, $Z_1 = Z \sin(K\bar{x}_{j,j+1})$, $Z_2 = Z \sin(Kx_j)$, and $\bar{x}_{j,j+1} = (x_{j+1} + x_j)/2$. One can fourier transform along the y-axis to momentum space to simplify the system to

$$\mathcal{H}(t) = - \sum h e^{iZ_1 \sin\omega t} c_{jk}^\dagger c_{j+1,k} + h e^{iZ_2 \cos(\omega t) - ika} c_{jk}^\dagger c_{jk} + h.c.$$

$$= - \sum_{jk} h_{j,j+1}(t) c_{jk}^\dagger c_{j+1,k} + h_{jk}(t) c_{jk}^\dagger c_{jk} + h.c. \quad (3.16)$$

We next impose Floquet theory and take fourier time-domain transforms of the Hamiltonian. Both of the terms take the following form

$$\begin{aligned}
h_{j,j+1,n} &= \frac{1}{T} \int_0^T h_{j,j+1}(t) e^{-in\omega t} dt \\
&= \frac{h}{T} \int_0^T e^{iZ_1 \sin \omega t - in\omega t} dt \\
&= \frac{h}{2\pi} \int_0^{2\pi} e^{iZ_1 \sin \tau - in\tau} d\tau \\
&= hJ_n(Z_1)
\end{aligned} \tag{3.17}$$

$$h_{j+1,j,n} = h(-1)^n J_n(Z_1) \tag{3.18}$$

$$\begin{aligned}
h_{jk,n} &= \frac{1}{T} \int_0^T h_{jk}(t) e^{-in\omega t} dt \\
&= \frac{h}{T} e^{-ika} \int_0^T e^{-iZ_2 \cos(\omega t) - in\omega t} dt \\
&= \frac{h}{2\pi} e^{-ika} \int_0^{2\pi} e^{-iZ_2 \cos \tau - in\tau} d\tau \\
&= \frac{h}{2\pi} e^{-in\pi/2 - ika} \int_0^{2\pi} e^{-iZ_2 \cos \tau - in\tau + in\pi/2} d\tau \\
&= h e^{-in\pi/2 - ika} J_n(Z_2)
\end{aligned} \tag{3.19}$$

$$h_{jk,n}^* = h e^{+in\pi/2 + ika} J_n(Z_2) \tag{3.20}$$

The Hamiltonian after fourier transform is

$$H_n = -h \sum_{jk} J_n(Z_1) \left(c_{jk}^\dagger c_{j+1,k} + (-1)^n c_{j+1,k}^\dagger c_{jk} \right) + 2 \cos \left(ka + \frac{n\pi}{2} \right) J_n(Z_2) c_{jk}^\dagger c_{jk} \tag{3.21}$$

We now build the quasienergy matrix \bar{Q} that has matrix elements

$$\bar{Q}_{m,m+n} = H_n - m\hbar\omega\delta_{n0} \quad (3.22)$$

The quasienergy matrix by definition is infinite in Floquet theory and thus not possible to solve at least numerically. However, since we are interested in the behavior at zeroth mode and depending on the strength of laser light energy, $\hbar\omega$, we choose a cutoff mode $|m| \leq m_c$, where m_c is a positive integer such that higher modes do not contribute to the zeroth modes behavior. Notice we have two cutoffs, one for x-axis radius and for light modes. This translates to a matrix with dimensions $(N_r N_m)^2$, $N_r = (2 * r_c + 1)$, and $N_m = (2 * m_c + 1)$.

3.4 Floquet LLs in Dirac systems

Dirac electrons can be represented with a generic model Hamiltonian like 2D graphene monolayer,

$$H^D = v_F(\sigma_x \Pi_x + \sigma_y \Pi_y), \quad (3.23)$$

where $\Pi = \mathbf{p} - q\mathbf{A}^D(t)$, here \mathbf{A}^D is the vector potential, \mathbf{p} is the momentum operator, v_F is the Fermi velocity of Dirac fermions, q is charge, and σ the Pauli matrices vector in 2D. We have two linearly polarized laser lights with the electric field components

$$\begin{aligned} \mathbf{E}_1 &= E \cos(\omega t) \mathbf{x}, \\ \mathbf{E}_2 &= E \sin(Kx) \sin(2\omega t) \mathbf{y}, \end{aligned} \quad (3.24)$$

where second light is spatially inhomogeneous. It is important to note that second light need to have twice higher frequency than first. This is basic requirement to have LLs spectrum in Dirac systems. Further, one light is propagating along y-axis and polarization is along x-axis, and the other is propagating along x-axis and polarization along y-axis. The ω is frequency of light with

time t , $K = 2\pi/d$ with d being the spatial period of the electric field with amplitude E . This form of the field leads ($\mathbf{E} = -\frac{\partial \mathbf{A}^D}{\partial t}$) to the following vector potential \mathbf{A}^D

$$\mathbf{A}^D(t) = \frac{E}{\omega} \langle -\sin(\omega t), \frac{1}{2} \sin(Kx) \cos(2\omega t), 0 \rangle, \quad (3.25)$$

Substituting Eq. (??) into Eq. (3.23), we arrive at

$$H^D(t) = H_0^D + \sigma_x V_1 \sin(\omega t) - \sigma_y V_2 \cos 2(\omega t), \quad (3.26)$$

where $H_0^D = v_F(\sigma_x p_x + \sigma_y p_y)$, $V_1 = v_F V$, and $V_2 = \frac{1}{2} v_f V \sin(Kx)$. Because of the time-translation symmetry through $A(t+T) = A(t)$ with $T = 2\pi/\omega$, one can apply the Floquet theory [60, 71, 79] and obtain an effective Hamiltonian from Eq. (3.26). After performing the Fourier transform of the time-periodicity, first and second order expansion in $\hbar\omega$ terms leads to the final effective Hamiltonian in Eq. (3.26) as

$$H_{\text{eff}}^D = H_0^D - \frac{v_F V_1^2 \sigma_y p_y}{\hbar^2 \omega^2} + \frac{V_1^2 V_2 \sigma_y}{2\hbar^2 \omega^2} - \frac{v_F \sigma_x (V_2^2 p_x + p_x V_2^2)}{8\hbar^2 \omega^2}. \quad (3.27)$$

In Eq. (3.27), first order term in $\hbar\omega$ that leads to gap at the Dirac point in usual circularly polarized light experiments [73, 75] is zero here due to inhomogeneous nature of laser lights. This effective Hamiltonian can be simplified in the long wavelength limit to

$$H_{\text{eff}}^D = v_F \sigma_x p_x + v_F \sigma_y \left[\left(1 - \frac{v_F^2 V^2}{\hbar^2 \omega^2} \right) p_y + \frac{K v_F^2 V^3}{4\hbar^2 \omega^2} x \right]$$

$$H_{\text{eff}}^D = v_F \sigma_x p_x + v_F \sigma_y (C p_y + q B^D x) \quad (3.28)$$

In obtaining Eq. (3.28), last term in Eq. (3.27) is second order in space and thus zero in the long wavelength limit for the spatially inhomogeneous modulation. Further, we have $B^D = \frac{K q^2 v_F^2 E^3}{4\hbar^2 \omega^5}$.

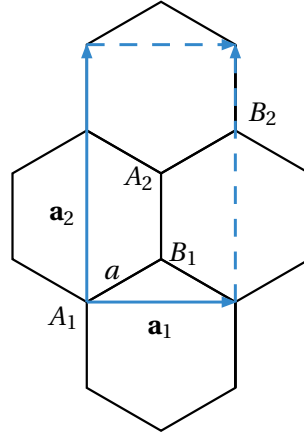
In accordance with Eqs. (3.27) and (3.28), there is least anisotropy in the Dirac spectrum in

addition to zero gap. Diagonalizing the Hamiltonian in Eq. (3.28), we obtained the eigenvalues for Dirac system as

$$E_n^D = v_F^2 \sqrt{\frac{nKq^3 E^3}{2\hbar\omega^5}} \quad (3.29)$$

which is similar to graphene LLs spectrum in the limit of equal velocities. We can have gapped Dirac spectrum by using uniform circularly polarized laser light as observed in experiments [73,75] or by using any substrate like hBN. It is also important to note that the effective magnetic field strength obtained for Dirac case in Eq. (3.29) is directly proportional to third order of the electric field and inversely proportional to the product of spatial period and fifth order of the frequency of the polarized light $\propto (E^3/(a\omega^5))$. This factor of the laser lights can be tuned and thus effective magnetic field can be enhanced in such nonequilibrium situations.

3.4.1 Dirac Numerical Approach



We now look beyond perturbation theory. In doing so we will have to solve the system numerically, which we will describe next. The incident laser light doesn't allow for translation symmetry along the x-axis for our Dirac honeycomb system. We consider a simple model using 4 atoms in a unit cell, the lattice vectors are $\mathbf{a}_1 = \sqrt{3}a\mathbf{x}$ and $\mathbf{a}_2 = 3a\mathbf{y}$, as can be seen in figure ?? . Our Hamiltonian takes the following form

$$H = - \sum_{j'l'\alpha, jl\beta} h_{jl\beta}^{j'l'\alpha} C_{j'l'\alpha}^\dagger C_{jl\beta} + h.c., \quad (3.30)$$

where t is the hopping amplitude, j, l are unit cell index in x and y , and $\alpha, \beta = A_1, A_2, B_1, B_2$. To include the vector potential from Eq. (3.25) in the tight-binding model we consider a finite system defined by $r_c \geq \max(|x_{i\alpha}|, |y_{i\beta}|)$. Using a Peierls substitution we can write the hopping term as

$$\begin{aligned} h_{jl\beta}^{j'l'\alpha} &= h \exp \left[i\phi_0 \left\{ (x_{j'l'}^\alpha - x_{jl}^\beta) \sin \omega t - \frac{1}{2} \sin \left(K \frac{x_{j'l'}^\alpha + x_{jl}^\beta}{2} \right) (y_{j'l'}^\alpha - y_{jl}^\beta) \cos 2\omega t \right\} \right] \\ &= h \exp [iX_1 \sin(\omega t) - iX_2 \cos(2\omega t)] \end{aligned} \quad (3.31)$$

where . One can fourier transform along the y -axis to momentum space to simplify our system to

$$H = - \sum_{jk} \left[\Psi_{jk}^\dagger H_{j,j} \Psi_{jk} + \Psi_{j,k}^\dagger H'_{j,j+1,k} \Psi_{j+1,k} + h.c. \right], \quad (3.32)$$

where $\Psi_{jk} = [C_{jkA_1}, C_{jkB_1}, C_{jkA_2}, C_{jkB_2}]^T$. The two matrices are

$$H_{j,j} = \begin{bmatrix} 0 & 0 & 0 & 0 \\ t_{jlB_1}^{jLA_1} & 0 & 0 & 0 \\ 0 & t_{jlA_2}^{jLB_1} & 0 & 0 \\ 0 & 0 & t_{jlB_2}^{jLA_2} & 0 \end{bmatrix}$$

and

$$H'_{j,j+,k} = \begin{bmatrix} 0 & t_{jlB_1}^{j+1,LA_1} & 0 & t_{jlB_2}^{j+1,L+1,A_1} e^{i\mathbf{k} \cdot \mathbf{a}_2} \\ 0 & 0 & 0 & 0 \\ 0 & 0 & 0 & t_{jlB_2}^{j+1,LA_2} \\ 0 & 0 & 0 & 0 \end{bmatrix},$$

where $\mathbf{k} = k\mathbf{y}$. The Hamiltonian dimension is reduced to $N_S \times N_S$, with $N_S = 2r_c + 1$.

For Floquet theorem we next consider how to construct the Quasienergy operator \bar{Q} . We first need to calculate the fourier time transform of our Hamiltonian. Each component of the matrix can be written as the following

$$\begin{aligned} H_{ab,n} &= \frac{1}{T} \int_0^T H_{ab} e^{-in\omega t} dt \\ &= \frac{1}{2\pi} \int_0^{2\pi} e^{iX_1 \sin(\tau) - iX_2 \cos(2\tau) - in\tau} d\tau. \end{aligned} \quad (3.33)$$

This integral form is close to a Bessel function but has no elementary solution thus we solve it numerically. The quasienergy matrix \bar{Q} then has matrix elements

$$\bar{Q}_{m,m+n} = H_n - m\hbar\omega\delta_{n0} \quad (3.34)$$

We choose a cutoff for mode m , $|m| \leq m_c$, where m_c is a positive integer. This means we will have $N_m = 2m_c + 1$ diagonal blocks, where each block is a $N_S \times N_S$ matrix, H_n .

3.5 Discussion and conclusion

Results can be explained with the help of existing experiments [73,75] and can provide an estimate for the strength of the effective magnetic field to observe LLs and QHE. Analytical structure of Eq. (3.29) and Eq. (??) is primarily responsible for the LLs spectrum in both the Dirac and Schrödinger systems, respectively. Although such results are valid for other 2D materials or Schrödinger systems, however, for simplicity, we will consider parameters realized for graphene or topological insulators [73,75]. In these experiments [73,75], the strength of the electric field used is 1×10^7 V/m to 1×10^8 V/m and the frequency of the light varies from 120 meV to 191 meV.

In case of Dirac electrons, we calculate the effective magnetic field strength using Eq. (3.29). For a fixed value of the spatial period of 120 nm and frequency of laser light $\hbar\omega = 191$ meV, the strength of the effective magnetic field is ≈ 10 Tesla for electric field strength of 5×10^7 V/m [75]. Moreover, by reducing the spatial period to 12 nm, we obtain the effective magnetic field ≈ 98 Tesla for fixed frequency ($\hbar\omega = 191$ meV) and electric field (5×10^7 V/m). This is due to the fact that effective magnetic field is directly proportional to electric field and inversely proportional to the spatial period of light according to Eq. (3.29). Similarly, keeping the spatial period constant and increasing the electric field strength, we can increase the strength of the effective magnetic field for larger frequencies only. However, for the frequency $\hbar\omega = 191$ meV, we can not go beyond 5×10^7 V/m value of the electric field irrespective of the spatial period. This limitation is due to the factor "C" in Eq. (3.29). Further, using lower light frequency ($\hbar\omega = 120$ meV) as realized in topological insulators experiments [73], the critical strength of the electric field is 2×10^7 V/m beyond which magnetic field will become negative. Additionally, for larger frequency of 220 meV, the maximum value of electric field 7×10^7 V/m can be used. It is also important and interesting to note that negative values of the effective magnetic field at larger strengths of light's electric field are fruitful. This is because positive or negative values of the effective magnetic field means (see Eq. (3.28)) that magnetic field is applied either from positive z-axis or negative z-axis. **This estimate of parameters is equally valid for frequency space expansion results (Fig. 1) obtained numerically and degenerate perturbation (Fig. 2) analysis.**

In case of Schrödinger electrons in conventional 2DEG systems, the effective magnetic field strength can be obtained using Eq. (??). For a fixed value of the spatial period of 100 nm and light frequency of $\hbar\omega = 191$ meV, the strength of the effective magnetic field is 1 Tesla using electric field of 5×10^7 V/m. Further, by reducing the spatial period to 10 nm and keeping the electric field (5×10^7 V/m) and frequency of light ($\hbar\omega = 191$ meV) fixed, we obtain the effective magnetic field ≈ 106 Tesla. This can be understood from Eq. (??). In contrast to Dirac case, by increasing the strength of electric field of light, we can increase the strength of the effective magnetic field values. For example, for fixed period of 100 nm and frequency ($\hbar\omega = 191$

meV), the effective magnetic field is 17 Tesla for 2×10^8 V/m. Next, we see the impact of increasing or decreasing frequency and keeping period (100 nm) and electric field (5×10^7 V/m) fixed. For decreasing frequency to 120 meV, we obtain larger effective magnetic field (4.3 Tesla) while increasing frequency leads to smaller effective magnetic field (0.7 Tesla at 220 meV light frequency). **This estimate of parameters is equally valid for frequency space expansion results (Fig. 1) obtained numerically and degenerate perturbation (Fig. 2) analysis.**

In conclusion, we have shown Floquet LLs and the QHE using two linearly polarized lights for graphene-like 2D and conventional 2DEG systems. While using these laser lights, we need at least one or both polarized lights to be spatially inhomogeneous. We have presented results using frequency space expansion method, degenerate Floquet perturbation theory, tight binding models and numerical model calculations. All the results are agreed well to show Floquet LLs in experimentally accessible parameters range. Also, it is interesting to note that we are flexible to use different values of the electric field strength, frequency or spatial period of the light to realize QHE and control the strength of the effective magnetic field. Therefore, we believe that Floquet LLs and QHE can be observed in the experiments for moderate strength of the spatially inhomogeneous lights **as shown in Figs. 1 and 2**. Moreover, we expect the potential to host new nano-electronics in nonequilibrium systems.

Chapter 4

Conclusion and Discussion

What makes gauge potential unique in creating/tuning/manipulating new topoglical systems Applications

Appendix A

Superconducting Triangular Islands

A.1 Kitaev chain

A pair of Majorana fermions can be defined in terms of spinless operators a_j, a_j^\dagger , where j labels general quantum numbers, as

$$c_{2j-1} = a_j + a_j^\dagger \tag{A.1}$$

$$c_{2j} = -i(a_j - a_j^\dagger)$$

which are hermitian conjugates of themselves. Conversely,

$$a_j = \frac{1}{2}(c_{2j-1} + i c_{2j}), \tag{A.2}$$

$$a_j^\dagger = \frac{1}{2}(c_{2j-1} - i c_{2j})$$

For a general mean-field Hamiltonian

$$H = \sum_{jl} h_{jl} a_j^\dagger a_l \tag{A.3}$$

where h is a Hermitian matrix, it can be transformed to the Majorana fermion representation as follows:

$$\begin{aligned}
H &= \frac{1}{4} \sum_{jl} h_{jl} (c_{2j-1} - i c_{2j}) (c_{2l-1} + i c_{2l}) \\
&= \frac{1}{4} \sum_{jl} (h_{jl} c_{2j-1} c_{2l-1} - i h_{jl} c_{2j} c_{2l-1} + i h_{jl} c_{2j-1} c_{2l} + h_{jl} c_{2j} c_{2l}) \\
&= \frac{i}{4} \sum_{jl} (c_{2j-1}, c_{2j}) \begin{pmatrix} -i h_{jl} & h_{jl} \\ -h_{jl} & -i h_{jl} \end{pmatrix} \begin{pmatrix} c_{2l-1} \\ c_{2l} \end{pmatrix} \\
&\equiv \frac{i}{4} \sum_{mn} A_{mn} c_m c_n
\end{aligned} \tag{A.4}$$

where the matrix A anti-Hermitian since

$$H^\dagger = -\frac{i}{4} \sum_{mn} A_{mn}^* c_n c_m = H \tag{A.5}$$

which leads to $A_{mn}^* = -A_{nm}$. If the Hamiltonian does not preserve particle number, i.e., it is a BdG Hamiltonian, we have, similarly

$$H = \sum_{jl} \left(h_{jl} a_j^\dagger a_l + \Delta_{jl} a_j a_l + \Delta_{jl}^\dagger a_j^\dagger a_l^\dagger \right) \tag{A.6}$$

supposing we do not double count the terms in the normal part of the Hamiltonian. Then

$$H = \frac{i}{4} \sum_{jl} (c_{2j-1}, c_{2j}) \begin{pmatrix} -i h - i(\Delta + \Delta^\dagger) & h + (\Delta - \Delta^\dagger) \\ -h + (\Delta - \Delta^\dagger) & -i h + i(\Delta + \Delta^\dagger) \end{pmatrix}_{jl} \begin{pmatrix} c_{2l-1} \\ c_{2l} \end{pmatrix} \tag{A.7}$$

On the other hand, the BdG Hamiltonian can be written as

$$\begin{aligned}
H &= \frac{1}{2} \sum_j h_{jj} + \sum_{jl} \left(\frac{1}{2} h_{jl} a_j^\dagger a_l - \frac{1}{2} h_{lj} a_j a_l^\dagger + \Delta_{jl} a_j a_l + \Delta_{jl}^\dagger a_j^\dagger a_l^\dagger \right) \\
&= \frac{1}{2} \text{Tr}(h) + \sum_{jl} (a_j^\dagger, a_j) \begin{pmatrix} \frac{1}{2} h & \Delta^\dagger \\ \Delta & -\frac{1}{2} h^T \end{pmatrix}_{jl} \begin{pmatrix} a_l \\ a_l^\dagger \end{pmatrix} \\
&\equiv \frac{1}{2} \text{Tr}(h) + a^\dagger \begin{pmatrix} \frac{1}{2} h & \Delta^\dagger \\ \Delta & -\frac{1}{2} h^T \end{pmatrix} a
\end{aligned} \tag{A.8}$$

where $a \equiv (a_1, a_2, \dots, a_1^\dagger, a_2^\dagger, \dots)^T$. Suppose the BdG Hamiltonian can be diagonalized by a Bogoliubov transformation:

$$\tilde{a}_j^\dagger = a_l^\dagger U_{1,lj} + a_k U_{2,kj} \tag{A.9}$$

$$\tilde{a}_j = a_l U_{1,lj}^* + a_k^\dagger U_{2,kj}^*$$

Preserving the anticommutation relation suggests

$$\begin{aligned}
\delta_{ij} &= \{\tilde{a}_i, \tilde{a}_j^\dagger\} = \{a_l U_{1,li}^* + a_k^\dagger U_{2,ki}^*, a_{l'}^\dagger U_{1,l'j} + a_{k'} U_{2,k'j}\} \\
&= U_{1,li}^* U_{1,l'j} + U_{2,ki}^* U_{2,k'j} = (U_1^\dagger U_1 + U_2^\dagger U_2)_{ij} \\
0 &= \{\tilde{a}_i, \tilde{a}_j\} = \{a_l U_{1,li}^* + a_k^\dagger U_{2,ki}^*, a_{l'} U_{1,l'j} + a_{k'}^\dagger U_{2,k'j}^*\} \\
&= U_{1,li}^* U_{2,l'j} + U_{2,ki}^* U_{1,k'j} = (U_1^\dagger U_2^* + U_2^\dagger U_1^*)_{ij} \\
0 &= \{\tilde{a}_i^\dagger, \tilde{a}_j^\dagger\} = \{a_l^\dagger U_{1,li} + a_k U_{2,ki}, a_{l'}^\dagger U_{1,l'j} + a_{k'} U_{2,k'j}\} \\
&= U_{1,li} U_{2,l'j} + U_{2,ki} U_{1,k'j} = (U_1^\dagger U_2^* + U_2^\dagger U_1^*)_{ij}^*
\end{aligned} \tag{A.10}$$

The above identities simply indicate

$$\mathcal{U} \equiv \begin{pmatrix} U_1 & U_2 \\ U_2^* & U_1^* \end{pmatrix} \quad (\text{A.11})$$

is a unitary matrix. Therefore one can diagonalize the BdG Hamiltonian using usual unitary matrices obtained from the eigenvectors of the matrix in the last line of Eq. A.98:

$$\begin{aligned} H &= \frac{1}{2} \text{Tr}(h) + \tilde{a}^\dagger U^\dagger \begin{pmatrix} \frac{1}{2}h & \Delta^\dagger \\ \Delta & -\frac{1}{2}h^T \end{pmatrix} U \tilde{a} \\ &\equiv \frac{1}{2} \text{Tr}(h) + \frac{1}{2} \tilde{a}^\dagger \begin{pmatrix} \epsilon & 0 \\ 0 & -\epsilon \end{pmatrix} \tilde{a} \\ &= \frac{1}{2} \sum_j h_{jj} + \frac{1}{2} \sum_j (\epsilon_j \tilde{a}_j^\dagger \tilde{a}_j - \epsilon_j \tilde{a}_j \tilde{a}_j^\dagger) \\ &= \frac{1}{2} \sum_j h_{jj} + \sum_j \epsilon_j (\tilde{a}_j^\dagger \tilde{a}_j - \frac{1}{2}) \end{aligned} \quad (\text{A.12})$$

where $\epsilon \equiv \text{Diag}[\epsilon_1, \epsilon_2, \dots]$. To see why U can transform the BdG Hamiltonian into such a diagonal matrix with opposite eigenvalues at the same positions in the upper-left and lower-right blocks, we check these two terms explicitly

$$\begin{aligned} &\frac{1}{2} (\epsilon_1 \tilde{a}_j^\dagger \tilde{a}_j - \epsilon_2 \tilde{a}_j \tilde{a}_j^\dagger) \\ &= \frac{\epsilon_1}{2} (a_l^\dagger U_{1,lj} + a_k U_{2,kj}) (a_{l'} U_{1,l'j}^* + a_{k'}^\dagger U_{2,k'j}^*) - \frac{\epsilon_2}{2} (a_{l'} U_{1,l'j}^* + a_{k'}^\dagger U_{2,k'j}^*) (a_l^\dagger U_{1,lj} + a_k U_{2,kj}) \\ &= \frac{1}{2} (\epsilon_1 U_{1,lj} U_{1,l'j}^* - \epsilon_2 U_{2,lj}^* U_{2,l'j}) a_l^\dagger a_{l'} + \frac{1}{2} (\epsilon_1 U_{2,kj} U_{2,k'j}^* - \epsilon_2 U_{1,kj}^* U_{1,k'j}) a_k a_{k'}^\dagger \\ &+ \frac{1}{2} (\epsilon_1 U_{1,lj} U_{2,k'j}^* - \epsilon_2 U_{2,lj}^* U_{1,k'j}) a_l^\dagger a_{k'}^\dagger + \frac{1}{2} (\epsilon_1 U_{2,kj} U_{1,l'j}^* - \epsilon_2 U_{1,kj}^* U_{2,l'j}) a_k a_{l'} \end{aligned} \quad (\text{A.13})$$

Comparing them with the original BdG Hamiltonian Eq. A.98, we can conclude that

$$\epsilon_1 U_{1,lj} U_{1,l'j}^* - \epsilon_2 U_{2,lj}^* U_{2,l'j} = -(\epsilon_1 U_{2,l'j} U_{2,lj}^* - \epsilon_2 U_{1,l'j}^* U_{1,lj}) \quad (\text{A.14})$$

$$\epsilon_1 U_{1,lj} U_{2,k'j}^* - \epsilon_2 U_{2,lj}^* U_{1,k'j} = (\epsilon_1 U_{2,k'j} U_{1,lj}^* - \epsilon_2 U_{1,k'j}^* U_{2,lj})^*$$

or equivalently

$$(\epsilon_1 - \epsilon_2)(U_{1,lj} U_{1,l'j}^* + U_{2,l'j} U_{2,lj}^*) = 0 \quad (\text{A.15})$$

$$0 = 0$$

The first equation therefore dictates $\epsilon_1 = \epsilon_2$. However, note that ϵ_j does not have to be all positive. If the original normal state Hamiltonian can be diagonalized into a form

$$H = \sum_j \tilde{\epsilon}_j b_j^\dagger b_j \quad (\text{A.16})$$

where $\tilde{\epsilon}_j$ can be either positive or negative, the state with the lowest possible energy from the system is

$$|\Omega\rangle = \prod_{\tilde{\epsilon}_k < 0} b_k^\dagger |0\rangle \quad (\text{A.17})$$

where $|0\rangle$ is the true vacuum with no particles in any sense. This is the ground state, and its parity is therefore determined by the number of single-particle eigenstates that have negative energies.

From the same perspective, one can define the ground state of the BdG Hamiltonian Eq. A.12 for a specific set of Fermion operators \tilde{a}_j , as

$$|\Omega_{\text{BdG}}\rangle = \prod_{\epsilon_j < 0} \tilde{a}_j^\dagger |0_{\text{BdG}}\rangle \quad (\text{A.18})$$

where $|0_{\text{BdG}}\rangle$ is certain “vacuum state” for the given set of \tilde{a}_j :

$$\tilde{a}_j |0_{\text{BdG}}\rangle = 0, \forall j \quad (\text{A.19})$$

The number of particles in the ground state is therefore determined by the number of negative ϵ_j . However, the sign of ϵ_j in the present case does not have absolute meaning. For example, supposing $\epsilon_{j_0} < 0$, the following Bogoliubov transformation

$$\tilde{a}'_{j_0} = \tilde{a}_{j_0}^\dagger \quad (\text{A.20})$$

$$\tilde{a}_{j_0}'^\dagger = \tilde{a}_{j_0}$$

that only interchanges the creation and annihilation operators for a single j_0 and keeps the others unchanged, leads to a different ground state

$$|\Omega'_{\text{BdG}}\rangle = \prod_{\epsilon_j < 0, j \neq j_0} \tilde{a}_j^\dagger |0_{\text{BdG}}\rangle \quad (\text{A.21})$$

since the number of negative energy eigenstates decreases by one. The transformation in Eq. A.20 therefore neither preserves particle number nor particle parity. This can be explicitly checked. The particle number operator in the \tilde{a}_j representation is

$$N = \sum_j \tilde{a}_j^\dagger \tilde{a}_j \quad (\text{A.22})$$

Therefore

$$N' = \sum_{j \neq j_0} \tilde{a}_j^\dagger \tilde{a}_j + \tilde{a}_{j_0} \tilde{a}_{j_0}^\dagger = N + (1 - 2\tilde{a}_{j_0}^\dagger \tilde{a}_{j_0}) \quad (\text{A.23})$$

The latter equation also means that when the j_0 state is occupied in Ω_{BdG} , i.e., $\tilde{a}_{j_0}^\dagger \tilde{a}_{j_0} |\Omega_{\text{BdG}}\rangle = |\Omega_{\text{BdG}}\rangle$, the transformation decreases the total number of particles by 1. Conversely, if it is un-

occupied ($\epsilon_{j_0} > 0$), or $\tilde{a}_{j_0}^\dagger \tilde{a}_{j_0} |\Omega_{\text{BdG}}\rangle = 0$, the transformation increases the particle number by one.

The fermion parity operator can be defined by

$$P = \prod_j (1 - 2a_j^\dagger a_j) \quad (\text{A.24})$$

so that $P = 1$ if the number of occupied states is even, and -1 otherwise. Alternatively, since

$$a_j^\dagger a_j = \frac{1}{4}(c_{2j-1} - ic_{2j})(c_{2j-1} + ic_{2j}) = \frac{1}{2}(1 + ic_{2j-1}c_{2j}) \quad (\text{A.25})$$

P can be written in the Majorana representation as

$$P = \prod_j (-ic_{2j-1}c_{2j}). \quad (\text{A.26})$$

Eq. [A.20](#) transforms P by changing

$$1 - 2\tilde{a}_{j_0}^\dagger \tilde{a}_{j_0} \rightarrow 1 - 2\tilde{a}'_{j_0} \tilde{a}'_{j_0}{}^\dagger = -(1 - \tilde{a}_{j_0}^\dagger \tilde{a}'_{j_0}) \quad (\text{A.27})$$

and hence indeed changes P .

We can also understand why the BdG Hamiltonian preserves P but not N . Due to the following commutation relations:

$$[a_j^\dagger a_l, a_j^\dagger a_j] = a_j^\dagger a_l a_j^\dagger a_j - a_j^\dagger a_j a_j^\dagger a_l = -a_j^\dagger a_l \quad (\text{A.28})$$

$$[a_j^\dagger a_l, a_l^\dagger a_l] = a_j^\dagger a_l a_l^\dagger a_l - a_l^\dagger a_l a_j^\dagger a_l = a_j^\dagger a_l$$

$$[a_j^\dagger a_l^\dagger, a_j^\dagger a_j] = a_j^\dagger a_l^\dagger a_j^\dagger a_j - a_j^\dagger a_j a_j^\dagger a_l^\dagger = -a_j^\dagger a_l^\dagger$$

$$[a_j^\dagger a_l^\dagger, a_l^\dagger a_l] = a_j^\dagger a_l^\dagger a_l^\dagger a_l - a_l^\dagger a_l a_j^\dagger a_l^\dagger = -a_j^\dagger a_l^\dagger$$

$$[a_j a_l, a_j^\dagger a_j] = a_j a_l a_j^\dagger a_j - a_j^\dagger a_j a_j a_l = a_j a_l$$

$$[a_j a_l, a_l^\dagger a_l] = a_j a_l a_l^\dagger a_l - a_l^\dagger a_l a_j a_l = a_j a_l$$

and

$$[a_j^\dagger a_l, (1 - 2a_j^\dagger a_j)(1 - 2a_l^\dagger a_l)] = (1 - 2a_j^\dagger a_j)[a_j^\dagger a_l, (1 - 2a_l^\dagger a_l)] + [a_j^\dagger a_l, (1 - 2a_j^\dagger a_j)](1 - 2a_l^\dagger a_l) \quad (\text{A.29})$$

$$= -2(1 - 2a_j^\dagger a_j)a_j^\dagger a_l + 2a_j^\dagger a_l(1 - 2a_l^\dagger a_l)$$

$$= -2a_j^\dagger a_l + 4a_j^\dagger a_l + 2a_j^\dagger a_l - 4a_j^\dagger a_l = 0$$

$$[a_j a_l, (1 - 2a_j^\dagger a_j)(1 - 2a_l^\dagger a_l)] = (1 - 2a_j^\dagger a_j)[a_j a_l, (1 - 2a_l^\dagger a_l)] + [a_j a_l, (1 - 2a_j^\dagger a_j)](1 - 2a_l^\dagger a_l)$$

$$= -2(1 - 2a_j^\dagger a_j)a_j a_l - 2a_j a_l(1 - 2a_l^\dagger a_l)$$

$$= -2a_j a_l - 2a_j a_l + 4a_j a_l = 0$$

we have

$$[H, N] = 2 \sum_{jl} (\Delta_{jl} a_j a_l - \Delta_{jl}^\dagger a_j^\dagger a_l^\dagger) \quad (\text{A.30})$$

$$[H, P] = 0$$

Since $[H, P] = 0$, there are common eigenstates of H and P , or that they can be simultaneously diagonalized by some unitary transformation. However, since P is not a one-body operator, its unitary transformation in general cannot be written as multiplications of $2N \times 2N$ matrices as the BdG Hamiltonian. We therefore need to understand how the Bogoliubov transformation Eq. A.9 transforms P . To this end we first write Eq. A.9 into a block form

$$(\tilde{a}^\dagger, \tilde{a}) = (a^\dagger, a)\mathcal{U} \quad (\text{A.31})$$

where $a \equiv (a_1, a_2, \dots, a_N)$ and so on. On the other hand, Eqs. A.2 and A.1 can be written as

$$(c_o, c_e) = (a^\dagger, a) \begin{pmatrix} 1 & i \\ 1 & -i \end{pmatrix}, \quad (a^\dagger, a) = (c_o, c_e) \begin{pmatrix} \frac{1}{2} & \frac{1}{2} \\ -\frac{i}{2} & \frac{i}{2} \end{pmatrix} \quad (\text{A.32})$$

where $c_o \equiv (c_1, c_3, \dots, c_{2N-1})$ and $c_e \equiv (c_2, c_4, \dots, c_{2N})$. The above equations then lead to

$$\begin{aligned} (\tilde{c}_o, \tilde{c}_e) &= (c_o, c_e) \begin{pmatrix} \frac{1}{2} & \frac{1}{2} \\ -\frac{i}{2} & \frac{i}{2} \end{pmatrix} \mathcal{U} \begin{pmatrix} 1 & i \\ 1 & -i \end{pmatrix} \\ &= (c_o, c_e) \begin{pmatrix} \text{Re}(U_1 + U_2) & -\text{Im}(U_1 - U_2) \\ \text{Im}(U_1 + U_2) & \text{Re}(U_1 - U_2) \end{pmatrix} \\ &= (c_o, c_e) \mathcal{O} \end{aligned} \quad (\text{A.33})$$

or equivalently

$$\tilde{c}_{2j-1} = c_{2k-1} \mathcal{O}_{k,j} + c_{2k} \mathcal{O}_{N+k,j} \quad (\text{A.34})$$

$$\tilde{c}_{2j} = c_{2k-1} \mathcal{O}_{k,N+j} + c_{2k} \mathcal{O}_{N+k,N+j}$$

Since all elements of \mathcal{O} are real,

$$\mathcal{O}^T \mathcal{O} = \mathcal{O}^\dagger \mathcal{O} = \begin{pmatrix} \frac{1}{2} & \frac{1}{2} \\ -\frac{i}{2} & \frac{i}{2} \end{pmatrix} \mathcal{U}^\dagger \mathcal{U} \begin{pmatrix} 1 & i \\ 1 & -i \end{pmatrix} = \mathbb{I} \quad (\text{A.35})$$

Namely, \mathcal{O} is a real orthogonal matrix. As a result we have

$$1 = \det(\mathcal{O}^T \mathcal{O}) = (\det\{\mathcal{O}\})^2 \quad (\text{A.36})$$

which necessarily means $\det\{\mathcal{O}\} = \pm 1$. From linear algebra we know that an arbitrary special orthogonal matrix, i.e., $\det\{\mathcal{O}\} = +1$, can always be written as

$$\mathcal{O} = e^A \quad (\text{A.37})$$

where $A = -A^T$ is a real skew-symmetric matrix. But no such general expressions exist for those \mathcal{O} with $\det \mathcal{O} = -1$. For later convenience we reorganize the elements of \mathcal{O} so that they are labeled in the same way as the Majorana operators. Namely

$$\mathcal{O}_{k,j} \rightarrow \mathcal{O}_{2k-1,2j-1} \quad (\text{A.38})$$

$$\mathcal{O}_{N+k,j} \rightarrow \mathcal{O}_{2k,2j-1}$$

$$\mathcal{O}_{k,N+j} \rightarrow \mathcal{O}_{2k-1,2j}$$

$$\mathcal{O}_{N+k,N+j} \rightarrow \mathcal{O}_{2k,2j}$$

This does not affect the orthogonality of \mathcal{O} .

To see how \mathcal{O} transforms P , we start from Eq. A.26 and note that it can be written as

$$P = (-i)^N \prod_{j=1}^N (c_{2j-1} c_{2j}) = \text{pf}(\mathcal{C}) \quad (\text{A.39})$$

where

$$\mathcal{C} \equiv \begin{pmatrix} C_1 & & \\ & \ddots & \\ & & C_N \end{pmatrix}, C_j \equiv \begin{pmatrix} 0 & -ic_{2j-1}c_{2j} \\ ic_{2j-1}c_{2j} & 0 \end{pmatrix} \quad (\text{A.40})$$

The pfaffian pf for an arbitrary skew-symmetric matrix is defined as

$$\text{pf}(A) = \frac{1}{2^n n!} \sum_{\sigma \in S_{2n}} \text{sgn}(\sigma) \prod_{i=1}^n a_{\sigma(2i-1), \sigma(2i)} \quad (\text{A.41})$$

where A is a $2n \times 2n$ skew-symmetric matrix, S_{2n} is the permutation group of order $2n$. For skew-symmetric tridiagonal A with $A_{2j-1, 2j} = -A_{2j, 2j-1} = b_j$ and all other elements zero, $\text{pf}(A) = \prod_{j=1}^n b_j$. Eq. A.39 is valid since all the $-ic_{2j-1}c_{2j}$ commute with one another and can be viewed as c-numbers.

Our goal is to convert the complicated transformation rule of P under \mathcal{O} to something that is more manageable. To this end we generalize the \mathcal{C} matrix above to the following:

$$\mathcal{C}_{mn} = \begin{cases} 0 & m = n \\ -ic_m c_n & m \neq n \end{cases} \quad (\text{A.42})$$

Apparently $\mathcal{C} = -\mathcal{C}^T$ and one can still calculate its pfaffian. To simplify the calculation we use the following equivalent definition of the pfaffian:

$$\text{pf}(A) = \sum_{\alpha \in \Pi} A_\alpha \quad (\text{A.43})$$

where A_α is

$$A_\alpha = \text{sgn}(\pi_\alpha) a_{i_1, j_1} a_{i_2, j_2} \cdots a_{i_n, j_n} \quad (\text{A.44})$$

and the permutation π_α and its set Π are constructed in the following way: Consider a partition of $\{1, 2, \dots, 2n\}$ into unordered pairs and define α as such a partition

$$\alpha = \{(i_1, j_1), (i_2, j_2), \dots, (i_n, j_n)\} \quad (\text{A.45})$$

so that there are $(2n)!/(2^n n!)$ such partitions. The permutation π_α is defined as

$$\pi_\alpha \equiv \begin{pmatrix} 1 & 2 & 3 & 4 & \dots & 2n-1 & 2n \\ i_1 & j_1 & i_2 & j_2 & \dots & i_n & j_n \end{pmatrix} \quad (\text{A.46})$$

For our \mathcal{C} this means the counterpart of A_α is

$$\text{sgn}(\pi_\alpha)(-i)^N c_{m_1} c_{n_1} c_{m_2} c_{n_2} \dots c_{m_N} c_{n_N} = \prod_{j=1}^N (-i c_{2j-1} c_{2j}) \quad (\text{A.47})$$

since $\text{sgn}(\pi_\alpha)$ is exactly compensated by the anticommutation relation of the Majorana fermions.

We therefore have

$$P = \frac{2^N N!}{(2N)!} \text{pf}(\mathcal{C}) \quad (\text{A.48})$$

We next consider the transformation of \mathcal{C} by \mathcal{O} :

$$\tilde{\mathcal{C}}_{mn} = -i \tilde{c}_m \tilde{c}_n = -i \sum_{i \neq j} \mathcal{O}_{mi} \mathcal{O}_{nj} c_i c_j = (\mathcal{O}^T \mathcal{C} \mathcal{O})_{mn} \quad (\text{A.49})$$

which is nothing but the usual similarity transformation of the matrix \mathcal{C} . We therefore immediately get

$$\begin{aligned} \tilde{P} &= \frac{2^N N!}{(2N)!} \text{pf}(\tilde{\mathcal{C}}) = \frac{2^N N!}{(2N)!} \text{pf}(\mathcal{O}^T \mathcal{C} \mathcal{O}) = \frac{2^N N!}{(2N)!} \text{pf}(\mathcal{C}) \det(\mathcal{O}) \\ &= \det(\mathcal{O}) P \end{aligned} \quad (\text{A.50})$$

Therefore the Bogoliubov transformation \mathcal{O} preserves the parity if $\det(\mathcal{O}) = +1$, and changes the parity if $\det(\mathcal{O}) = -1$.

Using the above transformation rule of P under a general Bogoliubov transformation we can now understand the meaning of ground state parity in [8]. Start from an arbitrary state that is an eigenstate of P with even parity, we have

$$P|\psi\rangle = |\psi\rangle \quad (\text{A.51})$$

Under a Bogoliubov transformation, the state itself is unchanged, but $P \rightarrow \tilde{P}$, since the meaning of particles is different. We then have

$$\tilde{P}|\psi\rangle = \det(\mathcal{O})P|\psi\rangle = \det(\mathcal{O})|\psi\rangle \quad (\text{A.52})$$

Namely, because the Bogoliubov transformation redefines particles and hence the parity operator, an even-parity state can become an odd-parity state in the new definition of the parity operator. Therefore for a given BdG Hamiltonian, the meaning of its ground state parity must be relative, and we need to choose a reference in order to discuss the parity. Such a reference is the ground state of the “canonical form” of the BdG Hamiltonian:

$$\begin{aligned} H_{\text{canonical}} &= \sum_m \epsilon_m (\tilde{a}_m^\dagger \tilde{a}_m - \frac{1}{2}) = \frac{i}{2} \sum_m \tilde{c}_{2m-1} \tilde{c}_{2m} \\ &\equiv \frac{i}{2} \sum_m \epsilon_m b'_m b''_m, \quad \epsilon_m \geq 0 \end{aligned} \quad (\text{A.53})$$

where the crucial requirement is that all the eigenenergies are non-negative. For a given BdG Hamiltonian such a canonical form is uniquely fixed, and we can use its ground state as a reference for the parity and the parity operator. The ground state of $H_{\text{canonical}}$ is defined by

$$\tilde{a}_m |\Omega_{\text{canonical}}\rangle = 0 \quad \forall m \in [1, N]. \quad (\text{A.54})$$

and the “reference” or canonical parity operator is

$$P_{\text{canonical}} \equiv \prod_{m=1}^N (-i b'_m b''_m). \quad (\text{A.55})$$

Since there are no \tilde{a} particles in $|\Omega_{\text{canonical}}\rangle$, we must have

$$P_{\text{canonical}}|\Omega_{\text{canonical}}\rangle = |\Omega_{\text{canonical}}\rangle \quad (\text{A.56})$$

Namely $|\Omega_{\text{canonical}}\rangle$ has even parity. We can then ask the following question: What is the parity of $|\Omega_{\text{canonical}}\rangle$ in the sense of particles in the original BdG Hamiltonian, i.e., a_j ? This requires us to evaluate

$$\begin{aligned} P_{\text{BdG}}|\Omega_{\text{canonical}}\rangle &\equiv \prod_j (-i c_{2j-1} c_{2j}) |\Omega_{\text{canonical}}\rangle = \det(\mathcal{O}) P_{\text{canonical}}|\Omega_{\text{canonical}}\rangle \\ &= \det(\mathcal{O}) |\Omega_{\text{canonical}}\rangle \end{aligned} \quad (\text{A.57})$$

Namely, the parity is equal to the determinant of the orthogonal transformation that transforms c to b' and b'' . More precisely,

$$\begin{pmatrix} b'_1 \\ b''_1 \\ \vdots \\ b'_N \\ b''_N \end{pmatrix} = \mathcal{O} \begin{pmatrix} c_1 \\ c_2 \\ \vdots \\ c_{2N-1} \\ c_{2N} \end{pmatrix} \quad (\text{A.58})$$

and

$$\mathcal{O} A \mathcal{O}^T = \begin{pmatrix} 0 & \epsilon_1 & & \\ -\epsilon_1 & 0 & & \\ & & \ddots & \\ & & & 0 & \epsilon_N \\ & & & -\epsilon_N & 0 \end{pmatrix} \quad (\text{A.59})$$

where A is introduced in Eq. A.4, and our \mathcal{O} is the matrix W in [8]. Eq. A.59 therefore leads to a convenient formula for calculating $\det(\mathcal{O})$:

$$\text{pf}(\mathcal{O} A \mathcal{O}^T) = \det(\mathcal{O}) \text{pf}(A) = \text{pf} \begin{pmatrix} 0 & \epsilon_1 & & \\ -\epsilon_1 & 0 & & \\ & & \ddots & \\ & & & 0 & \epsilon_N \\ & & & -\epsilon_N & 0 \end{pmatrix} = \prod_m \epsilon_m \geq 0 \quad (\text{A.60})$$

Therefore

$$\det(\mathcal{O}) = \left(\prod_m \epsilon_m \right) [\text{pf}(A)]^{-1} \quad (\text{A.61})$$

Since $\det(\mathcal{O}) = \pm 1$ we only need the signs of the two quantities on the right hand side of the above equation. If none of the ϵ_m vanishes, $(\prod_m \epsilon_m) > 0$, we finally arrive at

$$\det(\mathcal{O}) = \text{sgn}[\text{pf}(A)] \quad (\text{A.62})$$

Namely,

$$\begin{aligned}
 P_{\text{BdG}}|\Omega_{\text{canonical}}\rangle &= \det(\mathcal{O})|\Omega_{\text{canonical}}\rangle \\
 &= \text{sgn}[\text{pf}(A)]|\Omega_{\text{canonical}}\rangle
 \end{aligned}
 \tag{A.63}$$

A.2 Vector potential and gauge invariance

In this section we address the question of how to understand the Peierls substitution in BdG Hamiltonian.

Although the superconductivity order parameter appears to break the U(1) gauge symmetry, all physical observables are still gauge invariant. More explicitly, consider a general tight-binding BdG Hamiltonian

$$H = \sum_{ij,\alpha\beta} \left(t_{ij}^{\alpha\beta} c_{i\alpha}^\dagger c_{j\beta} + \Delta_{ij,\alpha\beta} c_{i\alpha} c_{j\beta} - \frac{\mu}{2} c_{i\alpha}^\dagger c_{i\alpha} + \text{h.c.} \right) \equiv \frac{1}{2} C^\dagger h C \quad (\text{A.64})$$

where i, j label position, α, β label any internal degrees of freedom, and $C = (\{c_{i\alpha}\}, \{c_{i\alpha}^\dagger\})^T$. H has the eigensolutions

$$H|\psi_n\rangle = \epsilon_n|\psi_n\rangle \quad (\text{A.65})$$

$$|\psi_n\rangle = d_{\psi_n}^\dagger |\Omega\rangle = \sum_{i\alpha\sigma} c_{i\alpha}^\sigma |\Omega\rangle U_{i\alpha\sigma,n}$$

where $|\Omega\rangle$ is the BCS ground state, $\sigma = \pm$ distinguishes the creation (particle) and annihilation (creation for hole) operators, and U is a Bogoliubov transformation matrix which is unitary for fermions. Substituting $|\psi\rangle$ into the eigenequation leads to

$$U^\dagger h U = \text{Diag}[\{\epsilon_n\}] \quad (\text{A.66})$$

where the pairing potential satisfies the gap equation

$$\begin{aligned} \Delta_{ij,\alpha\beta} &= Z^{-1} \text{Tr}[V_{j\beta,i\alpha} c_{j\beta}^\dagger c_{i\alpha}^\dagger e^{-\frac{1}{k_B T} H}] \\ &= \sum_n f(\epsilon_n) (U^\dagger \mathbb{V} U)_{nn} \end{aligned} \quad (\text{A.67})$$

where \mathbb{V} is a matrix with the only nonzero element being $\mathbb{V}_{j\beta+,i\alpha-} = V_{j\beta,i\alpha}$, f is the Fermi-Dirac distribution function.

We now show that physical observables are gauge invariant. A gauge transformation corresponds to

$$\mathbf{A} \rightarrow \mathbf{A}' = \mathbf{A} + \nabla\chi \quad (\text{A.68})$$

where \mathbf{A} is the vector potential. \mathbf{A} enters the tight-binding Hamiltonian implicitly through the Peierls substitution:

$$c_{i\alpha}^\dagger \rightarrow \tilde{c}_{i\alpha}^\dagger = e^{-\frac{ie}{\hbar} \int_0^{\mathbf{r}_i} \mathbf{A} \cdot d\mathbf{l}} c_{i\alpha}^\dagger \quad (\text{A.69})$$

and we can understand Eq. (A.64) as that written for certain \mathbf{A} already absorbed into the definitions of t and Δ . The gauge transformation leads to

$$c_{i\alpha}^\dagger \rightarrow c_{i\alpha}^\dagger e^{-\frac{ie}{\hbar} \chi_i} \quad (\text{A.70})$$

The Hamiltonian therefore becomes

$$\begin{aligned} H \rightarrow H' &= \sum_{ij,\alpha\beta} \left[t_{ij}^{\alpha\beta} e^{-\frac{ie}{\hbar}(\chi_i - \chi_j)} c_{i\alpha}^\dagger c_{j\beta} + \Delta_{ij,\alpha\beta} e^{\frac{ie}{\hbar}(\chi_i + \chi_j)} c_{i\alpha} c_{j\beta} - \frac{\mu}{2} c_{i\alpha}^\dagger c_{i\alpha} + \text{h.c.} \right] \\ &= \frac{1}{2} C^\dagger U_\chi h U_\chi^\dagger C \end{aligned} \quad (\text{A.71})$$

where

$$U_\chi = \text{Diag}[\{e^{-\frac{ie}{\hbar} \chi_i}\}, \{e^{\frac{ie}{\hbar} \chi_i}\}] \quad (\text{A.72})$$

As a result, the BdG eigenvalues as well as all other physical observables represented in terms of Bogoliubov quasiparticles are invariant under the gauge transformation.

The above derivation includes, however, an assumption. Namely the pairing potential $\Delta_{ij,\alpha\beta}$ stays unchanged. This is indeed the case, since

$$\begin{aligned}
\Delta'_{ij,\alpha\beta} &= Z'^{-1} \text{Tr}[V_{j\beta,i\alpha} c_{j\beta}^\dagger c_{i\alpha}^\dagger e^{-\frac{ie}{\hbar}(\chi_i + \chi_j)} e^{-\frac{1}{k_B T} H'}] \\
&= \sum_n f(\epsilon_n) (U^\dagger U_\chi^\dagger U_\chi \mathbb{V} U_\chi^\dagger U_\chi U) \\
&= \Delta_{ij,\alpha\beta}
\end{aligned} \tag{A.73}$$

A.3 Analytic solution of the Kitaev triangle

In this section we present some analytic results related to the Kitaev triangle.

We start from the 1D Kitaev chain Hamiltonian with complex nearest-neighbor hopping $-te^{i\phi}$ and p -wave pairing $\Delta e^{i\theta}$ in the Kitaev limit ($t = \Delta > 0, \mu = 0$):

$$H = \sum_n \left(-te^{i\phi} c_n^\dagger c_{n+1} + \Delta e^{i\theta} c_n c_{n+1} + \text{h.c.} \right) \tag{A.74}$$

In the Majorana fermion basis $a_n = c_n + c_n^\dagger$, $b_n = -i(c_n - c_n^\dagger)$ the Hamiltonian becomes

$$H = -\frac{it}{2} \sum_n \left[(S_\phi - S_\theta) a_n a_{n+1} + (S_\phi + S_\theta) b_n b_{n+1} + (C_\phi - C_\theta) a_n b_{n+1} - (C_\phi + C_\theta) b_n a_{n+1} \right] \tag{A.75}$$

where $S_\phi \equiv \sin \phi$, $C_\phi \equiv \cos \phi$, etc. Therefore, when $\phi = \theta$, a_n becomes decoupled from a_{n+1} and b_{n+1} , and a_1 drops out from the Hamiltonian. Similarly, when $\phi = \theta + \pi$, b_1 becomes isolated. To find the other MZM, we note that when $\phi = \theta$, terms involving a_N and b_N in the Hamiltonian are

$$H_N = -it b_{N-1} (S_\phi b_N - C_\phi a_N). \tag{A.76}$$

Considering the unitary transformation

$$\begin{pmatrix} a'_N \\ b'_N \end{pmatrix} \equiv \begin{pmatrix} C_\phi & -S_\phi \\ S_\phi & C_\phi \end{pmatrix} \begin{pmatrix} a_N \\ b_N \end{pmatrix} \quad (\text{A.77})$$

we have

$$H_N = i t b_{N-1} a'_N \quad (\text{A.78})$$

Therefore the other MZM is $b'_N = S_\phi a_N + C_\phi b_N$. Similarly, when $\phi = \theta + \pi$ the other MZM is $a'_N \equiv C_\phi a_N - S_\phi b_N$.

We now consider the three edges of the Kitaev triangle separately. The MZM due to each edge are respectively

$$1-2: \quad a_1, b_2 \quad (\text{A.79})$$

$$2-3: \quad b_2, \frac{1}{2}a_3 + \frac{\sqrt{3}}{2}b_3$$

$$3-1: \quad a_1, \frac{\sqrt{3}}{2}a_3 + \frac{1}{2}b_3$$

One can therefore see that the two MZM at site 3 are not compatible with each other. To get the non-MZM eigenstates, we write down the remaining terms of the Hamiltonian in the Majorana

basis

$$H = -\frac{it}{2} \left(-2b_1 a_2 - \sqrt{3} a_2 a_3 + a_2 b_3 + \sqrt{3} b_1 b_3 - b_1 a_3 \right) \quad (\text{A.80})$$

$$= \frac{1}{2} (b_1, a_2, a_3, b_3) h \begin{pmatrix} b_1 \\ a_2 \\ a_3 \\ b_3 \end{pmatrix}$$

$$h \equiv -it \begin{pmatrix} 0 & -1 & -\frac{1}{2} & \frac{\sqrt{3}}{2} \\ 1 & 0 & -\frac{\sqrt{3}}{2} & \frac{1}{2} \\ \frac{1}{2} & \frac{\sqrt{3}}{2} & 0 & 0 \\ -\frac{\sqrt{3}}{2} & -\frac{1}{2} & 0 & 0 \end{pmatrix} = t \left(-\frac{1}{2} \sigma_0 \tau_y - \frac{1}{2} \sigma_z \tau_y - \frac{1}{2} \sigma_y \tau_z + \frac{\sqrt{3}}{2} \sigma_x \tau_y \right)$$

h has the following symmetry:

$$O = \left(\frac{\sqrt{3}}{2} \sigma_x - \frac{1}{2} \sigma_z \right) \tau_y \quad (\text{A.81})$$

We therefore rotate the Hamiltonian so that O becomes diagonal using the following unitary operator

$$U = e^{-\frac{i\pi}{3} \sigma_y} \otimes e^{i\frac{\pi}{4} \tau_x} \quad (\text{A.82})$$

which leads to

$$U^\dagger O U = \text{Diag}(1, -1, -1, 1) \quad (\text{A.83})$$

U therefore block-diagonalizes h as

$$U^\dagger h U = \frac{t}{2} \begin{pmatrix} 1 & & -1 \\ & -1 & 1 \\ & 1 & -3 \\ -1 & & 3 \end{pmatrix} \quad (\text{A.84})$$

which can then be diagonalized by

$$V = \begin{pmatrix} \frac{1+\sqrt{2}}{\sqrt{4+2\sqrt{2}}} & 0 & \frac{1-\sqrt{2}}{\sqrt{4-2\sqrt{2}}} & 0 \\ 0 & \frac{1+\sqrt{2}}{\sqrt{4+2\sqrt{2}}} & 0 & \frac{1-\sqrt{2}}{\sqrt{4-2\sqrt{2}}} \\ 0 & \frac{1}{\sqrt{4+2\sqrt{2}}} & 0 & \frac{1}{\sqrt{4-2\sqrt{2}}} \\ \frac{1}{\sqrt{4+2\sqrt{2}}} & 0 & \frac{1}{\sqrt{4-2\sqrt{2}}} & 0 \end{pmatrix} \quad (\text{A.85})$$

as

$$V^\dagger U^\dagger h U V = t \times \text{Diag} \left(1 - \frac{\sqrt{2}}{2}, -1 + \frac{\sqrt{2}}{2}, 1 + \frac{\sqrt{2}}{2}, -1 - \frac{\sqrt{2}}{2} \right) \quad (\text{A.86})$$

We therefore have the two lowest excited states

$$\begin{aligned} \psi_{+1} &= (b_1, a_2, a_3, b_3) U \begin{pmatrix} \frac{1+\sqrt{2}}{\sqrt{4+2\sqrt{2}}} \\ 0 \\ 0 \\ \frac{1}{\sqrt{4+2\sqrt{2}}} \end{pmatrix} = (b_1, a_2, a_3, b_3) \times \frac{1}{4\sqrt{2+\sqrt{2}}} \begin{pmatrix} 1 + \sqrt{2} - \sqrt{3}i \\ (1 + \sqrt{2})i - \sqrt{3} \\ i + \sqrt{3} + \sqrt{6} \\ 1 + (\sqrt{3} + \sqrt{6})i \end{pmatrix} \\ \psi_{-1} &= (b_1, a_2, a_3, b_3) U \begin{pmatrix} 0 \\ \frac{1+\sqrt{2}}{\sqrt{4+2\sqrt{2}}} \\ \frac{1}{\sqrt{4+2\sqrt{2}}} \\ 0 \end{pmatrix} = (b_1, a_2, a_3, b_3) \times \frac{1}{4\sqrt{2+\sqrt{2}}} \begin{pmatrix} (1 + \sqrt{2})i - \sqrt{3} \\ 1 + \sqrt{2} - \sqrt{3}i \\ 1 + (\sqrt{3} + \sqrt{6})i \\ i + \sqrt{3} + \sqrt{6} \end{pmatrix} \end{aligned} \quad (\text{A.87})$$

The first excited states can therefore be understood as a hybridization between the “bulk” states of the 1-2 bond and the fermion on site 3.

We next consider the braiding process and particularize to the $\phi_1 \rightarrow \phi_2$ step. The Hamiltonian in the fermion basis becomes

$$\begin{aligned}
H = & -e^{ix} c_1^\dagger c_2 + c_1 c_2 + e^{-ix} c_1 c_2^\dagger - c_1^\dagger c_2^\dagger \\
& + -e^{-\frac{\pi}{3}i} c_2^\dagger c_3 + e^{\frac{2\pi}{3}i} c_2 c_3 + e^{\frac{\pi}{3}i} c_2 c_3^\dagger - e^{-\frac{2\pi}{3}i} c_2^\dagger c_3^\dagger \\
& + e^{(-\frac{\pi}{3}-x)i} c_1 c_3^\dagger - e^{-\frac{2\pi}{3}i} c_1 c_3 - e^{(\frac{\pi}{3}+x)i} c_1^\dagger c_3 + e^{\frac{2\pi}{3}i} c_1^\dagger c_3^\dagger
\end{aligned} \tag{A.88}$$

where we have temporarily omitted the energy unit t . We then have

$$\begin{aligned}
[c_1^\dagger, H] &= c_2 + e^{-ix} c_2^\dagger + e^{(-\frac{\pi}{3}-x)i} c_3^\dagger - e^{-\frac{2\pi}{3}i} c_3 \\
[c_1, H] &= -e^{ix} c_2 - c_2^\dagger - e^{(\frac{\pi}{3}+x)i} c_3 + e^{\frac{2\pi}{3}i} c_3^\dagger \\
&= -e^{ix} \left[c_2 + e^{-ix} c_2^\dagger - e^{-\frac{2\pi}{3}i} c_3 + e^{(-\frac{\pi}{3}-x)i} c_3^\dagger \right]
\end{aligned} \tag{A.89}$$

Therefore

$$[e^{\frac{ix}{2}} c_1^\dagger + e^{-\frac{ix}{2}} c_1, H] = 0 \tag{A.90}$$

Namely we have an MZM:

$$\tilde{a}_1 \equiv e^{\frac{ix}{2}} c_1^\dagger + e^{-\frac{ix}{2}} c_1 = \frac{1}{2} e^{\frac{ix}{2}} (a_1 - ib_1) + \frac{1}{2} e^{-\frac{ix}{2}} (a_1 + ib_1) = C_{\frac{x}{2}} a_1 + S_{\frac{x}{2}} b_1 \tag{A.91}$$

To find the other MZM, we calculate the commutators between the other fermion operators with the Hamiltonian:

$$\begin{aligned}
[c_2^\dagger, H] &= e^{ix} c_1^\dagger - c_1 - e^{-\frac{i\pi}{3}} c_3 + e^{\frac{i\pi}{3}} c_3^\dagger \\
[c_2, H] &= -e^{-ix} c_1 + c_1^\dagger + e^{\frac{i\pi}{3}} c_3^\dagger - e^{-\frac{i\pi}{3}} c_3 \\
[c_3^\dagger, H] &= e^{-\frac{i\pi}{3}} c_2^\dagger + e^{-\frac{i\pi}{3}} c_2 - e^{\frac{i\pi}{3}} c_1 + e^{i(\frac{\pi}{3}+x)} c_1^\dagger \\
[c_3, H] &= -e^{\frac{i\pi}{3}} c_2 - e^{\frac{i\pi}{3}} c_2^\dagger + e^{-\frac{i\pi}{3}} c_1^\dagger - e^{-i(\frac{\pi}{3}+x)} c_1
\end{aligned} \tag{A.92}$$

Therefore

$$\begin{aligned}
[c_2 - c_2^\dagger, H] &= (1 - e^{-ix}) c_1 + (1 - e^{ix}) c_1^\dagger \\
[e^{\frac{i\pi}{6}} (e^{i\frac{2\pi}{3}} c_3^\dagger + c_3), H] &= e^{\frac{i\pi}{6}} (1 - e^{-i(\frac{\pi}{3}+x)}) c_1 + e^{-\frac{i\pi}{6}} (1 - e^{i(\frac{\pi}{3}+x)}) c_1^\dagger
\end{aligned} \tag{A.93}$$

However

$$-\frac{1 - e^{-ix}}{e^{\frac{i\pi}{6}} (1 - e^{-i(\frac{\pi}{3}+x)})} = -\frac{2 - 2\cos x}{e^{\frac{i\pi}{6}} (1 - e^{-i(\frac{\pi}{3}+x)}) (1 - e^{ix})} = \frac{1 - \cos x}{\cos(x + \frac{\pi}{6}) - \frac{\sqrt{3}}{2}} \tag{A.94}$$

Thus the following is the other MZM:

$$\begin{aligned}
\tilde{b}_{23} &\equiv -iN \left(\left[\cos\left(x + \frac{\pi}{6}\right) - \frac{\sqrt{3}}{2} \right] (c_2 - c_2^\dagger) + (1 - \cos x) \left(e^{\frac{i\pi}{6}} c_3 - e^{-\frac{i\pi}{6}} c_3^\dagger \right) \right) \\
&= N \left(\left[\cos\left(x + \frac{\pi}{6}\right) - \frac{\sqrt{3}}{2} \right] b_2 + (1 - \cos x) \left(\frac{1}{2} a_3 + \frac{\sqrt{3}}{2} b_3 \right) \right)
\end{aligned} \tag{A.95}$$

where N is a normalization factor. When $x = 0$ only the first term survives since

$$\lim_{x \rightarrow 0} \frac{1 - \cos x}{\cos(x + \frac{\pi}{6}) - \frac{\sqrt{3}}{2}} = 0 \tag{A.96}$$

while when $x = -\frac{\pi}{3}$ only the second term survives.

A.4 Kitaev Triangle and Peierls substitution

We start with a spinless or spin-polarized p -wave superconductor

$$\mathcal{H} = \sum_{\langle j,l \rangle} (-tc_j^\dagger c_l + \Delta e^{i\theta_{jl}} c_j c_l + h.c.) - \sum_j \mu c_j^\dagger c_j, \quad (\text{A.97})$$

where t is the hopping amplitude, Δ is the amplitude of (2D) p -wave pairing, μ is the chemical potential, θ_{jl} is the polar angle of $\mathbf{r}_{jl} = \mathbf{r}_l - \mathbf{r}_j$, consistent with $\{c_l^\dagger, c_j^\dagger\} = 0$.

We will now include a gauge potential via a Peierls substitution as

$$\begin{aligned} c_j^\dagger &\rightarrow c_j^\dagger \exp\left(-\frac{ie}{\hbar} \int_0^{\mathbf{r}_j} \mathbf{A} \cdot d\mathbf{l}\right), \\ c_j^\dagger c_l &\rightarrow c_j^\dagger c_l \exp\left(\frac{ie}{\hbar} \int_{\mathbf{r}_j}^{\mathbf{r}_l} \mathbf{A} \cdot d\mathbf{l}\right) \\ &\rightarrow c_l^\dagger c_j e^{i\phi_{jl}}, \\ \phi_{jl} &= \frac{e}{\hbar} \int_{\mathbf{r}_j}^{\mathbf{r}_l} \mathbf{A} \cdot d\mathbf{l} = -\phi_{lj} \end{aligned} \quad (\text{A.98})$$

The modified Hamiltonian is then

$$\mathcal{H} = \sum_{\langle j,l \rangle} (-te^{i\phi_{jl}} c_j^\dagger c_l + \Delta e^{i\theta_{jl}} c_j c_l + h.c.) - \sum_j \mu c_j^\dagger c_j, \quad (\text{A.99})$$

The complex fermion operator can be written in the Majorana Fermion basis, a superposition of two Majorana fermions $c_j = \frac{1}{2}(a_j + ib_j)$. Due to the nature of Majorana fermions, $a_j^\dagger = a_j$, the creation operator is $c_j^\dagger = \frac{1}{2}(a_j - ib_j)$. It is quickly seen after substitution we arrive at

$$c_j^\dagger c_j = \frac{1}{2}(1 + i a_j b_j), \quad (\text{A.100})$$

$$c_j^\dagger c_l = \frac{1}{4}(a_j a_l + b_j b_l + i a_j b_l - i b_j a_l), \quad (\text{A.101})$$

$$c_j c_l = \frac{1}{4}(a_j a_l - b_j b_l + i a_j b_l + i b_j a_l). \quad (\text{A.102})$$

The hopping term in MF basis are

$$-t(e^{i\phi_{jl}} c_j^\dagger c_l + e^{-i\phi_{jl}} c_l^\dagger c_j) = -\frac{it}{2}(\sin\phi_{jl}(a_j a_l + b_j b_l) + \cos\phi_{jl}(a_j b_l - b_j a_l)), \quad (\text{A.103})$$

the order parameter terms are

$$\Delta(e^{i\theta_{jl}} c_j^\dagger c_l^\dagger + e^{-i\theta_{jl}} c_j c_l) = \frac{i\Delta}{2}(\sin\theta_{jl}(a_l a_j - b_l b_j) + \cos\theta_{jl}(a_l b_j + b_l a_j)). \quad (\text{A.104})$$

Our Hamiltonian in MF basis is then

$$\begin{aligned} \mathcal{H} = & -\frac{i}{2} \sum_{\langle j,l \rangle} [(t \sin\phi_{jl} - \Delta \sin\theta_{jl}) a_j a_l + (t \sin\phi_{jl} + \Delta \sin\theta_{jl}) b_j b_l \\ & + (t \cos\phi_{jl} - \Delta \cos\theta_{jl}) a_j b_l - (t \cos\phi_{jl} + \Delta \cos\theta_{jl}) b_j a_l] \\ & - \frac{i\mu}{2} \sum_j a_j b_j \end{aligned} \quad (\text{A.105})$$

For concreteness we consider a 1-D chain in the Kitaev limit $t = \Delta$, $\mu = 0$, and choose $\phi_{jl} = 0$ (either zero or a perpendicular gauge potential). The Kitaev chain is resultant with $\mathcal{H} = -\sum_{j,j+1} i t b_j a_{j+1}$ and hosting MZM a_1 and b_N .

Appendix B

Floquet Landau levels

B.1 Quantum harmonic oscillator

We will quickly derive this energy solution and derive ladder operators. Rewrite the quantum harmonic oscillator as (and dropping the operator hat)

$$H = \frac{1}{2m} (p_x^2 + m^2 \omega^2 x^2),$$

then complete the square by adding "zero"

$$\begin{aligned} H &= \frac{1}{2m} ([m\omega x - i p_x][m\omega x + i p_x] - i m\omega [x p_x - p_x x]) \\ &= \frac{1}{2m} ([m\omega x - i p_x][m\omega + i p_x] + m\hbar\omega) \\ &= \frac{1}{2m} (\tilde{a}^\dagger \tilde{a} + m\hbar\omega) \\ &= \hbar\omega \left(\frac{\tilde{a}^\dagger \tilde{a}}{2m\hbar\omega} + \frac{1}{2} \right) \\ &= \hbar\omega \left(a^\dagger a + \frac{1}{2} \right), \end{aligned} \tag{B.1}$$

where $a = \frac{1}{\sqrt{2}} \left(\sqrt{\frac{m\omega}{\hbar}} x + i \frac{p_x}{\sqrt{m\hbar\omega}} \right)$. We have simplified the Hamiltonian into new creation and annihilation operators, called ladder operators, which we will now show how they work. Also note $[a, a^\dagger] = 1$. Let looks at how the operator commutes with the Hamiltonian

$$\begin{aligned}
[H, a] &= Ha - aH = \hbar\omega \left(a^\dagger aa + \frac{a}{2} - aa^\dagger a - \frac{a}{2} \right) \\
&= \hbar\omega(a^\dagger a - (1 + a^\dagger a))a \\
&= -\hbar\omega a, \quad \text{and}
\end{aligned} \tag{B.2}$$

$$\begin{aligned}
[H, a^\dagger] &= Ha^\dagger - a^\dagger H = \hbar\omega \left(a^\dagger aa^\dagger + \frac{a^\dagger}{2} - a^\dagger a^\dagger a - \frac{a^\dagger}{2} \right) \\
&= \hbar\omega a^\dagger (aa^\dagger - a^\dagger a) \\
&= \hbar\omega a^\dagger.
\end{aligned} \tag{B.3}$$

SOME TRANSITION TO ACTING Ha on Psi.

$$\begin{aligned}
H|\psi_n\rangle &= E_n|\psi_n\rangle. \\
Ha^\dagger|\psi_n\rangle &= (a^\dagger H + \hbar\omega a^\dagger)|\psi_n\rangle \\
Ha^\dagger|\psi_n\rangle &= (E_n + \hbar\omega)a^\dagger|\psi_n\rangle. \\
Ha|\psi_n\rangle &= (E_n - \hbar\omega)a|\psi_n\rangle.
\end{aligned} \tag{B.4}$$

Being careful notice

$$\begin{aligned}
H|\psi_0\rangle &= E_0|\psi_0\rangle \\
Ha|\psi_0\rangle &= (E_0 - \hbar\omega)a|\psi_0\rangle,
\end{aligned} \tag{B.5}$$

however, E_0 is the minimum so $E_0 - \hbar\omega$ cannot exist and thus

$$a|\psi_0\rangle = 0 \quad (\text{B.6})$$

Again we look at the ground state energy

$$\begin{aligned} \langle\psi_0|H|\psi_0\rangle &= \langle\psi_0|\hbar\omega(a^\dagger a + 1/2)|\psi_0\rangle \\ E_0 &= \hbar\omega\langle\psi_0|a^\dagger a|\psi_0\rangle + \frac{\hbar\omega}{2}\langle\psi_0|\psi_0\rangle \\ E_0 &= \frac{\hbar\omega}{2}. \end{aligned} \quad (\text{B.7})$$

Then for the given eigenstates

$$a^\dagger|\psi_0\rangle, \quad a^\dagger a^\dagger|\psi_0\rangle, \quad a^\dagger a^\dagger a^\dagger|\psi_0\rangle, \quad \dots$$

with eigenvalues

$$\frac{3}{2}\hbar\omega, \quad \frac{5}{2}\hbar\omega, \quad \frac{7}{2}\hbar\omega, \quad \dots$$

Which we can generalize to

$$|\psi_n\rangle \propto (a^\dagger)^n|\psi_0\rangle,$$

with the eigenenergy

$$E_n = \hbar\omega\left(n + \frac{1}{2}\right).$$

With our goal complete we continue on to determine how the ladder operators evolve the state.

We can now renormalize our proportional expression

$$|\psi_{n+1}\rangle = c a^\dagger |\psi_n\rangle$$

$$1 = \langle \psi_{n+1} | \psi_{n+1} \rangle = |c|^2 (\langle \psi_n | a^\dagger) (a^\dagger | \psi_n \rangle)$$

$$= |c|^2 \langle \psi_n | a a^\dagger | \psi_n \rangle$$

$$= |c|^2 \langle \psi_n | \frac{H}{\hbar\omega} + \frac{1}{2} | \psi_n \rangle$$

$$= |c|^2 \left(\frac{E_n}{\hbar\omega} + \frac{1}{2} \right)$$

$$= |c|^2 (n+1)$$

$$|c| = \frac{1}{\sqrt{n+1}}$$

which give the following relation

$$|\psi_{n+1}\rangle = \frac{a^\dagger}{\sqrt{n+1}} |\psi_n\rangle. \quad (\text{B.8})$$

Similarly we find

$$|\psi_{n-1}\rangle = \frac{a}{\sqrt{n}} |\psi_n\rangle. \quad (\text{B.9})$$

Thus $a^\dagger a |\psi_n\rangle = n |\psi_n\rangle$. The energy of the system is definitively

$$E_n = \hbar\omega \left(n + \frac{1}{2} \right) \quad (\text{B.10})$$

B.2 Dirac equation in the presence of a magnetic field

We now focus on how the presence of a magnetic field affects the Dirac equation. The Dirac Hamiltonian with vector potential

$$\mathcal{H} = v_f \boldsymbol{\sigma} \cdot (\hat{\mathbf{p}} - q\hat{\mathbf{A}}) \quad (\text{B.11})$$

Using the previous definition, $\mathbf{A} = Bx\mathbf{y}$, the Hamiltonian becomes

$$\mathcal{H} = v_f \sigma_x \hat{p}_x + v_f \sigma_y (\hat{p}_y - qB\hat{x}) \quad (\text{B.12})$$

Like Schrodinger's equation we use the same ansatz wavefunction and arrive at

$$\begin{aligned} \mathcal{H} &= v_f \sigma_x \hat{p}_x - v_f \sigma_y (qB\hat{x} - \hbar k_y) \\ \mathcal{H} &= v_f \sigma_x \hat{p}_x - v_f \sigma_y qB\hat{x}, \end{aligned} \quad (\text{B.13})$$

where we recognize the x term is just shifted by a constant like earlier. In matrix form the Hamiltonian looks like

$$\begin{aligned} \mathcal{H} &= i v_f qB \begin{bmatrix} 0 & \hat{x} - i \frac{\hat{p}_x}{qB} \\ \hat{x} + i \frac{\hat{p}_x}{qB} & 0 \end{bmatrix} \\ \mathcal{H} &= i v_f \sqrt{2m\hbar\omega} \begin{bmatrix} 0 & a^\dagger \\ a & 0 \end{bmatrix} \end{aligned}$$

The form of the Hamiltonian can be quickly solved by squaring then acting on a wavefunction

$$|\mathcal{H}|^2 = 2m\hbar\omega v_f^2 \begin{bmatrix} a^\dagger a & 0 \\ 0 & a a^\dagger \end{bmatrix}$$

We focus on the first element of the matrix

$$\begin{aligned}
\langle \psi_n | |\mathcal{H}_{11}|^2 | \psi_n \rangle &= \langle \psi_n | E_n^2 | \psi_n \rangle \\
&= 2m\hbar\omega v_f^2 \langle \psi_n | a^\dagger a | \psi_n \rangle \\
&= 2m\hbar\omega v_f^2 \langle \psi_n | n | \psi_n \rangle \\
E_n^2 &= 2m\hbar\omega n v_f^2 \\
E_n &= \pm v_f \sqrt{2m\hbar\omega n}
\end{aligned} \tag{B.14}$$

B.3 Van-Vleck expansion of modulated circularly polarized light on a 2DEG

We start with the Schrodinger equation in 2D with a vector potential field

$$H(t) = \frac{1}{2m} [(p_x - qA_x(t))^2 + (p_y - qA_y(t))^2] \tag{B.15}$$

where $\mathbf{A}(t) = \langle -V_1 \sin \omega t, V_2 \cos \omega t \rangle$, $V_1 = E/\omega$ and $V_2 = V_1 \cos Kx$. Which is made up of two electromagnetic wave sources. The time dependent Hamiltonian becomes

$$H(t) = \frac{1}{2m} \left[p_x^2 + p_y^2 + 2qV_1 \sin \omega t p_x - 2qV_2 \cos \omega t p_y + \frac{q^2(V_1^2 + V_2^2)}{2} - \frac{q^2(V_1^2 - V_2^2)}{2} \cos 2\omega t \right]. \tag{B.16}$$

The Van Vleck expansion uses a high frequency expansion from degenerate perturbation. The Hamiltonian of such an expansion is as follows

$$H = H^{F(0)} + H^{F(1)} + H^{F(2)} + H^{F(3)} + \dots \tag{B.17}$$

where each term is a Floquet Hamiltonian

$$H^{F(0)} = 0 \quad (\text{B.18})$$

$$H^{F(1)} = H_0 \quad (\text{B.19})$$

$$H^{F(2)} = \sum_{m \neq 0} \frac{[H_m, H_{-m}]}{m\hbar\omega} \quad (\text{B.20})$$

$$H^{F(3)} = \sum_{m \neq 0} \left(\frac{[H_{-m}, [H_0, H_m]]}{2(m\hbar\omega)^2} + \sum_{m' \neq 0, m} \frac{[H_{-m'}, [H_{m'-m}, H_m]]}{3mm'(\hbar\omega)^2} \right) \quad (\text{B.21})$$

The H_m terms are Fourier time-domain transforms of the time dependent Hamiltonian

$$H_n = \frac{1}{T} \int_0^T H(t) e^{-in\omega t} dt = H_{-n}^\dagger \quad (\text{B.22})$$

Notice our Hamiltonian has modes $m = [-2, 2]$, due to orthogonality we need only compute three integrals.

$$H_0 = \frac{1}{2m} \left(p_x^2 + p_y^2 + \frac{q^2}{2} (V_1^2 + V_2^2) \right) \quad (\text{B.23})$$

$$H_{\pm 1} = -\frac{1}{2m} (qV_2 p_y \pm iqV_1 p_x) \quad (\text{B.24})$$

$$H_{\pm 2} = -\frac{1}{2m} \left(\frac{q^2}{4} (V_1^2 - V_2^2) \right) \quad (\text{B.25})$$

We can now begin writing out all the commutator relations seen above. Some of the commutators are related by transpose or Hermitian conjugate. As an example in $H^{F(2)}$ the transpose reduces the sum down by

$$\frac{[H_m, H_{-m}]}{m\hbar\omega} + \frac{[H_{-m}, H_m]}{-m\hbar\omega} = \frac{[H_m, H_{-m}]}{m\hbar\omega} + \frac{[H_m, H_{-m}]}{m\hbar\omega} \quad (\text{B.26})$$

$$= 2 \frac{[H_m, H_{-m}]}{m\hbar\omega} \quad (\text{B.27})$$

Alternatively, an example in $H^{F(3)}$ the Hermitian conjugate reduces the sum down by

$$\begin{aligned} [H_{-m'}, [H_{m'-m}, H_m]]^\dagger &= [[H_{m'-m}, H_m]^\dagger, H_{-m'}^\dagger] \\ &= [[H_m^\dagger, H_{m'-m}^\dagger], H_{m'}] \\ &= [[H_{-m}, H_{m-m'}], H_{m'}] \\ &= [H_{m'}, [H_{m-m'}, H_{-m}]] \end{aligned} \quad (\text{B.28})$$

or in general the following identity

$$[A, [B, C]]^\dagger = [A^\dagger, [B^\dagger, C^\dagger]]. \quad (\text{B.29})$$

With the symmetry in modes we have the following simplification

$$[H_{-m'}, [H_{m'-m}, H_m]] + [H_{m'}, [H_{m-m'}, H_{-m}]] = [H_{-m'}, [H_{m'-m}, H_m]] + h.c. \quad (\text{B.30})$$

We now focus on the $H^{F(2)}$ term which looks like

$$H^{F(2)} = \frac{2}{\hbar\omega} ([H_1, H_{-1}] + \frac{1}{2}[H_2, H_{-2}]) \quad (\text{B.31})$$

$$\begin{aligned}
[H_1, H_{-1}] &= \frac{q^2}{4m^2} [qV_2p_y + iV_1p_x, qV_2p_y - iV_1p_x] \\
&= \frac{iq^2V_1p_y}{4m^2} ([p_x, V_2] - [V_2, p_x]) \\
&= -\frac{iq^2V_1p_y}{2m^2} [V_2, p_x] \\
&= \frac{\hbar q^2V_1p_y}{2m^2} \partial_x V_2
\end{aligned}$$

$$[H_2, H_{-2}] = \frac{q^4}{64m^2} [V_1^2 - V_2^2, V_1^2 - V_2^2] = 0 \quad (\text{B.32})$$

$$H^{F(2)} = \frac{q^2V_1p_y}{m^2\omega} \partial_x V_2 \quad (\text{B.33})$$

For the 3rd order terms there are several combinations that end up being zero because they require $H_{|m|\geq 3}$ which are zero from our earlier Fourier transforms. We need compute the following commutations:

$$[H_1, [H_0, H_{-1}]] \quad (\text{B.34})$$

$$[H_2, [H_0, H_{-2}]] \quad (\text{B.35})$$

$$[H_1, [H_1, H_{-2}]] \quad (\text{B.36})$$

$$[H_2, [H_{-1}, H_{-1}]] \quad (\text{B.37})$$

$$[H_{-1}, [H_2, H_{-1}]]. \quad (\text{B.38})$$

$$\begin{aligned}
[H_1, [H_0, H_{-1}]] &= \frac{q^2}{8m^3} [V_2 p_y + i V_1 p_x, [p_x^2 + p_y^2 + \frac{q^2}{2} (V_1^2 + V_2^2), V_2 p_y - i V_1 p_x]] \\
&= \frac{q^2}{8m^3} [V_2 p_y + i V_1 p_x, p_y [p_x^2, V_2] - i \frac{q^2}{2} V_1 [V_2^2, p_x]] \\
&= \frac{q^2}{8m^3} (p_y^2 [V_2, [p_x^2, V_2]] + i V_1 p_y [p_x, [p_x^2, V_2]] - i \frac{q^2}{2} V_1 p_y [V_2, [V_2^2, p_x]] + \frac{q^2}{2} V_1^2 [p_x, [V_2^2, p_x]]) \\
[H_1, [H_0, H_{-1}]] + h.c. &= \frac{q^2}{4m^3} (p_y^2 [V_2, [p_x^2, V_2]] + \frac{q^2}{2} V_1^2 [p_x, [V_2^2, p_x]]) \tag{B.39}
\end{aligned}$$

notice, the imaginary term cancels out when considering the Hermitian conjugate.

$$\begin{aligned}
[H_2, [H_0, H_{-2}]] &= \frac{q^4}{128m^3} [V_1^2 - V_2^2, [p_x^2 + p_y^2 + \frac{q^2}{2} (V_1^2 + V_2^2), V_1^2 - V_2^2]] \\
&= -\frac{q^4}{128m^3} [V_1^2 - V_2^2, [p_x^2, V_2^2]] \\
&= \frac{q^4}{128m^3} [V_2^2, [p_x^2, V_2^2]] \\
[H_2, [H_0, H_{-2}]] + h.c. &= \frac{q^4}{64m^3} [V_2^2, [p_x^2, V_2^2]] \tag{B.40}
\end{aligned}$$

$$\begin{aligned}
[H_1, [H_1, H_{-2}]] &= -\frac{q^4}{32m^3} [V_2 p_y + i V_1 p_x, [V_2 p_y + i V_1 p_x, V_1^2 - V_2^2]] \\
&= \frac{q^4}{32m^3} [V_2 p_y + i V_1 p_x, i V_1 [p_x, V_2^2]] \\
&= \frac{q^4}{32m^3} V_1 (i p_y [V_2, [p_x, V_2^2]] - V_1 [p_x, [p_x, V_2^2]]) \\
[H_1, [H_1, H_{-2}]] + h.c. &= \frac{q^4 V_1^2}{16m^3} [p_x, [V_2, p_x^2]] \tag{B.41}
\end{aligned}$$

$$\begin{aligned}
[H_2, [H_{-1}, H_{-1}]] &= -\frac{q^4}{32m^3} [V_1^2 - V_2^2, [V_2 p_y - i V_1 p_x, V_2 p_y - i V_1 p_x]] \\
&= -\frac{q^4}{32m^3} [V_1^2 - V_2^2, -i V_1 p_y [V_2, p_x] - i V_1 p_y [p_x, V_2]] \\
&= 0
\end{aligned} \tag{B.42}$$

$$\begin{aligned}
[H_{-1}, [H_2, H_{-1}]] &= -\frac{q^4}{32m^3} [V_2 p_y - i V_1 p_x, [V_1^2 - V_2^2, V_2 p_y - i V_1 p_x]] \\
&= -\frac{q^4}{32m^3} [V_2 p_y - i V_1 p_x, i V_1 [V_2^2, p_x]] \\
&= -\frac{q^4}{32m^3} V_1 (i p_y [V_2, [V_2^2, p_x]] + V_1 [p_x, [V_2^2, p_x]]) \\
[H_{-1}, [H_2, H_{-1}]] + h.c. &= -\frac{q^4 V_1^2}{16m^3} [p_x, [V_2^2, p_x]]
\end{aligned} \tag{B.43}$$

$$\begin{aligned}
H^{F(3)} &= \frac{1}{2\hbar^2\omega^2} [H_{-1}, [H_0, H_1]] + \frac{1}{8\hbar^2\omega^2} [H_{-2}, [H_0, H_2]] + \frac{1}{6\hbar^2\omega^2} [H_1, [H_1, H_{-2}]] \\
&+ \frac{1}{6\hbar^2\omega^2} [H_2, [H_{-1}, H_{-1}]] - \frac{1}{3\hbar^2\omega^2} [H_{-1}, [H_2, H_{-1}]] + h.c.
\end{aligned} \tag{B.44}$$

$$\begin{aligned}
&= \frac{q^2}{8m^3\hbar^2\omega^2} \left(p_y^2 [V_2, [p_x^2, V_2]] + \frac{q^2}{2} V_1^2 [p_x, [V_2^2, p_x]] \right) + \frac{q^4}{8^3 m^3 \hbar^2 \omega^2} [V_2^2, [p_x^2, V_2^2]] \\
&+ \frac{q^4}{96m^3\hbar^2\omega^2} V_1^2 [p_x, [V_2, p_x^2]] + \frac{q^4}{48m^3\hbar^2\omega^2} [p_x, [V_2^2, p_x]]
\end{aligned} \tag{B.45}$$

$$= \frac{q^2 p_y^2}{8m^3\hbar^2\omega^2} [V_2, [p_x^2, V_2]] + \frac{9q^4 V_1^2}{96m^3\hbar^2\omega^2} [p_x, [V_2^2, p_x]] \tag{B.46}$$

The Hamiltonian with $p_y = 0$ becomes

$$\begin{aligned}
H &= \frac{1}{2m} \left(p_x^2 + \frac{q^2}{2} (V_1^2 + V_2^2) \right) + \frac{9q^4 V_1^2}{96m^3 \hbar^2 \omega^2} [p_x, [V_2^2, p_x]] \\
&= \frac{1}{2m} \left(p_x^2 + \frac{q^2}{2} (V_1^2 + V_2^2) \right) - \frac{9q^4 V_1^2}{48m^3 \omega^2} ((\partial_x V_2)^2 + V_2 \partial_x^2 V_2)
\end{aligned} \tag{B.47}$$

Letting $V_2 = \frac{E}{\omega} \sin Kx$, $\partial_x V_2 = \frac{EK}{\omega} \cos Kx$, and $\partial_x^2 V_2 = -\frac{EK^2}{\omega} \sin Kx$ we arrive at

$$H = \frac{1}{2m} \left(p_x^2 + \frac{q^2 E^2}{2\omega^2} (1 + \sin^2 Kx) \right) - \frac{9q^4 E^4 K^2}{48m^3 \omega^6} (\cos^2 Kx - \sin^2 Kx) \tag{B.48}$$

In the limit $Kx \ll 1$ it becomes

$$\begin{aligned}
H &= \frac{1}{2m} \left(p_x^2 + \frac{q^2 E^2}{2\omega^2} (1 + K^2 x^2) \right) - \frac{9q^4 E^4 K^2}{48m^3 \omega^6} (1 - 2K^2 x^2) \\
H &= \frac{1}{2m} \left(p_x^2 + \left(\frac{q^2 E^2 K^2}{2\omega^2} + \frac{9q^4 E^4 K^4}{48m^2 \omega^6} \right) x^2 \right) + \frac{q^2 E^2}{4m\omega^2} - \frac{9q^4 E^4 K^2}{48m^3 \omega^6}
\end{aligned} \tag{B.49}$$

B.4 Tight-binding model 2DEG

We start with a nearest-neighbor single-orbital tight-binding Hamiltonian on a square lattice

$$\mathcal{H} = \sum_{j,l} -h(c_{j,l}^\dagger c_{j+1,l} + c_{j,l}^\dagger c_{j,l+1} + h.c.) \tag{B.50}$$

The incident laser beam as a vector potential is as follows

$$\mathbf{A}(\mathbf{r}, t) = \frac{E}{\omega} \langle -\sin \omega t, \cos(Kx) \cos \omega t \rangle. \tag{B.51}$$

Using the following approximation for smoothly varying vector potential fields

$$\int_{\mathbf{r}_a}^{\mathbf{r}_b} \mathbf{A}(\mathbf{r}, t) \cdot d\mathbf{l} \approx \mathbf{A}\left(\frac{\mathbf{r}_b + \mathbf{r}_a}{2}, t\right) \cdot (\mathbf{r}_b - \mathbf{r}_a) \quad (\text{B.52})$$

and using Peierls substitution the Hamiltonian becomes

$$\mathcal{H}(t) = - \sum_{j,l} (h_{j,j+1}(t) c_{j,l}^\dagger c_{j+1,l} + h_{l,l+1}(t) c_{j,l}^\dagger c_{j,l+1} + h.c.), \quad (\text{B.53})$$

where

$$\begin{aligned} h_{j,j+1}(t) &\approx h \exp\left(-i \frac{eEa}{\hbar\omega} \frac{x_{j+1} - x_j}{a} \sin\omega t\right) \\ &= h \exp(-i\phi_0 \sin\omega t) \end{aligned} \quad (\text{B.54})$$

$$\begin{aligned} h_{l,l+1}(t) &\approx h \exp\left(i \frac{eEa}{\hbar\omega} \frac{y_{l+1} - y_l}{a} \cos(Kx_j) \cos\omega t\right) \\ &= h \exp(i\phi_0 \cos(Kx_j) \cos\omega t). \end{aligned} \quad (\text{B.55})$$

The incident laser beam allows for translation symmetry along the y-axis, so we can reduce the dimension of the Hamiltonian with the following Fourier transform

$$c_{j,l}^\dagger = \frac{1}{\sqrt{N_y}} \sum_k c_{j,k}^\dagger e^{iky \cdot \mathbf{r}_l} = \frac{1}{\sqrt{N_y}} \sum_k c_{j,k}^\dagger e^{ikla}. \quad (\text{B.56})$$

The Hamiltonian then becomes

$$\mathcal{H}(t) = \sum_{j,k} (h_{l,l+1}(t) e^{-ika} + h_{l,l+1}^*(t) e^{ika}) c_{j,k}^\dagger c_{j,k} + (h_{j,j+1}(t) c_{j,k}^\dagger c_{j+1,k} + h.c.) \quad (\text{B.57})$$

$$= \sum_{j,k} 2h \cos(\phi_0 \cos(Kx_j) \cos\omega t - ka) c_{j,k}^\dagger c_{j,k} + (h e^{i\phi_0 \sin\omega t} c_{j,k}^\dagger c_{j+1,k} + h.c.). \quad (\text{B.58})$$

Making use of Floquet theory we can make the Hamiltonian time-independent with the following time Fourier transform

$$\mathcal{H}_{ab,n}(k) = \frac{1}{T} \int_0^T \mathcal{H}_{ab}(k, t) e^{-in\omega t} dt \quad (\text{B.59})$$

$$= \frac{1}{2\pi} \int_0^{2\pi} \mathcal{H}_{ab}(k, t) e^{-in\tau} d\tau \quad (\text{B.60})$$

where a, b represent the matrix index of the previous Hamiltonian and n is the n -th order mode of light. We will make use of the following Hansen-Bessel integral formulas

$$J_n(z) = \frac{1}{2\pi} \int_0^{2\pi} e^{in\tau - z \sin \tau} d\tau = \frac{1}{2\pi} \int_0^{2\pi} e^{in\tau - in\pi/2 + z \cos \tau} d\tau, \quad (\text{B.61})$$

note that the integral bound can be the same due to the integrand being periodic from $[0, 2\pi]$.

Recall, Bessel function identities for $n \in \mathbb{Z}$

$$J_n(-z) = (-1)^n J_n(z) \quad (\text{B.62})$$

$$J_{-n}(z) = (-1)^n J_n(z) \quad (\text{B.63})$$

The terms for given k become the following time Fourier transforms

$$\begin{aligned}
\mathcal{H}_{j,j,n}(k) &= -\frac{h}{2\pi} \int_0^{2\pi} \left(e^{i\phi_0 \cos(Kx_j) \cos \tau - ika - in\tau} + e^{-i\phi_0 \cos(Kx_j) \cos \tau + ika - in\tau} \right) d\tau \\
&= -h \left(\frac{e^{-ika}}{2\pi} \int_0^{2\pi} e^{iz \cos \tau - in\tau} d\tau + \frac{e^{ika}}{2\pi} \int_0^{2\pi} e^{-iz \cos \tau - in\tau} d\tau \right) \\
&= -h \left(\frac{e^{-ika - in\pi/2}}{2\pi} \int_0^{2\pi} e^{iz \cos \tau - in\tau + in\pi/2} d\tau + \frac{e^{ika - in\pi/2}}{2\pi} \int_0^{2\pi} e^{-iz \cos \tau - in\tau + in\pi/2} d\tau \right) \\
&= -he^{-in\pi/2} \left(J_{-n}(z) e^{-ika} + J_{-n}(-z) e^{ika} \right) \\
&= -hJ_n(z) e^{-in\pi/2} (e^{ika} + e^{-ika + in\pi}) \\
&= -hJ_n(z) (e^{i(ka - n\pi/2)} + e^{-i(ka - n\pi/2)}) \\
&= -2hJ_n(\phi_0 \cos(Kx_j)) \cos(ka - n\pi/2)
\end{aligned} \tag{B.64}$$

and

$$\begin{aligned}
\mathcal{H}_{j,j+1,n} &= -\frac{h}{2\pi} \int_0^{2\pi} e^{-i\phi_0 \sin \tau - in\tau} d\tau \\
&= -hJ_{-n}(\phi_0) \\
&= -h(-1)^n J_n(\phi_0)
\end{aligned} \tag{B.65}$$

$$\begin{aligned}
\mathcal{H}_{j+1,j,n} &= -\frac{h}{2\pi} \int_0^{2\pi} e^{i\phi_0 \sin \tau - in\tau} d\tau \\
&= -hJ_{-n}(-\phi_0) \\
&= -hJ_n(\phi_0)
\end{aligned} \tag{B.66}$$

This completes finding all the matrix terms for the quasienergy matrix \bar{Q} for a 2DEG tight binding model with incident inhomogeneous laser light.

B.5 Tight-binding model Dirac

We start with a nearest-neighbor single-orbital tight-binding Hamiltonian

$$\mathcal{H} = - \sum_{jl\alpha, j'l'\beta} hc_{jl\alpha}^\dagger c_{j'l'\beta} + h.c. \quad (\text{B.67})$$

The incident laser beam in vector potential forms looks like

$$\mathbf{A}(\mathbf{r}, t) = \frac{E}{\omega} \langle -\sin \omega t, \frac{1}{2} \sin(Kx) \cos 2\omega t \rangle. \quad (\text{B.68})$$

Using the following approximation for smoothly varying vector potential fields

$$\int_{\mathbf{r}_{j,l}^\alpha}^{\mathbf{r}_{j',l'}^\beta} \mathbf{A}(\mathbf{r}, t) \cdot d\mathbf{l} \approx \mathbf{A} \left(\frac{\mathbf{r}_{j',l'}^\beta + \mathbf{r}_{j,l}^\alpha}{2}, t \right) \cdot (\mathbf{r}_{j',l'}^\beta - \mathbf{r}_{j,l}^\alpha) \quad (\text{B.69})$$

where

$$\mathbf{a}_1 = \sqrt{3}a\mathbf{x} \quad (\text{B.70})$$

$$\mathbf{a}_2 = 3a\mathbf{y} \quad (\text{B.71})$$

$$\mathbf{r}_{jl}^{A_1} = j\mathbf{a}_1 + l\mathbf{a}_2 \quad (\text{B.72})$$

$$\mathbf{r}_{jl}^{B_1} = (j + \frac{1}{2})\mathbf{a}_1 + (l + \frac{1}{6})\mathbf{a}_2 \quad (\text{B.73})$$

$$\mathbf{r}_{jl}^{A_2} = (j + \frac{1}{2})\mathbf{a}_1 + (l + \frac{1}{2})\mathbf{a}_2 \quad (\text{B.74})$$

$$\mathbf{r}_{jl}^{B_2} = (j + 1)\mathbf{a}_1 + (l + \frac{2}{3})\mathbf{a}_2. \quad (\text{B.75})$$

Applying a Peierls substitution the Hamiltonian becomes

$$\begin{aligned}
\mathcal{H}(t) = & - \sum_{jl} h_{jlA_1}^{j l B_1}(t) c_{jlA_1}^\dagger c_{jlB_1} + h_{jlB_1}^{j l A_2}(t) c_{jlB_1}^\dagger c_{jlA_2} + h_{jlA_2}^{j l B_2}(t) c_{jlA_2}^\dagger c_{jlB_2} \\
& + h_{jlB_1}^{j+1, l A_1}(t) c_{jlB_1}^\dagger c_{j+1, l A_1} + h_{jlB_2}^{j+1, l A_2}(t) c_{jlB_2}^\dagger c_{j+1, l A_2}(t) \\
& + h_{jlB_2}^{j+1, l+1, A_1}(t) c_{jlB_2}^\dagger c_{j+1, l+1, A_1} + h.c.
\end{aligned} \tag{B.76}$$

where in general

$$h_{jl\alpha}^{j'l'\beta}(t) \approx h \exp \left[i\phi_0 \left(-\frac{x_{j'l'}^\beta - x_{jl}^\alpha}{a} \sin \omega t + \frac{y_{j'l'}^\beta - y_{jl}^\alpha}{2a} \sin \left(K \frac{x_{j'l'}^\beta + x_{jl}^\alpha}{2} \right) \cos 2\omega t \right) \right]. \tag{B.77}$$

More explicitly for each term

$$h_{jlA_1}^{j l B_1}(t) \approx h \exp \left[i\phi_0 \left(-\frac{\sqrt{3}}{2} \sin \omega t + \frac{1}{4} \sin \left(\sqrt{3} K a (j + \frac{1}{4}) \right) \cos 2\omega t \right) \right] \tag{B.78}$$

$$h_{jlB_1}^{j l A_2}(t) \approx h \exp \left[i\phi_0 \left(\frac{1}{2} \sin \left(\sqrt{3} K a (j + \frac{1}{2}) \right) \cos 2\omega t \right) \right] \tag{B.79}$$

$$h_{jlA_2}^{j l B_2}(t) \approx h \exp \left[i\phi_0 \left(-\frac{\sqrt{3}}{2} \sin \omega t + \frac{1}{4} \sin \left(\sqrt{3} K a (j + \frac{3}{4}) \right) \cos 2\omega t \right) \right] \tag{B.80}$$

$$h_{jlB_1}^{j+1, l A_1}(t) \approx h \exp \left[i\phi_0 \left(-\frac{\sqrt{3}}{2} \sin \omega t - \frac{1}{4} \sin \left(\sqrt{3} K a (j + \frac{3}{4}) \right) \cos 2\omega t \right) \right] \tag{B.81}$$

$$h_{jlB_2}^{j+1, l A_2}(t) \approx h \exp \left[i\phi_0 \left(-\frac{\sqrt{3}}{2} \sin \omega t - \frac{1}{4} \sin \left(\sqrt{3} K a (j + \frac{5}{4}) \right) \cos 2\omega t \right) \right] \tag{B.82}$$

$$h_{jlB_2}^{j+1, l+1, A_1}(t) \approx h \exp \left[i\phi_0 \left(\frac{1}{2} \sin \left(\sqrt{3} K a (j + 1) \right) \cos 2\omega t \right) \right] \tag{B.83}$$

The incident laser beam allows for translation symmetry along the y-axis, so we can reduce the dimension of the Hamiltonian with the following Fourier transform

$$c_{jl\alpha}^\dagger = \frac{1}{N_y} \sum_k c_{jk\alpha}^\dagger e^{iky \cdot \mathbf{R}_l} = \frac{1}{N_y} \sum_k c_{jk\alpha}^\dagger e^{ik(3la)} \quad (\text{B.84})$$

The Hamiltonian then becomes

$$\begin{aligned} \mathcal{H}(t) = & - \sum_{jk} h_{jlA_1}^{jLB_1}(t) c_{jkA_1}^\dagger c_{jkB_1} + h_{jlB_1}^{jLA_2}(t) c_{jkB_1}^\dagger c_{jkA_2} + h_{jlA_2}^{jLB_2}(t) c_{jkA_2}^\dagger c_{jkB_2} \\ & + h_{jlB_1}^{j+1,LA_1}(t) c_{jkB_1}^\dagger c_{j+1,kA_1} + h_{jlB_2}^{j+1,L,A_2}(t) c_{jkB_2}^\dagger c_{j+1,kA_2}(t) \\ & + h_{jlB_2}^{j+1,l+1,A_1}(t) e^{-i3ka} c_{jkB_2}^\dagger c_{j+1,kA_1} + h.c. \end{aligned} \quad (\text{B.85})$$

Making use of Floquet theory we can make the Hamiltonian time-independent with the following time domain Fourier transform

$$\mathcal{H}_{ab,n}(k) = \frac{1}{2\pi} \int_0^{2\pi} \mathcal{H}_{ab}(k, t) e^{-in\tau} d\tau \quad (\text{B.86})$$

where a, b represent the amtrix indes of the previous Hamiltonian and n is the n -th order mode of light. Each term has the general following form

$$\mathcal{H}_{ab,n}(k) = \frac{1}{2\pi} \int_0^{2\pi} e^{iZ_1 \sin \tau + iZ_2 \cos 2\tau - in\tau} d\tau \quad (\text{B.87})$$

which looks a lot like the Hansen-Bessel integral function. However, because of the linear combination of $\sin \tau$ and $\cos 2\tau$, there is no elementary solution to the integral as currently defined.

I think if it was a linear combination of $\sin \tau$ and $\cos \tau$ we could use an addition of sines identity and maybe get a Hansen-Bessel integral. A moot point for this project since we need the $\cos 2\tau$ term to match the continuum models expectation of Landau levels. We thus solve the integral numerically for each given n . After the time domain Fourier transform the Hamiltonian can be

reduced to the following matrix form

$$\mathcal{H} = - \sum_{jk} \left[\Psi_{jk}^\dagger \mathcal{H}_{jj} \Psi_{jk} + \Psi_{jk}^\dagger \mathcal{H}'_{j,j+1}(k) \Psi_{j+1,k} + h.c. \right] \quad (\text{B.88})$$

$$\mathcal{H}_{jj} = \begin{bmatrix} 0 & h_{jlA_1}^{jLB_2} & 0 & 0 \\ 0 & 0 & h_{jlB_1}^{jLA_2} & 0 \\ 0 & 0 & 0 & h_{jlA_2}^{jLB_2} \\ 0 & 0 & 0 & 0 \end{bmatrix}$$

$$\mathcal{H}'_{j,j+1}(k) = \begin{bmatrix} 0 & 0 & 0 & 0 \\ h_{jlB_1}^{j+1,LA_1} & 0 & 0 & 0 \\ 0 & 0 & 0 & 0 \\ e^{-i3ka} h_{jlB_2}^{j+1,L+1,A_1} & 0 & h_{jlB_2}^{j+1,LA_2} & 0 \end{bmatrix}$$

with $\Psi_{jk} = [c_{jkA_1}, c_{jkB_1}, c_{jkA_2}, c_{jkB_2}]^T$.

Chern number of Landau levels

In this section we discuss how to understand the Chern number of Landau levels. For two-dimensional periodic systems, the 2D Brillouin zone is a closed manifold, and one can define the Chern number as a topological invariant for the mapping between complex functions (ground state wavefunctions) and this manifold. However, for Landau levels the system does not have translational symmetry which causes a conceptual difficulty in defining Chern numbers.

To address this difficulty, let us start from the Chern number of typical 2D Bloch Hamiltonians. The Berry curvature of band n at crystal momentum \mathbf{k} is defined as

$$\Omega_{n\mathbf{k}} = \mathbf{z} \cdot (\nabla_{\mathbf{k}} \times \mathbf{A}_{n\mathbf{k}}) = \mathbf{z} \cdot (\nabla_{\mathbf{k}} \times \langle u_{n\mathbf{k}} | i \nabla_{\mathbf{k}} | u_{n\mathbf{k}} \rangle) \quad (\text{B.89})$$

The Chern number for band n , which must not touch other bands throughout the Brillouin zone, is defined as

$$C_n = \int \frac{d^2\mathbf{k}}{2\pi} \Omega_{n\mathbf{k}} \quad (\text{B.90})$$

However, according to Eq. (B.89), C_n can be rewritten into

$$\begin{aligned} C_n &= \int \frac{d^2\mathbf{k}}{2\pi} \partial_{k_x} \langle u_{n\mathbf{k}} | i \partial_{k_y} | u_{n\mathbf{k}} \rangle - \int \frac{d^2\mathbf{k}}{2\pi} \partial_{k_y} \langle u_{n\mathbf{k}} | i \partial_{k_x} | u_{n\mathbf{k}} \rangle \\ &= \frac{1}{2\pi} \int dk_x \partial_{k_x} \int dk_y \langle u_{n\mathbf{k}} | i \partial_{k_y} | u_{n\mathbf{k}} \rangle - \frac{1}{2\pi} \int dk_y \partial_{k_y} \int dk_x \langle u_{n\mathbf{k}} | i \partial_{k_x} | u_{n\mathbf{k}} \rangle \end{aligned} \quad (\text{B.91})$$

It is worth noting that the last result is related to the expectation value of polarization (or position operator) in a Bloch state:

$$\begin{aligned} \langle n\mathbf{k} | \mathbf{r} | n'\mathbf{k}' \rangle &= \int d^2\mathbf{r} \psi_{n'\mathbf{k}'}^\dagger(\mathbf{r}) \mathbf{r} \psi_{n\mathbf{k}}(\mathbf{r}) \\ &= \int d^2\mathbf{r} u_{n\mathbf{k}}^\dagger(\mathbf{r}) e^{-i\mathbf{k}\cdot\mathbf{r}} \mathbf{r} e^{i\mathbf{k}'\cdot\mathbf{r}} u_{n'\mathbf{k}'}(\mathbf{r}) \\ &= \int d^2\mathbf{r} u_{n\mathbf{k}}^\dagger(\mathbf{r}) e^{-i\mathbf{k}\cdot\mathbf{r}} (-i\partial_{\mathbf{k}'} e^{i\mathbf{k}'\cdot\mathbf{r}}) u_{n'\mathbf{k}'}(\mathbf{r}) \\ &= -i\partial_{\mathbf{k}'} \langle n\mathbf{k} | n'\mathbf{k}' \rangle + \int d^2\mathbf{r} u_{n\mathbf{k}}^\dagger(\mathbf{r}) e^{-i\mathbf{k}\cdot\mathbf{r}} e^{i\mathbf{k}'\cdot\mathbf{r}} [i\partial_{\mathbf{k}'} u_{n'\mathbf{k}'}(\mathbf{r})] \\ &= -i\delta_{nn'} \frac{(2\pi)^2}{V_{\text{uc}}} \partial_{\mathbf{k}'} \delta(\mathbf{k} - \mathbf{k}') + \int d^2\mathbf{r} u_{n\mathbf{k}}^\dagger(\mathbf{r}) e^{-i\mathbf{k}\cdot\mathbf{r}} e^{i\mathbf{k}'\cdot\mathbf{r}} [i\partial_{\mathbf{k}'} u_{n'\mathbf{k}'}(\mathbf{r})] \\ &= -i\delta_{nn'} \frac{(2\pi)^2}{V_{\text{uc}}} \partial_{\mathbf{k}'} \delta(\mathbf{k} - \mathbf{k}') + \sum_{\mathbf{R}} \int_{\text{uc}} d^2\mathbf{r} u_{n\mathbf{k}}^\dagger(\mathbf{r}) e^{i(\mathbf{k}' - \mathbf{k})\cdot\mathbf{r}} [i\partial_{\mathbf{k}'} u_{n'\mathbf{k}'}(\mathbf{r})] e^{i(\mathbf{k}' - \mathbf{k})\cdot\mathbf{R}} \\ &= -i\delta_{nn'} \frac{(2\pi)^2}{V_{\text{uc}}} \partial_{\mathbf{k}'} \delta(\mathbf{k} - \mathbf{k}') + \frac{(2\pi)^2}{V_{\text{uc}}} \delta(\mathbf{k} - \mathbf{k}') \int_{\text{uc}} d^2\mathbf{r} u_{n\mathbf{k}}^\dagger(\mathbf{r}) [i\partial_{\mathbf{k}'} u_{n'\mathbf{k}'}(\mathbf{r})] e^{i(\mathbf{k}' - \mathbf{k})\cdot\mathbf{R}} \\ &= \frac{(2\pi)^2}{V_{\text{uc}}} [i\delta_{nn'} \partial_{\mathbf{k}} \delta(\mathbf{k} - \mathbf{k}') + \langle u_{n\mathbf{k}} | i\partial_{\mathbf{k}} | u_{n'\mathbf{k}'} \rangle \delta(\mathbf{k} - \mathbf{k}')] \end{aligned} \quad (\text{B.92})$$

where we have used the normalization condition of 2D Bloch states $\langle n\mathbf{k}|n'\mathbf{k}'\rangle = \delta_{nn'} \frac{(2\pi)^2}{V_{uc}} \delta(\mathbf{k}-\mathbf{k}')$ with V_{uc} the unit cell volume or area. The above result means that

$$\begin{aligned} \frac{a_y}{2\pi} \int dk_y \langle n\mathbf{k}|\mathbf{r}|n\mathbf{k}\rangle &\equiv N\mathbf{r}_n(k_x) = \frac{a_y}{2\pi} \int dk_y \lim_{\mathbf{k}' \rightarrow \mathbf{k}} \langle n\mathbf{k}|\mathbf{r}|n\mathbf{k}'\rangle \\ &= \frac{a_y}{2\pi} N \int dk_y \langle u_{n\mathbf{k}}|i\partial_{\mathbf{k}}|u_{n\mathbf{k}}\rangle \end{aligned} \quad (\text{B.93})$$

where a_y is the lattice constant along y . Namely

$$\frac{1}{2\pi} \int dk_y \langle u_{n\mathbf{k}}|i\partial_{\mathbf{k}}|u_{n\mathbf{k}}\rangle = \frac{\mathbf{r}_n(k_x)}{a_y}. \quad (\text{B.94})$$

Therefore

$$\begin{aligned} C_n &= \frac{1}{a_y} \int dk_x \partial_{k_x} y_n(k_x) - \frac{1}{a_x} \int dk_y \partial_{k_y} x_n(k_y) \\ &= \frac{1}{a_y} \left[y_n|_{k_x=\frac{2\pi}{a_x}} - y_n|_{k_x=0} \right] - \frac{1}{a_x} \left[x_n|_{k_y=\frac{2\pi}{a_x}} - x_n|_{k_y=0} \right] \\ &\equiv \frac{\Delta y_n}{a_y} - \frac{\Delta x_n}{a_x} \end{aligned} \quad (\text{B.95})$$

In other words, the Chern number can be understood as an effect of adiabatic pumping. The parameter defining the pump is k_x (1st term in the above equation) or k_y (2nd term in the above equation). When the pumping parameter increases by a period, the expectation value of the position operator y_n (or x_n) for the given band does not necessarily return to itself. A nonzero change leads to the finite Chern number. A caveat that is not mentioned in many references or textbooks is that since $\mathbf{A}_{n\mathbf{k}}$ is not a gauge invariant quantity, the two individual terms in the last line of Eq. (B.95) are not separately well defined. Instead, one can choose a gauge so that $A_x(k_y=0) = A_x(k_y=\frac{2\pi}{a_y})$ [but $A_y(k_x=0) \neq A_y(k_x=\frac{2\pi}{a_x})$, since otherwise C_n always vanishes], so

that

$$C_n = \frac{\Delta y_n}{a_y}, \quad A_x \left(k_y + \frac{2\pi}{a_y} \right) = A_x(k_y) \quad (\text{B.96})$$

In this manner, the Chern number is equivalent to the change of the y -component of the center-of-mass position of the given Bloch state, when k_x changes by $2\pi/a_x$.

The above adiabatic pumping understanding of the Chern number can now be used to define the Chern number of Landau levels, for which the Hamiltonian can only be made translation invariant along one direction. The Landau level Hamiltonian for a uniform magnetic field $B\mathbf{z} = \nabla \times (Bx\mathbf{y}) = \nabla \times \mathbf{A}$ is

$$H = \frac{p_x^2}{2m} + \frac{(p_y + eBx)^2}{2m} \quad (\text{B.97})$$

Assuming the eigenfunctions are $\psi(x, y)$, we can first make use of the translation symmetry along y to define

$$\psi(x, y) = \frac{1}{2\pi} \int dk \phi(x, k) e^{iky} \quad (\text{B.98})$$

The inverse transform is

$$\psi(x, k) = \int dy \psi(x, y) e^{-iky} \quad (\text{B.99})$$

which is consistent with the direct transform since

$$\begin{aligned} \psi(x, k) &= \int dy \frac{1}{2\pi} \int dk' \phi(x, k') e^{i(k'-k)y} \\ &= \int dk' \phi(x, k') \delta(k' - k) = \phi(x, k) \end{aligned} \quad (\text{B.100})$$

Here we assume the wave functions are normalized as

$$\int d^2\mathbf{r} \psi^\dagger(x, y) \psi(x, y) = 1 \quad (\text{B.101})$$

which means

$$\begin{aligned} 1 &= \frac{1}{(2\pi)^2} \int d^2\mathbf{r} \int dk \int dk' \phi^\dagger(x, k) \phi(x, k') e^{i(k'-k)y} \\ &= \frac{1}{(2\pi)^2} \int dx \int dk \int dk' \phi^\dagger(x, k) \phi(x, k') 2\pi \delta(k' - k) \\ &= \frac{1}{2\pi} \int dx \int dk \phi^\dagger(x, k) \phi(x, k) \\ &= \int \frac{dk}{2\pi} \langle \phi(k) | \phi(k) \rangle \end{aligned} \quad (\text{B.102})$$

The k -dependent Hamiltonian is

$$\begin{aligned} H_k = e^{-iky} H e^{iky} &= \frac{p_x^2}{2m} + \frac{(\hbar k + eBx)^2}{2m} \\ &= \frac{p_x^2}{2m} + \frac{1}{2} m \left(\frac{eB}{m} \right)^2 \left(x + \frac{\hbar k}{eB} \right)^2 \end{aligned} \quad (\text{B.103})$$

which is a quantum harmonic oscillator with $\omega = eB/m \equiv \omega_c$. The eigensolutions are

$$\begin{aligned} H_k \phi_n(x, k) &= \hbar \omega \left(n + \frac{1}{2} \right) \phi_n(x, k), \\ \phi_n(x, k) &= \frac{1}{\sqrt{2^n n!}} \left(\frac{m\omega_c}{\hbar\pi} \right)^{\frac{1}{4}} e^{-\frac{m\omega_c(x-x_k)^2}{2\hbar}} H_n \left[\sqrt{\frac{m\omega}{\hbar}} (x - x_k) \right] \end{aligned} \quad (\text{B.104})$$

where H_n are the Hermite polynomials and $x_k \equiv -\frac{\hbar k}{eB}$. However, the above ϕ_n are normalized as

$$\int dx \phi_n^*(x, k) \phi_n(x, k) = 1 \quad (\text{B.105})$$

incompatible with our earlier definition in Eq. (B.102). To this end we choose a cutoff for the k integral and replace the normalization condition in Eq. (B.102) as

$$1 = \frac{1}{2\pi} \int_{-\frac{\pi}{a_y}}^{\frac{\pi}{a_y}} dk \langle \phi(k) | \phi(k) \rangle \quad (\text{B.106})$$

Since $\phi_n(x, k)$ depends on k only through a shift of x , we have

$$\frac{1}{2\pi} \int_{-\frac{\pi}{a_y}}^{\frac{\pi}{a_y}} dk \langle \phi_n(k) | \phi_n(k) \rangle = \frac{1}{a_y} \langle \phi_n(k=0) | \phi_n(k=0) \rangle \equiv \frac{1}{a_y} \langle \phi_n | \phi_n \rangle = \frac{1}{a_y} \quad (\text{B.107})$$

This means that the ϕ_n should be redefined so that Eq. (B.106) is satisfied:

$$\begin{aligned} \phi_n(x, k) &= \frac{\sqrt{a_y}}{\sqrt{2^n n!}} \left(\frac{m\omega_c}{\hbar\pi} \right)^{\frac{1}{4}} e^{-\frac{m\omega_c(x-x_k)^2}{2\hbar}} H_n \left[\sqrt{\frac{m\omega}{\hbar}} (x - x_k) \right] \\ \langle \phi_n | \phi_n \rangle &= a_y \end{aligned} \quad (\text{B.108})$$

We can now try to use the above interpretation of the Chern number to check if Landau levels indeed have $C = 1$. To this end we would rewrite Eq. (B.95) assuming k as a pumping parameter. But this requires us to re-interpret Eq. (B.94) \mathbf{r}_n defined there is for Bloch waves with a different normalization condition from that in Eq. (B.106). Regarding $|n\mathbf{k}\rangle$ as an eigenstate of the Hamiltonian playing the same role as $|\phi_n\rangle$, we have

$$\frac{a_x a_y}{(2\pi)^2} \int dk_x \int dk_y \langle n\mathbf{k} | n\mathbf{k} \rangle = \frac{a_x a_y}{(2\pi)^2} \int d^2\mathbf{k} \frac{(2\pi)^2}{a_x a_y} \delta(\mathbf{k}) = 1 \quad (\text{B.109})$$

In other words,

$$\frac{a_y}{2\pi} \int dk_y \langle n\mathbf{k} | \mathbf{r} | n\mathbf{k} \rangle = \frac{1}{N_y} \sum_{k_y} \langle n\mathbf{k} | \mathbf{r} | n\mathbf{k} \rangle \rightarrow \frac{1}{a_y} \langle \phi_n(k) | x | \phi_n(k) \rangle \equiv x_{nk} \quad (\text{B.110})$$

which corresponds to taking the expectation value of x in a given normalized eigenstate. Therefore Eq. (B.95) applicable to the present case should be

$$\begin{aligned} C_n &= -\frac{1}{2\pi} \int dk \partial_k \left(\frac{2\pi}{L_x} x_{nk} \right) \\ &= \frac{1}{L_x} \left(x_{nk=\frac{\pi}{a_y}} - x_{nk=-\frac{\pi}{a_y}} \right) \end{aligned} \quad (\text{B.111})$$

Due to the symmetry of $\phi_n(x, k) = \langle x | \phi_n(k) \rangle = \phi_n(x - x_k, k = 0)$, we have

$$\langle \phi_{nk} | x | \phi_{nk} \rangle = a_y x_k \quad (\text{B.112})$$

As a result

$$\begin{aligned} C_n &= \frac{1}{L_x} \frac{\hbar}{eB} \left(\frac{\pi}{a_y} + \frac{\pi}{a_y} \right) \\ &= \frac{\hbar}{e} \frac{1}{B a_y L_x} \equiv \frac{\Phi_0}{\Phi} N_y \end{aligned} \quad (\text{B.113})$$

where $N_y \equiv L_y / a_y$. However, this result is obtained by assuming that the period of k is $2\pi / a_y$. If one wraps the 2D system into a cylinder parallel to \mathbf{x} so that k is quantized into

$$k = \frac{2\pi}{L_y} m \quad (\text{B.114})$$

where m can be any integer. Then imagining that one inserts a flux (or phase) through the cylinder defined by

$$\Phi_x \equiv \frac{e}{\hbar} A L_y \quad (\text{B.115})$$

so that Φ_x enters the Landau level Hamiltonian as

$$H(\Phi_x) = \frac{p_x^2}{2m} + \frac{(p_y + \frac{\hbar}{L_y} \Phi_x + eBx)^2}{2m} \quad (\text{B.116})$$

Then apparently the Hamiltonian is symmetric under $\Phi_x \rightarrow \Phi_x + 2\pi$, so that Φ_x can be viewed as a pumping parameter. In the above language, this is equivalent to choosing k as the pumping parameter but defining its period as

$$\frac{2\pi}{a_y} \rightarrow \frac{2\pi}{L_y} \quad (\text{B.117})$$

The Chern number is thus defined as

$$\begin{aligned} C_n &= -\frac{1}{2\pi} \oint d\Phi_x \partial_{\Phi_x} \left(\frac{2\pi}{L_x} x_{nk} \right) \\ &= \frac{1}{L_x} \left(x_{nk=\frac{2\pi}{L_y}} - x_{nk=0} \right) \\ &= \frac{\Phi_0}{\Phi} \end{aligned} \quad (\text{B.118})$$

The final result above is, however, not necessarily an integer. To see what is wrong with it, let us now use the above cylinder picture to understand what is really going on when the flux Φ_x changes by 2π . Since the cylinder has periodic boundary condition along y , k is quantized as mentioned above, which restricts the eigenstates $|\phi_n(k)\rangle$. This further constrains the values of x_k , i.e., the center-of-mass of the wave functions $\phi_n(x, k) = \langle x | \phi_n(k) \rangle$:

$$\langle \phi_{nk} | x | \phi_{nk} \rangle = -\frac{2\pi m}{L_y} \frac{\hbar}{eB} = -\frac{\Phi_0}{BL_y} m \equiv -m\Delta x \quad (\text{B.119})$$

where we recover the original normalization of the Landau level wavefunctions Eq. (B.105). Note that from this we can also obtain the total number of electrons within a Landau level:

$$N = \frac{L_x}{\Delta x} = \frac{\Phi}{\Phi_0}. \quad (\text{B.120})$$

When Φ_x changes by a period, which is equivalent to k changing by $\frac{2\pi}{L_y}$ or m changes by 1, the center-of-mass of the Landau level wavefunction shifts along \mathbf{x} for all k by the same quantity

$\Phi_0/(BL_y)$, which is the same as their nearest neighbor spacing. Thus increasing Φ_x by 2π is equivalent to removing a Landau level wavefunction at the boundary of $x = -L_x/2$ and adding another one at $x = L_x/2$. That one electron is transported from one edge to the other edge is the Chern number. However, Eq. (B.118) does not describe this integer directly. A modification that leads to the direct correspondence is to multiply Eq. (B.118) by the total number of electrons N :

$$\begin{aligned}
C_n &= -\frac{N}{2\pi} \oint d\Phi_x \partial_{\Phi_x} \left(\frac{2\pi}{L_x} x_{nk}(\Phi_x) \right) \\
&= -\frac{1}{2\pi} \sum_k \oint d\Phi_x \partial_{\Phi_x} \left(\frac{2\pi}{L_x} x_{nk}(\Phi_x) \right) \\
&\equiv -\frac{1}{2\pi} \oint d\Phi_x \partial_{\Phi_x} \left(\frac{2\pi}{L_x} X_n(\Phi_x) \right) \\
&= \frac{1}{L_x} [X_n(2\pi) - X_n(0)]
\end{aligned} \tag{B.121}$$

where $X_n \equiv \sum_k x_{nk}$ is the X coordinate of the center of mass of *all* electrons multiplied by the number of electrons within a Landau level. The above formula can be generally applied to other systems that has translation symmetry only along one direction.

More specifically, suppose we have a Hamiltonian H with eigenstates labeled by discrete band indices n and some other quantum numbers q characterizing the degenerate states within a band, and the eigenstates are simply normalized as $\langle nq|nq \rangle = 1$, then

$$X_n = \sum_q \langle nq|x|nq \rangle \tag{B.122}$$

One can get C_n by diagonalizing the Hamiltonian so that $H|nq \rangle = \epsilon_n|nq \rangle$, adding the flux so that

$$H(\Phi_x)|nq(\Phi_x) \rangle = \epsilon_n(\Phi_x)|nq(\Phi_x) \rangle \tag{B.123}$$

and making sure that $\epsilon_n(\Phi_x)$ does not intersect with other bands as Φ_x increases by 2π . After that, calculate

$$X_n(\Phi_x = 2\pi) - X_n(\Phi_x = 0) \tag{B.124}$$

and divide the above result by the finite length of the system along x . The result, if nonzero, means the system has a finite Chern number despite the absence of translation symmetry.

If, however, that ϵ_n depends on q as well. Namely $\epsilon_n \rightarrow \epsilon_n(q)$, one can still define the Chern number by making sure that all eigenenergies $\epsilon_{nq}(\Phi_x)$ do not touch other bands as Φ_x increases by 2π . The final step of calculating the Chern number stays unchanged.

Bibliography

- [1] David J. Griffiths. *Introduction to Electrodynamics*. Cambridge University Press, Cambridge New York Port Melbourne New Delhi Singapore, fifth edition edition, 2024.
- [2] Alexander Altland and Ben Simons. *Condensed Matter Field Theory*. Cambridge University Press, Cambridge, United Kingdom ; New York, NY, third edition edition, 2023.
- [3] Charles Kittel. *Introduction to Solid State Physics*. Wiley, Hoboken, NJ, global edition, [9th edition] edition, 2018.
- [4] Xiangang Wan, Ari M. Turner, Ashvin Vishwanath, and Sergey Y. Savrasov. Topological semimetal and Fermi-arc surface states in the electronic structure of pyrochlore iridates. *Phys. Rev. B*, 83(20):205101, May 2011.
- [5] Su-Yang Xu, Ilya Belopolski, Nasser Alidoust, Madhab Neupane, Guang Bian, Chenglong Zhang, Raman Sankar, Guoqing Chang, Zhujun Yuan, Chi-Cheng Lee, Shin-Ming Huang, Hao Zheng, Jie Ma, Daniel S. Sanchez, BaoKai Wang, Arun Bansil, Fangcheng Chou, Pavel P. Shibayev, Hsin Lin, Shuang Jia, and M. Zahid Hasan. Discovery of a Weyl fermion semimetal and topological Fermi arcs. *Science*, 349(6248):613–617, August 2015.
- [6] Zhilin Li, Hongxiang Chen, Shifeng Jin, Di Gan, Wenjun Wang, Liwei Guo, and Xiaolong Chen. Weyl Semimetal TaAs: Crystal Growth, Morphology, and Thermodynamics. *Crystal Growth & Design*, 16(3):1172–1175, March 2016.
- [7] D. A. Ivanov. Non-Abelian Statistics of Half-Quantum Vortices in p -Wave Superconductors. *Phys. Rev. Lett.*, 86(2):268–271, January 2001.
- [8] A. Yu Kitaev. Unpaired Majorana fermions in quantum wires. *Phys.-Usp.*, 44(10S):131, October 2001.

- [9] Jason Alicea, Yuval Oreg, Gil Refael, Felix von Oppen, and Matthew P. A. Fisher. Non-Abelian statistics and topological quantum information processing in 1D wire networks. *Nature Phys*, 7(5):412–417, May 2011.
- [10] Jay D. Sau, Roman M. Lutchyn, Sumanta Tewari, and S. Das Sarma. Generic New Platform for Topological Quantum Computation Using Semiconductor Heterostructures. *Phys. Rev. Lett.*, 104(4):040502, January 2010.
- [11] A. Yu. Kitaev. Fault-tolerant quantum computation by anyons. *Annals of Physics*, 303(1):2–30, January 2003.
- [12] Chetan Nayak, Steven H. Simon, Ady Stern, Michael Freedman, and Sankar Das Sarma. Non-Abelian anyons and topological quantum computation. *Rev. Mod. Phys.*, 80(3):1083–1159, September 2008.
- [13] David Aasen, Michael Hell, Ryan V. Mishmash, Andrew Higginbotham, Jeroen Danon, Martin Leijnse, Thomas S. Jespersen, Joshua A. Folk, Charles M. Marcus, Karsten Flensberg, and Jason Alicea. Milestones Toward Majorana-Based Quantum Computing. *Phys. Rev. X*, 6(3):031016, August 2016.
- [14] N. Read and Dmitry Green. Paired states of fermions in two dimensions with breaking of parity and time-reversal symmetries and the fractional quantum Hall effect. *Phys. Rev. B*, 61(15):10267–10297, April 2000.
- [15] Jean-Pascal Brison. P-Wave Superconductivity and d-Vector Representation. In Hervé Bulou, Loïc Joly, Jean-Michel Mariot, and Fabrice Scheurer, editors, *Magnetism and Accelerator-Based Light Sources*, Springer Proceedings in Physics, pages 165–204, Cham, 2021. Springer International Publishing.
- [16] V. Mourik, K. Zuo, S. M. Frolov, S. R. Plissard, E. P. A. M. Bakkers, and L. P. Kouwenhoven. Signatures of Majorana Fermions in Hybrid Superconductor-Semiconductor Nanowire Devices. *Science*, 336(6084):1003–1007, May 2012.

- [17] Leonid P. Rokhinson, Xinyu Liu, and Jacek K. Furdyna. The fractional a.c. Josephson effect in a semiconductor–superconductor nanowire as a signature of Majorana particles. *Nature Phys*, 8(11):795–799, November 2012.
- [18] M. T. Deng, C. L. Yu, G. Y. Huang, M. Larsson, P. Caroff, and H. Q. Xu. Anomalous Zero-Bias Conductance Peak in a Nb–InSb Nanowire–Nb Hybrid Device. *Nano Lett.*, 12(12):6414–6419, December 2012.
- [19] T.-P. Choy, J. M. Edge, A. R. Akhmerov, and C. W. J. Beenakker. Majorana fermions emerging from magnetic nanoparticles on a superconductor without spin-orbit coupling. *Phys. Rev. B*, 84(19):195442, November 2011.
- [20] Bernd Braunecker and Pascal Simon. Interplay between Classical Magnetic Moments and Superconductivity in Quantum One-Dimensional Conductors: Toward a Self-Sustained Topological Majorana Phase. *Phys. Rev. Lett.*, 111(14):147202, October 2013.
- [21] Jelena Klinovaja, Peter Stano, Ali Yazdani, and Daniel Loss. Topological Superconductivity and Majorana Fermions in RKKY Systems. *Phys. Rev. Lett.*, 111(18):186805, November 2013.
- [22] S. Nadj-Perge, I. K. Drozdov, B. A. Bernevig, and Ali Yazdani. Proposal for realizing Majorana fermions in chains of magnetic atoms on a superconductor. *Phys. Rev. B*, 88(2):020407, July 2013.
- [23] Stevan Nadj-Perge, Ilya K. Drozdov, Jian Li, Hua Chen, Sangjun Jeon, Jungpil Seo, Allan H. MacDonald, B. Andrei Bernevig, and Ali Yazdani. Observation of Majorana fermions in ferromagnetic atomic chains on a superconductor. *Science*, 346(6209):602–607, October 2014.
- [24] Lucas Schneider, Philip Beck, Jannis Neuhaus-Steinmetz, Levente Rózsa, Thore Posske, Jens Wiebe, and Roland Wiesendanger. Precursors of Majorana modes and their length-

- dependent energy oscillations probed at both ends of atomic Shiba chains. *Nat. Nanotechnol.*, 17(4):384–389, April 2022.
- [25] Liang Fu and C. L. Kane. Superconducting proximity effect and Majorana fermions at the surface of a topological insulator. *Phys. Rev. Lett.*, 100(9):096407, March 2008.
 - [26] Pavan Hosur, Pouyan Ghaemi, Roger S. K. Mong, and Ashvin Vishwanath. Majorana Modes at the Ends of Superconductor Vortices in Doped Topological Insulators. *Phys. Rev. Lett.*, 107(9):097001, August 2011.
 - [27] Andrew C. Potter and Patrick A. Lee. Engineering a \mathbb{Z}_2 superconductor: Comparison of topological insulator and Rashba spin-orbit-coupled materials. *Phys. Rev. B*, 83(18):184520, May 2011.
 - [28] M. Veldhorst, M. Snelder, M. Hoek, C. G. Molenaar, D. P. Leusink, A. A. Golubov, H. Hilgenkamp, and A. Brinkman. Magnetotransport and induced superconductivity in Bi based three-dimensional topological insulators. *physica status solidi (RRL) – Rapid Research Letters*, 7(1-2):26–38, 2013.
 - [29] Chui-Zhen Chen, Ying-Ming Xie, Jie Liu, Patrick A. Lee, and K. T. Law. Quasi-one-dimensional quantum anomalous Hall systems as new platforms for scalable topological quantum computation. *Phys. Rev. B*, 97(10):104504, March 2018.
 - [30] Yongxin Zeng, Chao Lei, Gaurav Chaudhary, and Allan H. MacDonald. Quantum anomalous Hall Majorana platform. *Phys. Rev. B*, 97(8):081102, February 2018.
 - [31] Ying-Ming Xie, Xue-Jian Gao, Tai-Kai Ng, and K. T. Law. Creating Localized Majorana Zero Modes in Quantum Anomalous Hall Insulator/Superconductor Heterostructures with a Scissor, June 2021.
 - [32] Yuval Oreg, Gil Refael, and Felix von Oppen. Helical Liquids and Majorana Bound States in Quantum Wires. *Phys. Rev. Lett.*, 105(17):177002, October 2010.

- [33] Roman M. Lutchyn, Tudor D. Stanescu, and S. Das Sarma. Search for Majorana Fermions in Multiband Semiconducting Nanowires. *Phys. Rev. Lett.*, 106(12):127001, March 2011.
- [34] Andrew C. Potter and Patrick A. Lee. Topological superconductivity and Majorana fermions in metallic surface states. *Phys. Rev. B*, 85(9):094516, March 2012.
- [35] Jian Li, Titus Neupert, Zhijun Wang, A. H. MacDonald, A. Yazdani, and B. Andrei Bernevig. Two-dimensional chiral topological superconductivity in Shiba lattices. *Nat Commun*, 7(1):12297, July 2016.
- [36] Chao Lei, Hua Chen, and Allan H. MacDonald. Ultrathin Films of Superconducting Metals as a Platform for Topological Superconductivity. *Phys. Rev. Lett.*, 121(22):227701, November 2018.
- [37] Annica M. Black-Schaffer and Jacob Linder. Majorana fermions in spin-orbit-coupled ferromagnetic Josephson junctions. *Phys. Rev. B*, 84(18):180509, November 2011.
- [38] Falko Pientka, Alessandro Romito, Mathias Duckheim, Yuval Oreg, and Felix von Oppen. Signatures of topological phase transitions in mesoscopic superconducting rings. *New J. Phys.*, 15(2):025001, February 2013.
- [39] Michael Hell, Martin Leijnse, and Karsten Flensberg. Two-Dimensional Platform for Networks of Majorana Bound States. *Phys. Rev. Lett.*, 118(10):107701, March 2017.
- [40] Antonio Fornieri, Alexander M. Whiticar, F. Setiawan, Elías Portolés, Asbjørn C. C. Drachmann, Anna Keselman, Sergei Gronin, Candice Thomas, Tian Wang, Ray Kallaher, Geoffrey C. Gardner, Erez Berg, Michael J. Manfra, Ady Stern, Charles M. Marcus, and Fabrizio Nichele. Evidence of topological superconductivity in planar Josephson junctions. *Nature*, 569(7754):89–92, May 2019.
- [41] Hechen Ren, Falko Pientka, Sean Hart, Andrew T. Pierce, Michael Kosowsky, Lukas Lunczer, Raimund Schlereth, Benedikt Scharf, Ewelina M. Hankiewicz, Laurens W.

- Molenkamp, Bertrand I. Halperin, and Amir Yacoby. Topological superconductivity in a phase-controlled Josephson junction. *Nature*, 569(7754):93–98, May 2019.
- [42] Benedikt Scharf, Falko Pientka, Hechen Ren, Amir Yacoby, and Ewelina M. Hankiewicz. Tuning topological superconductivity in phase-controlled Josephson junctions with Rashba and Dresselhaus spin-orbit coupling. *Phys. Rev. B*, 99(21):214503, June 2019.
- [43] Tong Zhou, Matthieu C. Dartiailh, William Mayer, Jong E. Han, Alex Matos-Abiague, Javad Shabani, and Igor Žutić. Phase Control of Majorana Bound States in a Topological X Junction. *Phys. Rev. Lett.*, 124(13):137001, April 2020.
- [44] Jin-Peng Xu, Mei-Xiao Wang, Zhi Long Liu, Jian-Feng Ge, Xiaojun Yang, Canhua Liu, Zhu An Xu, Dandan Guan, Chun Lei Gao, Dong Qian, Ying Liu, Qiang-Hua Wang, Fu-Chun Zhang, Qi-Kun Xue, and Jin-Feng Jia. Experimental Detection of a Majorana Mode in the core of a Magnetic Vortex inside a Topological Insulator-Superconductor Bi_2Te_3 / NbSe_2 Heterostructure. *Phys. Rev. Lett.*, 114(1):017001, January 2015.
- [45] S. M. Albrecht, A. P. Higginbotham, M. Madsen, F. Kuemmeth, T. S. Jespersen, J. Nygård, P. Krogstrup, and C. M. Marcus. Exponential protection of zero modes in Majorana islands. *Nature*, 531(7593):206–209, March 2016.
- [46] Hao-Hua Sun, Kai-Wen Zhang, Lun-Hui Hu, Chuang Li, Guan-Yong Wang, Hai-Yang Ma, Zhu-An Xu, Chun-Lei Gao, Dan-Dan Guan, Yao-Yi Li, Canhua Liu, Dong Qian, Yi Zhou, Liang Fu, Shao-Chun Li, Fu-Chun Zhang, and Jin-Feng Jia. Majorana Zero Mode Detected with Spin Selective Andreev Reflection in the Vortex of a Topological Superconductor. *Phys. Rev. Lett.*, 116(25):257003, June 2016.
- [47] Dongfei Wang, Lingyuan Kong, Peng Fan, Hui Chen, Shiyu Zhu, Wen Yao Liu, Lu Cao, Yujie Sun, Shixuan Du, John Schneeloch, Ruidan Zhong, Genda Gu, Liang Fu, Hong Ding, and Hong-Jun Gao. Evidence for Majorana bound states in an iron-based superconductor. *Science*, 362(6412):333–335, October 2018.

- [48] Berthold Jäck, Yonglong Xie, Jian Li, Sangjun Jeon, B. Andrei Bernevig, and Ali Yazdani. Observation of a Majorana zero mode in a topologically protected edge channel. *Science*, 364(6447):1255–1259, June 2019.
- [49] Sujit Manna, Peng Wei, Yingming Xie, Kam Tuen Law, Patrick A. Lee, and Jagadeesh S. Moodera. Signature of a pair of Majorana zero modes in superconducting gold surface states. *Proceedings of the National Academy of Sciences*, 117(16):8775–8782, April 2020.
- [50] Geoffrey L. Fatin, Alex Matos-Abiague, Benedikt Scharf, and Igor Žutić. Wireless Majorana Bound States: From Magnetic Tunability to Braiding. *Phys. Rev. Lett.*, 117(7):077002, August 2016.
- [51] Jay D. Sau and S. Das Sarma. Realizing a robust practical Majorana chain in a quantum-dot-superconductor linear array. *Nat Commun*, 3(1):964, July 2012.
- [52] Martin Leijnse and Karsten Flensberg. Parity qubits and poor man’s Majorana bound states in double quantum dots. *Phys. Rev. B*, 86(13):134528, October 2012.
- [53] Tom Dvir, Guanzhong Wang, Nick van Loo, Chun-Xiao Liu, Grzegorz P. Mazur, Alberto Bordin, Sebastiaan L. D. ten Haaf, Ji-Yin Wang, David van Driel, Francesco Zatelli, Xiang Li, Filip K. Malinowski, Sasa Gazibegovic, Ghada Badawy, Erik P. A. M. Bakkers, Michael Wimmer, and Leo P. Kouwenhoven. Realization of a minimal Kitaev chain in coupled quantum dots. *Nature*, 614(7948):445–450, February 2023.
- [54] Torsten Karzig, Christina Knapp, Roman M. Lutchyn, Parsa Bonderson, Matthew B. Hastings, Chetan Nayak, Jason Alicea, Karsten Flensberg, Stephan Plugge, Yuval Oreg, Charles M. Marcus, and Michael H. Freedman. Scalable designs for quasiparticle-poisoning-protected topological quantum computation with Majorana zero modes. *Phys. Rev. B*, 95(23):235305, June 2017.

- [55] Andrew C. Potter and Patrick A. Lee. Multichannel Generalization of Kitaev's Majorana End States and a Practical Route to Realize Them in Thin Films. *Phys. Rev. Lett.*, 105(22):227003, November 2010.
- [56] Jian Li, Titus Neupert, B. Andrei Bernevig, and Ali Yazdani. Manipulating Majorana zero modes on atomic rings with an external magnetic field. *Nat Commun*, 7(1):10395, January 2016.
- [57] O. Pietzsch, S. Okatov, A. Kubetzka, M. Bode, S. Heinze, A. Lichtenstein, and R. Wiesendanger. Spin-Resolved Electronic Structure of Nanoscale Cobalt Islands on Cu(111). *Phys. Rev. Lett.*, 96(23):237203, June 2006.
- [58] Alessandro Romito, Jason Alicea, Gil Refael, and Felix von Oppen. Manipulating Majorana fermions using supercurrents. *Phys. Rev. B*, 85(2):020502, January 2012.
- [59] Kazuaki Takasan, Shuntaro Sumita, and Youichi Yanase. Supercurrent-induced topological phase transitions. *Phys. Rev. B*, 106(1):014508, July 2022.
- [60] *See Supplemental Material at [url].*
- [61] Jian Li, Hua Chen, Ilya K. Drozdov, A. Yazdani, B. Andrei Bernevig, and A. H. MacDonald. Topological superconductivity induced by ferromagnetic metal chains. *Phys. Rev. B*, 90(23):235433, December 2014.
- [62] Tudor E. Pahomi, Manfred Sigrist, and Alexey A. Soluyanov. Braiding Majorana corner modes in a second-order topological superconductor. *Phys. Rev. Res.*, 2(3):032068, September 2020.
- [63] Ryan V. Mishmash, Bela Bauer, Felix von Oppen, and Jason Alicea. Dephasing and leakage dynamics of noisy Majorana-based qubits: Topological versus Andreev. *Phys. Rev. B*, 101(7):075404, February 2020.

- [64] Gábor Széchenyi and András Pályi. Parity-to-charge conversion for readout of topological majorana qubits. *Phys. Rev. B*, 101:235441, Jun 2020.
- [65] Guan-Hao Feng and Hong-Hao Zhang. Probing robust Majorana signatures by crossed Andreev reflection with a quantum dot. *Phys. Rev. B*, 105(3):035148, January 2022.
- [66] K. v. Klitzing, G. Dorda, and M. Pepper. New method for high-accuracy determination of the fine-structure constant based on quantized hall resistance. *Phys. Rev. Lett.*, 45(6):494–497, August 1980.
- [67] K. S. Novoselov, A. K. Geim, S. V. Morozov, D. Jiang, M. I. Katsnelson, I. V. Grigorieva, Dubonos S. V., and A. A. Firsov. Two-dimensional gas of massless Dirac fermions in graphene. *Nature Physics*, 438:197, 2005.
- [68] Yuanbo Zhang, Yan-Wen Tan, Horst L. Stormer, and Philip Kim. Experimental observation of the quantum Hall effect and Berry’s phase in graphene. *Nature Physics*, 438:201, 2005.
- [69] A. H. Castro Neto, F. Guinea, N. M. R. Peres, K. S. Novoselov, and A. K. Geim. The electronic properties of graphene. *Rev. Mod. Phys.*, 81(1):109–162, January 2009.
- [70] Netanel H. Lindner, Gil Refael, and Victor Galitski. Floquet topological insulator in semiconductor quantum wells. *Nature Physics*, 7:490, 2011.
- [71] André Eckardt and Egidijus Anisimovas. High-frequency approximation for periodically driven quantum systems from a Floquet-space perspective. *New J. Phys.*, 17:093039, 2015.
- [72] Mikael C. Rechtsman, Julia M. Zeuner, Yonatan Plotnik, Yaakov Lumer, Daniel Podolsky, Felix Dreisow, Stefan Nolte, Mordechai Segev, and Alexander Szameit. Photonic floquet topological insulators. *Nature Physics*, 496:196, 2013.
- [73] Y. H. Wang, H. Steinberg, P. Jarillo-Herrero, and N. Gedik. Observation of floquet-bloch states on the surface of a topological insulator. *Science*, 342(6157):453–457, 2013.

- [74] Hongbin Zhang, Jiandong Yao, Jianmei Shao, Hai Li, Shuwei Li, Dinghua Bao, Chengxin Wang, and Guowei Yang. Anomalous photoelectric effect of a polycrystalline topological insulator film. *Scientific Reports*, 4:5876, 2014.
- [75] J. W. McIver, B. Schulte, F.-U. Stein, T. Matsuyama, G. Jotzu, G. Meier, and A. Cavalleri. Light-induced anomalous Hall effect in graphene. *Nature Physics*, 11:123, 2019.
- [76] Jon H. Shirley. Solution of the schrödinger equation with a hamiltonian periodic in time. *Phys. Rev.*, 138(4B):B979–B987, May 1965.
- [77] Hideo Sambe. Steady states and quasienergies of a quantum-mechanical system in an oscillating field. *Phys. Rev. A*, 7(6):2203–2213, June 1973.
- [78] Milena Grifoni and Peter Hänggi. Driven quantum tunneling. *Physics Reports*, 304:229, 1998.
- [79] M. Bukov, L. D’Alessio, and A. Polkovnikov. Universal high-frequency behavior of periodically driven systems: From dynamical stabilization to Floquet engineering. *Advances in Physics*, 64:139, 2015.
- [80] N. Goldman and J. Dalibard. Periodically driven quantum systems: Effective hamiltonians and engineered gauge fields. *Phys. Rev. X*, 4(3):031027, August 2014.
- [81] Saar Rahav, Ido Gilary, and Shmuel Fishman. Effective Hamiltonians for periodically driven systems. *Phys. Rev. A*, 68(1):013820, July 2003.
- [82] A. P. Itin and M. I. Katsnelson. Effective hamiltonians for rapidly driven many-body lattice systems: Induced exchange interactions and density-dependent hoppings. *Phys. Rev. Lett.*, 115(7):075301, August 2015.
- [83] Takahiro Mikami, Sota Kitamura, Kenji Yasuda, Naoto Tsuji, Takashi Oka, and Hideo Aoki. Brillouin-Wigner theory for high-frequency expansion in periodically driven sys-

- tems: Application to Floquet topological insulators. *Phys. Rev. B*, 93(14):144307, April 2016.
- [84] E. S. Mananga and T. Charpentier. Introduction of the Floquet-Magnus expansion in solid-state nuclear magnetic resonance spectroscopy. *The Journal of Chemical Physics*, 135:044109, 2011.
 - [85] T. Kuwahara, T. Mori, and K. Saito. Floquet–Magnus theory and generic transient dynamics in periodically driven many-body quantum systems. *Annals of Physics*, 367:96, 2016.
 - [86] A. López, A. Scholz, Z. Z. Sun, and J. Schliemann. Graphene with time-dependent spin-orbit coupling: Truncated Magnus expansion approach. *Eur. Phys. J. B*, 86:366, 2013.
 - [87] F. Casas, J. A. Oteo, and J. Ros. Floquet theory: Exponential perturbative treatment. *J. Phys. A*, 34:3379, 2001.
 - [88] Takuya Kitagawa, Takashi Oka, Arne Brataas, Liang Fu, and Eugene Demler. Transport properties of nonequilibrium systems under the application of light: Photoinduced quantum Hall insulators without Landau levels. *Phys. Rev. B*, 84(23):235108, December 2011.
 - [89] F. D. M. Haldane. Model for a quantum hall effect without landau levels: Condensed-matter realization of the "Parity Anomaly". *Phys. Rev. Lett.*, 61(18):2015–2018, October 1988.
 - [90] Andrei Kirilyuk, Alexey V. Kimel, and Theo Rasing. Ultrafast optical manipulation of magnetic order. *Rev. Mod. Phys.*, 82(3):2731–2784, September 2010.
 - [91] J. H. Mentink, K. Balzer, and M. Eckstein. Ultrafast and reversible control of the exchange interaction in Mott insulators. *Nature Communications*, 6:6708, 2015.

- [92] L. Stojchevska, I. Vaskivskyi, T. Mertelj, P. Kusar, D. Svetin, S. Brazovskii, and D. Mihailovic. Ultrafast switching to a stable hidden quantum state in an electronic crystal. *Science*, 344(6180):177–180, 2014.
- [93] Adolfo G. Grushin, Álvaro Gómez-León, and Titus Neupert. Floquet fractional chern insulators. *Phys. Rev. Lett.*, 112(15):156801, April 2014.
- [94] Mark S. Rudner and Netanel H. Lindner. Floquet topological insulators: From band structure engineering to novel non-equilibrium quantum phenomena. *arxiv*.
- [95] Ervand Kandelaki and Mark S. Rudner. Many-body dynamics and gap opening in interacting periodically driven systems. *Phys. Rev. Lett.*, 121(3):036801, July 2018.
- [96] G. Juzeliūnas and P. Öhberg. Slow light in degenerate fermi gases. *Phys. Rev. Lett.*, 93(3):033602, July 2004.
- [97] J. Ruseckas, G. Juzeliūnas, P. Öhberg, and M. Fleischhauer. Non-abelian gauge potentials for ultracold atoms with degenerate dark states. *Phys. Rev. Lett.*, 95(1):010404, June 2005.
- [98] Shi-Liang Zhu, Hao Fu, C.-J. Wu, S.-C. Zhang, and L.-M. Duan. Spin hall effects for cold atoms in a light-induced gauge potential. *Phys. Rev. Lett.*, 97(24):240401, December 2006.
- [99] Jean Dalibard, Fabrice Gerbier, Gediminas Juzeliūnas, and Patrik Öhberg. Colloquium: Artificial gauge potentials for neutral atoms. *Rev. Mod. Phys.*, 83(4):1523–1543, November 2011.
- [100] N Goldman, G Juzeliūnas, P Öhberg, and I B Spielman. Light-induced gauge fields for ultracold atoms. *Reports on Progress in Physics*, 77(12):126401, November 2014.